The role of ceramide [AP] for the structural assembly of stratum corneum lipid model membranes

D i s s e r t a t i o n

zur Erlangung des akademischen Grades

doctor rerum naturalium (Dr. rer. nat.)

vorgelegt der

Naturwissenschaftlichen Fakultät I

Biowissenschaften

der Martin-Luther-Universität Halle-Wittenberg

von

Frau Dipl.-Pharm. Annett Schröter, geb. Rüttinger

geboren am 10. Oktober 1979 in Halle (Saale)

Gutachter

1. Prof. Dr. Dr. h.c. Reinhard Neubert

2. Prof. Dr. Gerald Brezesinski

3. Prof. Dr. Daniel Huster

Tag der öffentlichen Verteidigung: 16.03.2010

Contents

Abbreviations and Symbols

AP	alpha-hydroxy phytosphingosine
BA	behenic acid
CA	cerotic acid
CER	ceramide
CHOL	cholesterol
ChS	cholesterol sulphate
d	membrane repeat distance
DSC	differential scanning calorimetry
EOS	omega-hydroxy sphingosine
FFA	free fatty acid
Fig.	figure
FT	Fourier transform
IR	infrared
λ	wavelength
LPP	long-periodicity-phase
NP	non-hydroxy phytosphingosine
PA	palmitic acid
θ	scattering angle theta
RH	relative humidity
SA	stearic acid
SANS	small angle neutron scattering
SAXD	small angle X-ray diffraction
SC	stratum corneum
SF	structure factor
SLD	scattering length density
SPP	short-periodicity-phase
T	temperature
TA	tetracosanoic acid
ν	wave number

1   Introduction

The mammalian skin, a highly complex and specialised organ covers an area of approximately $2m^2$ in case of an average human adult. With approximately 10% of the body mass is the skin the largest organ of the human being. It protects the organism from outside influences such as mechanical, physical (e.g. UV-Radiation) and chemical stress as well as against the invasion of pathogens. The skin is responsible for the maintenance of the homeostasis. The regulation of the thermal and water balance is one of its most important functions. Particularly, the prevention of dehydration made life outside of water possible as the skin barrier is responsible for the survival of the terrestrial animals without desiccation [1]. Consequently, the skin is subjected to a continuous process of regeneration [1, 2].

The skin is able to gather signals coming from the outside, to further process and transfer these signals. This enables the contact with the environment [3]. For this kind of communication different type of sensors such as pain and pressure are necessary and are present in the skin [4]. Such sensory functions of the skin are vital for the organism, because is has to "sense" its environment to react appropriately. For example the reflexive reaction to heat or other threatening stimuli are essential for survival.

The skin is further able perform endocrine functions as a variety of glands are incorporated in the skin, for example the synthesis of Vitamin D [5, 6] and the conversion of prohormones is taking place in there [7]. Additionally, the skin has an important role for the reproduction as pheromones are produced in the skin and therefore, it has an active role in the maintenance of a species. Moreover, visual signals and emotions are transferred via the skin.

Besides these functions of the incorporated organs the barrier function is the most important feature of the skin. Already in the 1940s it was suggested by Winsor and co-workers that the outermost layer of the skin, the stratum corneum (SC), is responsible for the barrier properties [8]. This superficial layer consists of dead cells, the corneocytes, which are further embedded in a matrix of multilamellar organised lipid membranes [9]. It is well known that the SC serves as barrier to transepidermal water loss [10, 11]. However, it was not until a series of experiments had been carried out before it was accepted that the *lipid* part of the SC plays an important role in the function of this barrier. With freeze-fracture electron microscopy a broad, multiple membranous structure was identified by Elias and co-workers [12] and it became evident that this structure fills most of the intercellular part of the SC.

For the pharmaceutical industry on the one hand due to its large area the skin offers the possibility of a directed pharmacotherapy, on the other hand it displays a challenge in the sense of overcoming the barrier, as a prerequisite to achieve a systemic effect. As the SC lipid matrix has been identified as the major diffusion-rate limiting pathway [13, 14], it is of interest to understand the nanostructure and the contribution of the different constituents, especially the lipids to the overall properties of the SC and for the comprehension of the drug penetration mechanism through the SC.

Many studies have been performed in order to receive more detailed information about the internal nanostructure of the SC and its properties. In previous studies it has been shown that X-ray and neutron scattering are very powerful tools for the investigation of the nanostructure of isolated SC [15-17] as well as SC model membranes constructed from extracted SC lipids [18, 15, 19-25]. As natural SC membranes are very complex, lipid model membranes will offer the possibility to gain a closer insight into the driving forces and mechanisms that govern the self assembling process of such lipid layers. Furthermore, using synthetic lipids is advantageous as issues due to the variability of the native lipids, for example the variability in the head group architecture can be overcome. Model membranes enable a systematic study of the impact of different lipids on the assembly and structural properties of the membranes. Many efforts have been undertaken to investigate the structure of model membranes based on eleven types of ceramides [26, 27]. Nevertheless, the information about the nanostructure was limited to the determination of the repeat distance. The investigation of a more simplistic, but realistic model membrane based only on one or two types of ceramides with neutron diffraction can give an insight into the internal nanostructure of the lipid bilayer as firstly shown by Kiselev and co-workers [28]. The scattering length density profiles received from neutron diffraction experiments allow for analysis of the internal structure of the SC lipid membrane as well as the water distribution function. It is generally accepted that the hydration level of the SC lipid matrix influences the penetration of substances through the SC [29-32]. Therefore, to gain insights into the water distribution through the SC lipid matrix and its manipulation is mandatory.

The aim of this thesis is to present fundamental insights into the organisation and nanostructure of stratum corneum model membranes with respect to the composition. For that purpose the influence of the free fatty acid chain length to a given SC model system based on ceramide [AP] was investigated (Chapters 4 and 5).

Chapter 6 concentrates on the structure-function-relationship of the ceramides. Therefore, artificial ceramides were employed which chemically differ only slightly from ceramide [AP]. Neutron diffraction experiments with SC lipid model membranes based on

these artificial ceramides were performed and the nanostructure was analysed and compared with the systems described in the preceding Chapters. Additionally, in order to receive more information about the role of ceramide [AP] for the spatial organisation of SC lipid model membranes, lipid systems containing both an artificial ceramide and ceramide [AP] were investigated with neutron diffraction.

The ultimate aim of such investigations is to develop a model membrane with mimics the stratum corneum as closely as possible. Therefore, in Chapter 7 a model system was investigated which contained both a short and long chain ceramide, along with cholesterol and a free fatty acid. Additionally, for the identification of the position of the fatty acid a specifically deuterated fatty acid was employed.

As the permeability of the stratum corneum is closely linked to the thermotropic state of the lipids the thermotropic phase behaviour of quaternary SC lipid matrices was monitored with differential scanning calorimetry, Raman spectroscopy and neutron diffraction (Chapter 8). This allowed the observation of changes in the internal nanostructure upon temperature alteration.

2   Skin fundamentals

2.1   Organisation and function of the mammalian skin

The skin can be divided into three layers, beginning at the outer layer, the **epidermis**, followed by the **dermis** (corium) and finally the innermost **subcutis** (hypodermis). The principal organisation is depicted in Fig. 2-1.
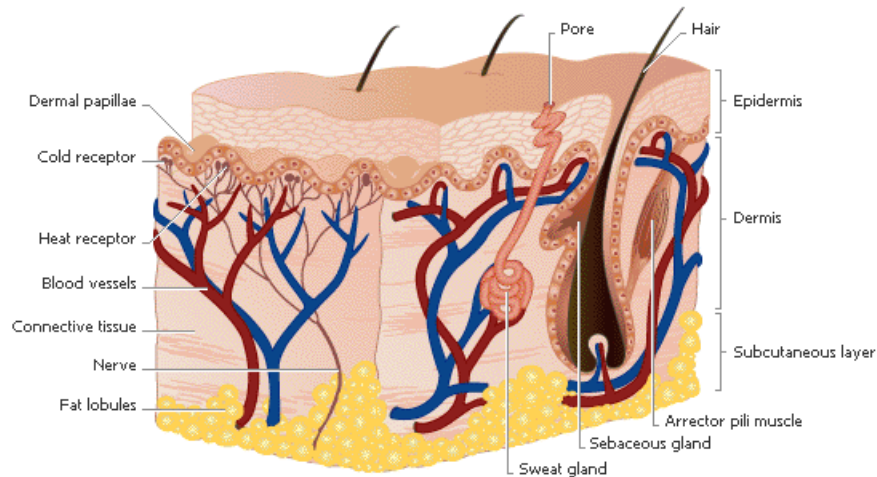
Fig. 2-1 Cross section of human skin according to [33]

The subcutis is a bridge between the overlying dermis and the body constituents with are underneath. The subcutis is a loose connective tissue containing fat lobes and it provides protection against cold and mechanical pressure. It includes the principal blood vessels as well as the principle nerves. Following the subcutis is the dermis which is typically 3 – 5 mm thick. Due to its high cohesiveness it is a supporting and connective tissue, predominately composed of collagen fibrils for support and elastic tissues for flexibility which are embedded in a mucopolysaccharide gel [34]. Embedded within the dermis are numerous structures such as vessels of the blood and lymphatic system, nerve endings, hair follicles, sebaceous and sweat glands. Due to the extensive vasculature of the dermis the regulation of the body temperature as well as the delivery of oxygen and nutrition and removal of waste products is guaranteed for the epidermis which is lacking in blood vessels.

The outermost layer, the epidermis is in itself a complex multilayer system with varying thickness. Four different layers can be differentiated, starting at the connection to the dermis with the stratum basale, followed by the stratum spinosum, stratum granulosum and finally the uppermost layer, the stratum corneum (see Fig. 2-2).
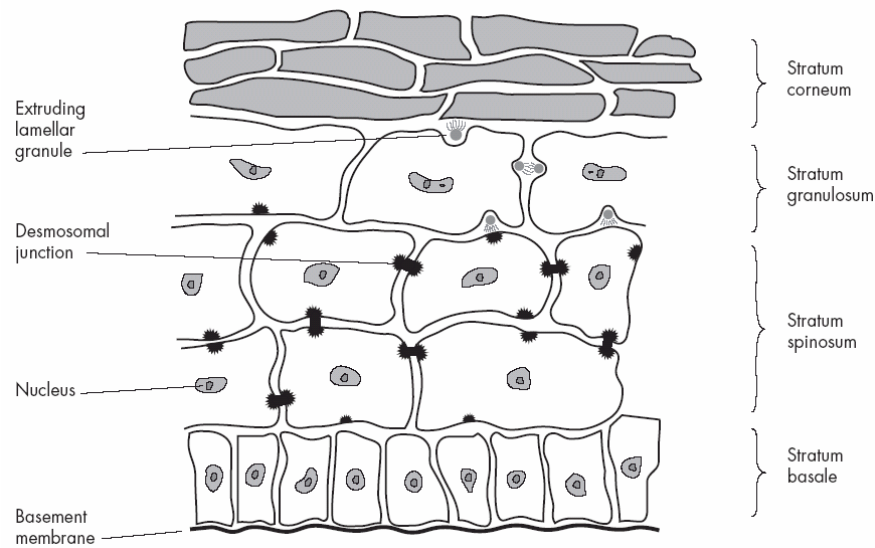
Fig. 2-2 Schematic presentation of the organisation of the epidermis. Modified according to [35].

The innermost epidermal layer, the stratum basale, also referred to as stratum germinativum is a single layer of columnar basal cells that remain attached to the basement membrane via hemidesmosomes. Those cells, the keratinocytes are the only cells of the epidermis which undergo cell division, then they migrate upwards to the skin surface while they change to dead coreless corneocytes. Furthermore, the stratum basale contains melanocytes which are responsible for the synthesis of the pigment melanin.

The following epidermal layer, the stratum spinosum consists of rows of keratinocytes which begin to differentiate and to synthesise keratin which aggregate to form tonofilaments. The tonofilaments condense and form desmosomes, the desmosomes connect the cell membranes of adjacent keratinocytes. In the upper layers of the stratum spinosum Odland and co-workers identified lamellar bodies, the now called Odland bodies [36]. Those membrane coated granules contain hydrolytic enzymes, glycoproteins and specific lipids [37]; the lipids are further of importance for the formation of the barrier of the stratum corneum [38].

The keratinocytes continue to differentiate, synthesise keratin and begin to flatten when they move to the subsequent layer, the stratum granulosum. The cells contain many dense and rigid tonofibrills and enzymes for degeneration of the vital cell components. In the course of the differentiation process the keratinocytes cornify to the metabolically inactive corneocytes. Additionally, as the cells approach the stratum corneum the enzymes release the components from the Odland bodies via exocytosis into the intercellular space, where a continuous lipid matrix is formed [38].

5

2.2   Stratum corneum

The final state of the epidermal cell differentiation is reached in the stratum corneum (SC). Typically this superficial layer comprises 10 to 15 cell layers and has a thickness of approximately 10 - 20 µm. It is made up of dead anucleate and keratinised cells, the terminally differentiated keratinocytes, the corneocytes. These cells are further embedded in a matrix of multilamellar organised lipid membranes [9]. The SC is often described as a brick wall-like structure, whereby the corneocytes resemble the bricks while the mortar is made up of the lipid bilayers [39, 37] (see Fig. 2-3).
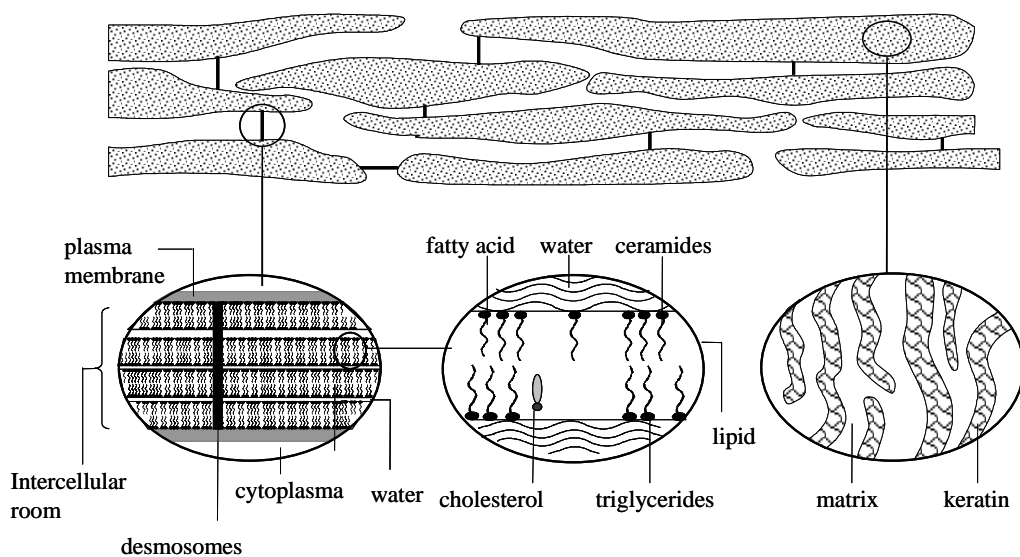
Fig. 2-3 Illustration of the organisation of the stratum corneum modified according to [40].

The flat corneocytes are further enclosed by a cornified envelop which is formed by the highly insoluble and chemically resistant proteins loricrin and involucrin. This protein envelop is covalently bound to ω-hydroxy acid-containing ceramides of a lipid envelope. Thus, this lipid envelop provides an anchor to the corneocytes and a link to the intercellular lipid membranes. This arrangement forms a rigid structure and an effective barrier against the penetration of foreign substances. Nevertheless, topically applied drugs can pass through the SC. However its multilamellar organised lipids are the major diffusion-rate limiting barrier, as shown by several transport studies [13, 14]. The knowledge and comprehension of the nanostructure and the relative properties of the SC on the molecular level, in particular of the SC lipids are essential for understanding of drug penetration through the SC as well as for the development of new dermal drug delivery systems.

2.2.1   The lipid composition within the stratum corneum

Since the intercellular lipid matrix of the stratum corneum is responsible for the barrier function of the mammalian skin, it depends on the physical state and structural organisation of these lipid membranes. The lipid composition of the stratum corneum lipid matrix is unique when compared to other biological membranes. The absence of phospholipids as a main component of biological membranes is one important feature that characterises the lipid composition as well as the properties of the SC [41]. Furthermore, the composition of the extractible lipids of the SC varies depending on the age and gender as well as the position of the skin [10, 42]. The major lipid classes that can be extracted from the SC are ceramides (CER), cholesterol (CHOL), and long chain free fatty acids (FFA). Small amounts of cholesterol sulphate and cholesterol esters are also present [43-46].

Ceramides

It is generally known, that the main constituent, the ceramides, play a key role in the structuring and hence the maintenance of the barrier function of the skin [47, 48]. They are a group of structurally heterogeneous sphingolipids and consist of a long chain fatty acid bound to the amino-group of a long chain di-or trihydroxy sphingoid base (sphingosine, phytosphingosine, and 6- hydroxysphingosine). The bound fatty acid of the ceramides can be hydroxylated at the α-position to the carbonyl oxygen, at the end of the hydrocarbon chain (ω-position) or contain no hydroxylation [48]. Up to now, 11 major ceramide classes have been identified within the SC lipid matrix [26, 27], but detailed information about their specific role for the barrier function of the SC remains to be presented (see Fig. 2-4).

The first nomenclature used to label the different ceramides was based on their mobility in the thin layer chromatography [49]. As the number of the identified ceramides increased, this method of labelling was insufficient. Therefore, the currently used nomenclature developed by Motta and co-workers [50] is based on the chemical structure of the ceramides. In this system the ceramides are labelled with letters, whereby the last letter assigns the type of sphingoid base (**S** … Sphingosine, **P**… Phytosphingosine, **H** … 6-Hydroxysphingosine). The long chain fatty acid bound to the amino group can be differentiated due to their hydroxylation. This was taken up in the nomenclature as amid-bound fatty acids without a hydroxyl group were labelled with the letter N (= non hydroxy), while ceramides with an omega and alpha hydroxylated fatty acid receive either the letter O or A, respectively. Furthermore, within the group of ceramide the exceptionally long ω-acylceramides exist, which are esterified with a long unsaturated fatty acid. In line with the way of labelling these ceramides receive the letter **E** (= esterified). Due to the esterified fatty

acid, those ceramides have a chain length of 30 – 32 carbon atoms [51]. As mentioned before, the role of each ceramide subspecies is not known or fully understood, however, there are several studies which report, that the existence of the ω-acylceramides is of importance for normal barrier function of the stratum corneum, especially due to the very long fatty acid chain [21, 52].
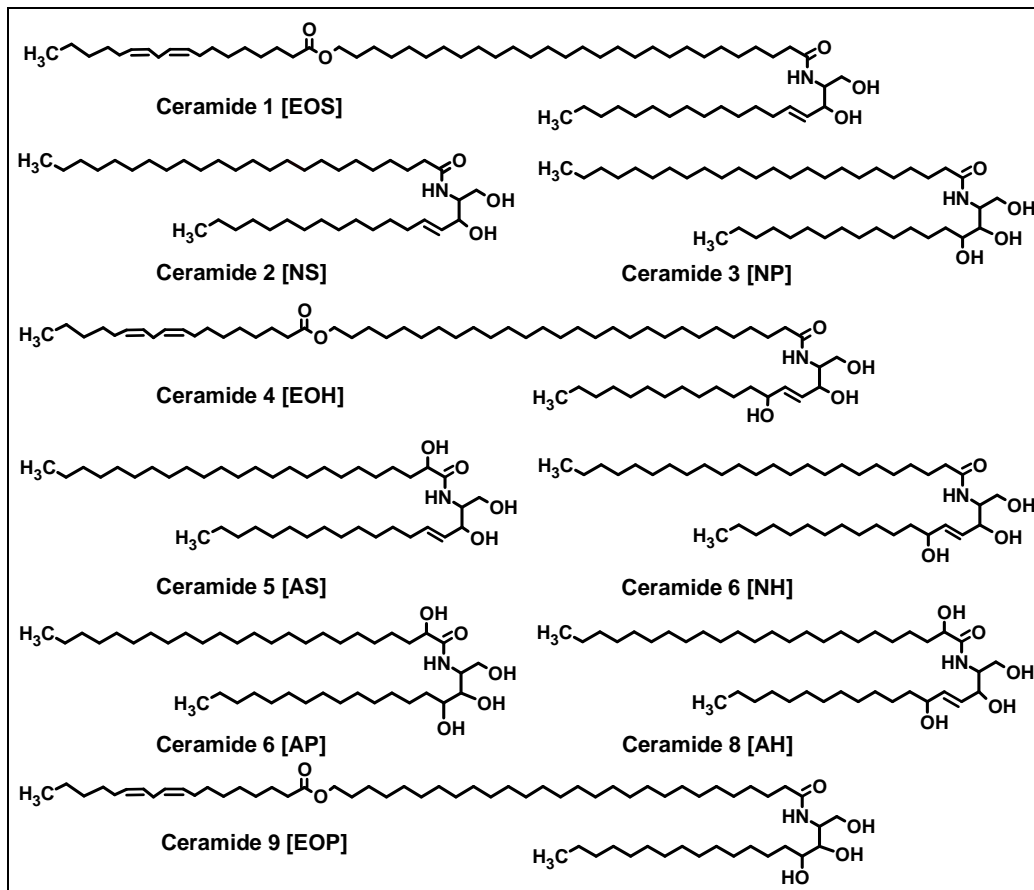
Fig. 2-4 Chemical structures of the ceramides found in the human stratum corneum. *S*: Sphingosine; *P*: Phytosphingosine; *H*: 6-Hydroxysphingosine, *N*: non hydroxy fatty acid, *A*: alpha-hydroxy fatty acid; *O*: ω-hydroxy fatty acid; *E*: esterified

Free fatty acids

The necessity of the free fatty acids (FFA) within the stratum corneum lipid matrix for normal barrier function was demonstrated by Mao-Qiang and co-workers, who found that after barrier disruption and inhibition of the fatty acid synthesis, the recovery of the barrier function is less pronounced, while after application of additional FFA, the barrier recovery improved significantly [53]. The free fatty acids found in the SC are predominately straight chained and saturated. They originate from the de-novo synthesis in the epidermis [48]. The range of the free fatty acid chain length varies from 16 to 30 carbon atoms, while the most abundant FFA in human SC are the 22- and 24-carbon entities [54, 55, 42]. Aside from the

small amount of cholesterol sulphate, the FFA are the only ionisable lipids in the SC, this may be important for the formation of lamellae [56].

Cholesterol

Cholesterol with its rigid ring system is an important and ubiquitous constituent of cell membranes. According to its structure, cholesterol inserts into the membrane with its hydrophobic steroid ring system and the aliphatic chain adjacent to the hydrophobic fatty acid tails of the ceramides and free fatty acids, while the hydroxyl group is oriented towards the aqueous phase [57]. Cholesterol modifies the properties of the lipid membranes depending on its concentration: in low concentrations the integration of cholesterol increases the order of the membrane by increasing the *trans* conformation of the chains and decreasing the tilt angle. This condensing effect of cholesterol on acyl chains results in a restriction of the mobility of the chains [58-60]. Due to this condensing effect the membrane permeability is decreased. On the other hand, the presence of cholesterol in high concentrations in phospholipid membranes inhibits the transition to the crystalline state due to the interference with closed packed fatty acid tails. Therefore, a high concentration of cholesterol increases the fluidity of membranes. As for stratum corneum lipid membranes cholesterol should also increase the fluidity of the otherwise rigid membrane when present in high concentrations [61].

The derivatives of cholesterol are only in small amounts present in the SC lipid fraction. Nevertheless, cholesterol sulphate for example is essential for the cohesion of cells and therefore, for the SC desquamation process. It plays a central role in the inhibition of proteases in SC, such enzymes are important for the degradation of the desmosomes. For example in patients with recessive X-linked ichthyosis it was found, that due to the steroid sulphatase deficiency its substrate cholesterol sulphate accumulates in stratum corneum [62]. This promotes the degradation of the desmosomes, an extremely important step in the desquamation process [63]. Therefore the scaling abnormality in recessive X-linked ichthyosis might be attributable to an accumulation of cholesterol sulphate within stratum corneum cell membrane domains [64].

2.3   State of the art in stratum corneum research

Conventional electron microscopy studies, in which the lipid samples are dehydrated, chemically fixed and stained by ruthenium tetroxide, have demonstrated that the intercellular lipids in the SC have a lamellar organisation with a repeating pattern of approximately 130 Å, consisting of a broad–narrow–broad sequence of electron lucent bands [65, 66]. This trilamellar organisation was also called long-periodicity-phase (LPP). Further, Ohta and co-workers [67] suggested the coexistence of 50 and 130 Å phases on the basis of X-ray diffraction studies on hairless mouse SC. In contrast, other studies relying on cryo-electron microscopy of vitreous human skin reported, that the trilamellar conformation could not be observed [68]. This discrepancy could be caused by morphological changes due to ruthenium tetroxide-fixation or dehydration in conventional sample preparation for electron microscopy. In line with this, several studies reported that chemical fixation by ruthenium tetroxide, applied by Madison and co-workers [65] in order to visualise lipid structures in transmission electron microscopy, led to severe changes in the skin's nanostructure [69].

The presence of the ω-acylceramide CER[EOS] in a suitable composition of other ceramides, cholesterol and a mixture of long chain free fatty acids (FFA) is regarded to be a prerequisite for the formation of the LPP [21]. However, Bouwstra and co-workers [70] stated that the addition of FFA to mixtures of *isolated* human ceramides and cholesterol promoted to the formation of the so-called short-periodicity-phase (SPP), while only the presence of FFA to mixtures of *synthetically derived* ceramides and cholesterol caused the formation of a dominant LPP as proclaimed by de Jager and co-workers [71, 72].

As mentioned above, the existence of the 130 Å lamellar repeat patterns in SC in vivo is currently a matter of debate, comprising many pros and cons about the organisation of the LPP and the inducing or preventing conditions for its formation. Apart from some conventional electron micrographs [66], the 130 Å repeat unit has only been observed in some small angle X-ray diffraction (SAXD) studies [73, 15], while it has not been confirmed in other SAXD studies [74], in cryo-transmission electron microscopy studies on native hydrated epidermis samples [68] or in neutron diffraction studies on hydrated SC [75]. From those various experimental results it can be concluded that the detection of the 130 Å repeating pattern cannot be regarded as an evidence for the biological relevance and correct preparation of the model systems applied.

To date, a detailed picture of the molecular organisation of lipids in the SC, in particular of the function of each ceramide subclass, has not been fully elucidated. It is clear, a profound knowledge of the physical properties of the SC lipids and of their interaction is essential for a

deeper understanding of the impact of each ceramide species, as well as all other lipid species, to the barrier function of the SC. First studies on human SC tried to elucidate the lipid organisation at a healthy state and made attempts to compare it diseased skin.

Based on these studies, most prominent theoretic SC lipid models concerning the lipid assembly were proposed and are still debated vigorously [66, 76, 19, 21-23, 77, 24, 78]. In the first studies, the samples contained no well-defined lipids, native SC material was used for the investigation of the organisation of the lipid matrix. Those lipids were only characterised by their head groups and chain length distribution. In principle, the SC lipid matrices can be studies in such a way, but it is difficult to find a correlation between lipid molecular structure and the organisation and thereby, validating each of the proposed models. Nowadays, a new possibility arises, using well-defined synthetic lipids, especially ceramides with defined acyl-chain and head group architecture. SC lipid model systems, prepared from those lipids in a fixed compositional ratio, improve the knowledge about the structural organisation of such mixture [79, 80, 72, 28]. In addition, the impact of each single lipid species and the interactions between the lipids as well as the influence of external parameters such as temperature, humidity and penetration enhancer molecules can be examined on a high level. Finally, this allows a better extrapolation to the *in-vivo* situation having well-defined SC lipid model membrane systems including the possibility to study the influence of enhancer molecules on the structure of the SC lipid model membranes on a molecular level.

2.4   Theoretical models of the stratum corneum lipid matrix

During the last years, several theoretical models proclaiming a possible structural organisation of the SC lipid matrix were developed and are still a matter of debate [66, 76, 19, 21-23, 77, 24, 78]. Among them, the most important ones are the *stacked monolayer model*, the *domain mosaic model*, the *sandwich model* and the *single gel phase model*.

The *stacked monolayer model* proposed by Swartzendruber, describes a lamellar molecular arrangement for the intercellular lipid matrix of SC, characterised by interdigitated alkyl chains of the ceramides in the stretched splayed chain conformation and by cholesterol specifically distributed between different layers. This lipid organisation could contribute to the intercellular broad-narrow-broad arrangement of lucent bands reported in classical transmission micrographs [66].
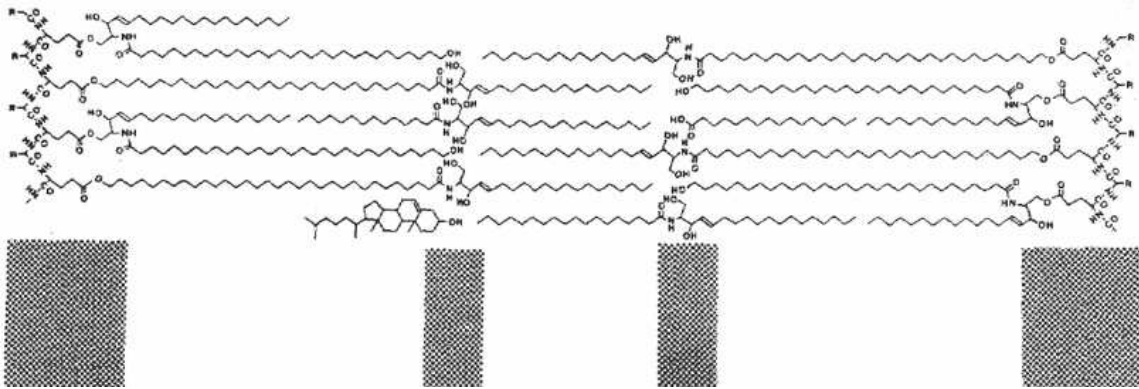
Fig. 2-5 Proposed molecular arrangement for the stacked monolayer model by Swartzendruber [66].

Forslind formulated the *domain mosaic model* [76], where the intercellular lipid matrix is treated as a multilamellar two-phase system with a discontinuous lamellar crystalline domain embedded in a continuous liquid crystalline domain. These structures are encircled by "grain borders", formed by lipids in the fluid crystalline state.
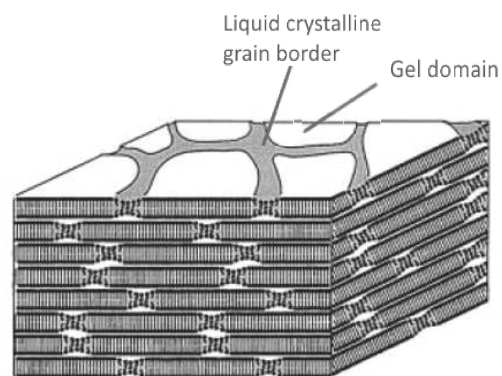
Fig. 2-6 Schematic illustration for the domain mosaic model presented by Forslind [76].

Unlike the side by side arrangement of the crystalline and liquid structures in one layer, the *sandwich model* suggested another lipid organisation [77]. The domains are located in separate layers in a trilayer arrangement, according to the broad-narrow-broad sequence of the long-periodicity-phase (LPP). The liquid sublattice is located in the central layer, formed mainly by the unsaturated linoleic moiety of the ω-acylceramides, namely CER[EOS], CER [EOP] and CER [EOH], and cholesterol. In the two neighbouring sublattices, the crystallinity increases gradually due to the presence of less mobile long-saturated hydrocarbon chains. Another feature is the small fraction of lipids constituting a fluid phase, which indicates that the central layer is a discontinuous phase.
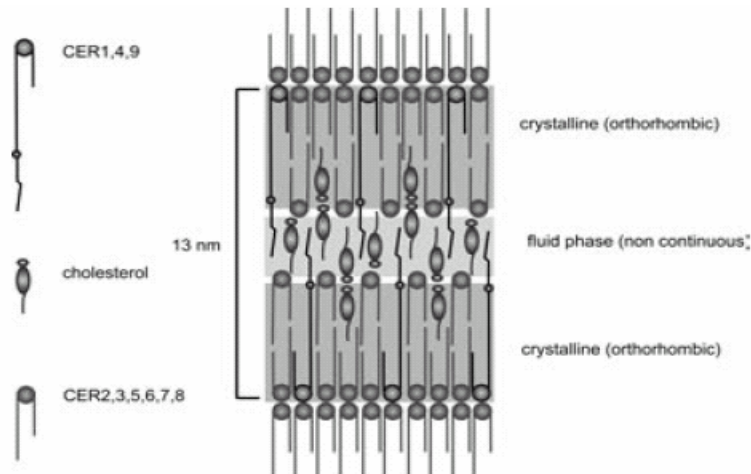
Fig. 2-7 Lipid organisation in the 13 nm lamellar phase according to the sandwich model.

The *single gel phase model* proposed by Norlén, differs significantly from the previously mentioned models and suggests, that the skin barrier is formed by a single coherent lamellar gel structure in the intercellular space of the SC [78]. The barrier structure shows no phase separation, neither between liquid crystalline and gel phases nor between different crystalline phases with hexagonal and orthorhombic chain packing, respectively. The proposed single lipid structure exhibits small water content, a low degree of mobility, and a low water permeability because of a dense-packing of the constituent lipids. Contrary to the *domain mosaic* and the *sandwich model*, where the ceramides are organised entirely in a hairpin conformation (i.e. with the two hydrocarbon chains pointing in the same direction), the *single gel phase model* Fig. 2-8 supposes both hairpin and splayed chain conformations (chains point away from a central polar head group in the opposite directions) of ceramides in the SC lipid matrix [78] (see Fig. 2-9).
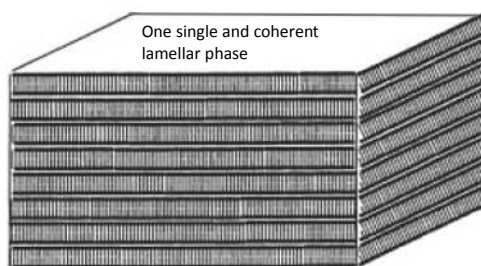
Fig. 2-8 Proposed illustration of the single gel phase model by Norlén [78].

Fig. 2-9 Possible conformation of ceramides. Left: Fully extended or splayed conformation. Right: Hairpin or on-sided conformation

Altogether, the theoretical models described above have one disadvantage. They cannot explain the structural alteration of the SC lipid matrix under hydration by water excess. Therefore, and because of the results obtained from the neutron diffraction studies [28, 81, 57] a new theoretical model to describe the structural arrangement of the SC lipid matrix was proposed by Kiselev, the so-called *armature reinforcement model* [82]. This

theoretical model of the SC lipid matrix is founded on the existence of the short chain CER[AP] molecules in the fully extended (FE) conformation [28, 82]. The phenomena of the chain flip transition of the CER[AP] molecules from the FE to the hairpin conformation was firstly described by Kiselev and co-workers [28] and further developed by him [82] to explain the of two following experimental facts:

i) the disappearance of the first diffraction order and stability of the second diffraction order under hydration in water excess of the SC isolated from the porcine skin [83], and

ii) the transformation of the long-periodicity-phase (LPP) to the short-periodicity-phase (SPP) for the case of SC extracted from human skin under hydration by water excess [15]. The main features of the *armature reinforcement model* are presented in Fig. 2-10.
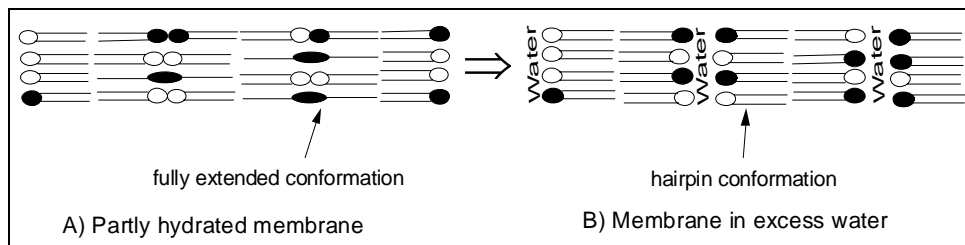
Fig. 2-10 Armature reinforcement model of the SC lipid bilayer. Transformation of SC membrane from partly dehydrated state to fully hydrated by water excess

The steric contact of the bilayer leaflets is created by the fully extended conformation of the ceramide molecules as shown in Fig. 2-10A. The introduction of excess water between the adjacent polar head groups forces the chain flip of the CER[AP] molecules from the FE to the hairpin conformation, thus creating an intermembrane space between the polar head groups (see Fig. 2-10B). In excess of water the four OH-groups of the CER[AP] molecule stabilise the hairpin conformation by forming hydrogen bonds.

From the energetically point of view the chain-flip transition is possible, as the required energy is lower when compared to the energy necessary for the flip-flop transition [84, 82]. There, the lipid molecules transverse from one part of the bilayer to the opposite part of the bilayer, while for the chain-flip transition only a chain of the ceramide molecule needs to change position. Further investigations are necessary to explicitly clarify this issue.

The results presented in this thesis further corroborate the *armature reinforcement model* and also give additional material for the debate of the importance of the short-periodicity-phase in relation to the long-periodicity-phase.

3   Fundamental concepts of the applied techniques

3.1   Differential scanning calorimetry

Differential scanning calorimetry (DSC) is a straightforward technique for the characterisation of induced changes of matter connected with changes in the energy content, in particular thermotropic phase behaviour of lipids [85]. In the DSC experiment the sample of interest and an appropriate inert reference sample are subjected to the same temperature program. As the temperature of both sample and reference increases their differential temperature remains zero ($\Delta T = 0$). If the sample undergoes a temperature-induced phase transition some part of the introduced heat is absorbed (endothermic reaction) or released (exothermic reaction). Consequently, the instrument needs to increase (or decrease) the heating energy to maintain the temperature of the sample equal to the reference. The differential or excess heat is recorded as a function of the temperature of the sample. Parameters, characterising phase transitions such as the heat of a phase transition and its temperature can be directly determined from the thermogram. The phase transition temperature can be determined by extrapolating the onset of the DSC peak, while the transition enthalpy ΔH can be determined by integrating the area under the DSC peak. The main advantage of the DSC method is that the measurements are fast and cover a wide temperature range.

DSC directly provides thermodynamic data but on a macroscopic scale. To interpret the results, information on the molecular level must be acquired by other methods. For that purpose scattering techniques such as neutron or X-ray diffraction as well as spectroscopic methods are in combination with DSC more appropriate [86].

3.2   Raman spectroscopy

Raman spectroscopy is a method for collecting vibrational spectra and is based on the interactions of molecules with electromagnetic radiation. Most photons of the monochromatic radiation scattered from an atom or molecule have the same energy (frequency) and wavelength as the incident photons (Rayleigh scattering). A small part of the scattered photons however, have a different, usually smaller frequency as the incident photons [87]. This difference in energy results in the infrared spectrum with Raman-active modes. Some of the incident photons of the monochromatic radiation transfer part of their

energy to the sample molecules, thereby initiating the excitation of molecule vibrations. The photons with now lower energy are emitted as scattered Raman radiation and the frequency (wave number) is detected. The difference between emitted scattered Raman radiation und incident radiation equates to the energy required for the excitation of the oscillation and can be assigned to the excited molecules vibrations.

A molecular vibration is Raman-active, when the vibration is accompanied by a change in the polarisability of the molecule (deformation of the electron shell of the molecule). Consequently, molecules possessing a strong dipole-character show only a small Raman scattering, while non-polar groups exhibit strong Raman-bands [88]. Therefore, Raman spectroscopy is a very suitable tool to characterise the non-polar parts of molecules, which in case of lipids comprise the degree of order and arrangement of the hydrocarbon chains [89, 90]. In principle, one differentiates between two types of vibration, one is termed *stretching* mode $\nu(CH_2)$, occurring when the molecules participate in a vibrational motion in direction of their bond, to and from each other. The second alternative, the *deformation* δ vibrations goes along with a change in the angle between two bonds.

Raman spectroscopy is a very useful tool in analysing the structure of molecules with long hydrocarbon chains [91]. In general, hydrocarbon chains in crystalline state are in a highly ordered "zig-zag" structure which contains a high number of *trans* conformers with small amounts of conformational perturbation, the *gauche* conformers. The hydrocarbon chains with *gauche*-sequences show a different vibrational behaviour compared to alkyl chains in *all-trans* conformation. For the structural characterisation different conformational sensitive Raman-bands have to be analysed for identification of the proportion of *gauche* next to *trans* conformers. Therefore, the spectral region between 2800 and 3000 cm^{-1} is examined in detail. This region consists of the symmetric and asymmetric CH$_2$ stretching vibrations [92, 93]. The position of the symmetric CH$_2$ stretching mode $\nu_s(CH_2)$ and the intensity ratio of the symmetric and asymmetric CH$_2$ stretching vibration can be used to evaluate the *gauche* to *trans*-ratio. The following rule can be applied: the lower the position of the $\nu_s(CH_2)$, the higher the content of *trans* conformers in the hydrocarbon chain [94, 95].

Furthermore, the region between 850 and 900 cm^{-1} exhibits the CH$_3$ rocking vibrations resulting from the chain ending, showing a sharp band at 890 cm^{-1} when the terminal C-C-bonds are in *trans* conformation. In contrast, a broad band positioned at 870 cm^{-1} indicates a *gauche* conformation at the chain's end [95].

Next to the chains order, conclusions about the chain packing in a crystalline subcell can be drawn from the Raman spectra [96] in the range of 1400 − 1500 cm^{-1} (CH$_2$ scissoring),

where the deformation vibrations are localised. Two arrangements of the chains can be differentiated, first, the orthorhombic or monoclinic chain packing, where two chains are packed together in a subcell and secondly, the hexagonal or triclinic chain packing with only one chain packed in the subcell. The CH_2 scissoring deformation shows a factor group splitting into three bands when orthorhombic chain packing is present, while two Raman bands of the CH_2 scissoring mode indicate a hexagonal chain packing [97].

3.3   Basic principles of neutron scattering

Neutron scattering is a particularly powerful tool for the investigation of biological relevant material. It can disclose structural and dynamical features, which are difficult to detect with other scattering techniques such as X-ray diffraction. In contrast to X-rays, which primarily interact with the electrons of an atom, the interaction of neutrons with the atomic nucleus is short-ranged. Therefore, neutrons are able to penetrate deeply into condensed matter. Furthermore, they are able to distinguish between different isotopes of the same element due to the different atomic mass of the isotopes nucleus. This difference in the scattering ability or contrast between various elements (particularly deuterium and hydrogen) is the main concept of neutron scattering and the main benefit for the investigation of biological samples [98-100].

Neutrons are uncharged elementary particles with a mass of $m=1.675 \cdot 10^{-27}$ kg and they exhibit a wave-like behaviour, whereby its wavelength λ is defined by

$$\lambda = \frac{h}{\vec{p}} = \frac{h}{m \cdot \vec{v}}$$

(3.1)

with h being the Planck's constant, while $\vec{p}$ is the momentum and $\vec{v}$ the velocity of the neutron particle. The wavelength used for the structure analysis of material is typically in the range of Å, the same order of magnitude as most interatomic distances. The neutron's momentum $\vec{p}$ is given by

$$\vec{p} = \hbar \cdot \vec{k} \, ,$$

(3.2)

with the Planck's constant combined to $\hbar = h / 2\pi$ and the neutron wave vector $\vec{k}$ defined as $\left| \vec{k} \right| = 2\pi / \lambda$.

In the scattering experiment a well collimated neutron beam with a defined wavelength λ irradiates a sample, whereby the neutrons are scattered in all directions depending on the interactions between the sample material and the neutrons. Therefore, when neutrons

interact with matter they undergo a change in momentum, meaning that the neutrons change direction and/ or velocity. Therefore, the structure and the dynamics of this matter can be determined by the measured changes in the energy and the momentum of the scattered neutrons. The change in momentum can be expressed by a momentum transfer vector, or *scattering vector* $\vec{Q}$, which is defined as the difference between incoming $\vec{k}_i$ and scattered $\vec{k}_s$ wave vectors:

$$\vec{Q} = \vec{k}_i - \vec{k}_s \tag{3.3}$$

In addition to a change in direction, the magnitude of $\vec{k}$ can also change as energy is transferred between incident neutrons and sample. As the law of energy preservation has to be followed, this can be expressed as

$$\Delta E = E_0 - E_1 = \hbar^2 \frac{\vec{k}_i^{\;2}}{2m} - \hbar^2 \frac{\vec{k}_s^{\;2}}{2m} \tag{3.4}$$

The scattering process is totally elastic when $\Delta E = 0$ therefore, $\left|\vec{k}_i\right|$ must be equal to $\left|\vec{k}_s\right|$. Transferring this to Eq. (3.3) the equation can be written as

$$\vec{Q} = 2\vec{k}_i \cdot sin\,\theta \tag{3.5}$$

with θ being the Bragg angle, which for crystalline materials appears at $\vec{Q}$-values equal to the reciprocal lattice spacing as

$$\left|\vec{Q}\right| = \frac{2\pi}{d} \tag{3.6}$$

with d being the characteristic spacing of a set of crystal planes. Carrying out the appropriate substitution with $\vec{k}_i = 2\pi/\lambda$ results in the Bragg formula:

$$\lambda = 2d \cdot sin\,\theta \tag{3.7}$$

For better understanding the difference between the terms "scattering" and "diffraction" has to be explained. Scattering results from the interaction of radiation with matter. In case the investigated material does not show a geometrical organisation, as in the case of a homogeneous dispersion of particles, the scattered wave traverse different distances, therefore, their relative phases are different. The data received in such a scattering experiment permits conclusions about the interaction of individual particles, their shape and size.

Diffraction on the other hand can be considered as a special type of scattering, whereby an organised structure such as a crystal is analysed. According to the Braggs law the

incident beams are diffracted at a defined angel 2θ, the diffraction occurring due to the interference between the waves scattered from the parallel planes (see Fig. 3-1).
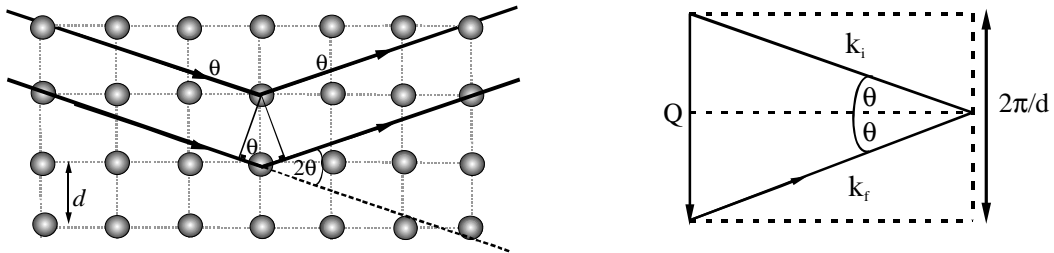
Fig. 3-1 Schematic presentation of the scattering process.
Left: Neutrons strike an array of atoms (spheres) from the left side and are scattered to the right. The planes of atoms separated by the distance d. The angle θ to the plans of atoms of the incident and the scattered beam are identical. *Right*: Change in the neutron's momentum Q. When Q points along the reciprocal lattice of the spacing $2\pi/d$, the Bragg condition for diffraction is met. The constructive interference leads to a diffraction peak (Bragg maximum)

The neutron scattering experiment now measures the scattering intensity I as a function of the scattering direction, the interpretation of the data offers information about the structure of the analysed sample. The incident neutron beam is often a plane wave ψ_i (in case of single, fixed nucleus), while the resulting scattered wave ψ_s is spherical and proportional to the scattering length b. The scattering length b is the measure of the scattering ability of the atomic nucleus, with the dimensions of length and is regarded as a real and known constant for a nucleus or isotope. The basic geometry of the scattering process is depicted in Fig. 3-2.
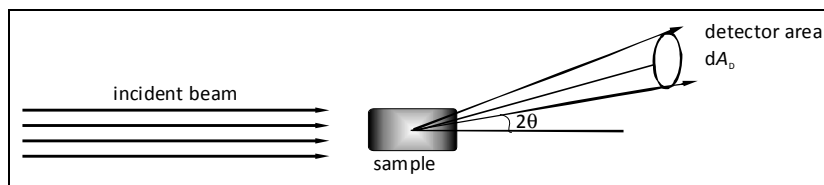
Fig. 3-2 Geometry of the scattering process depicting the incident plane wave, the sample, the spherical wave and the detector

In a typical neutron scattering experiment the number of scattered neutrons in a particular direction are counted, without regard to changes in the energy. The neutron flux which reaches the detector area is measured for a suitable time period. The spatial distribution of the neutron flux is called differential cross section which contains information about the *scattering length density* (SLD) of the sample. The amplitude of the scattered neutron wave is the so-called structure factor (SF).

3.3.1   Application of neutron diffraction for the investigation of stratum corneum lipid model membranes

All measurements were carried out using the membrane diffractometer V1 at the Berlin Neutron Scattering Centre of the "Helmholtz Zentrum Berlin für Materialien und Energie" (Berlin, Germany) with a cold source and a neutron wavelength λ of 5.23 Å. A two-dimensional position sensitive ^{3}He detector with a sensitive area of 19 cm x 19 cm and a pixel size of 1.5 mm x 1.5 mm was used. The distance from sample to detector amounted to 102.4 cm. For the measurement of the SC lipid model membranes the reflection setup was used to collect the data of the one-dimension diffraction experiment. A basic sketch of the scattering geometry is presented in Fig. 3-3.
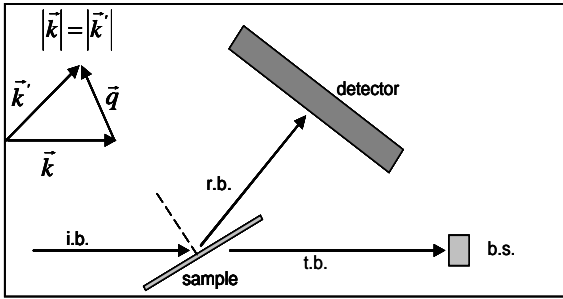
Fig. 3-3 Sketch of experiment geometry, whereby *i.b.* is incident beam, *r.b.* is reflected beam, *t.b.* is transmitted beam, while *b.s.* is beam stop. $\vec{k}$ and $\vec{k}'$ are the wave vectors of the incident and reflected neutrons, respectively, while $\vec{Q}$ assigns the scattering vector.

According to the standard diffraction notes, 2θ is the angle between the direction of the incident beam (transmitted beam) and the reflected beam, which is same as the angle between the vectors $\vec{k}$ and $\vec{k}'$ (see Fig. 3-3). An elastic scattering process was considered $\left|\vec{k}\right| = \left|\vec{k}'\right|$, thus the absolute value of the scattering vector $\vec{Q}$ (momentum transfer) can be written as

$$Q = \frac{4\pi \cdot sin(\theta)}{\lambda} \tag{3.8}$$

The integrated intensity of the diffraction peak depends on the number of layers N in the lipid film and is proportional to N^2. The width of the diffraction peak Δq depends on the resolution of the instrument Δq_1 and sample mosaicity Δq_2. The mosaicity of the sample is a property of mixed lipids and a result of the sample preparation, whereas the resolution of the instrument depends on the monochromator quality (Δλ/λ≈0.01), the angle resolution of the detector $\Delta\theta = \dfrac{\Delta x_d}{L_{sd}}$, and Bragg's angle θ

$$\frac{\Delta q_1}{q_1} = \sqrt{\left(\frac{\Delta\lambda}{\lambda}\right)^2 + \left(\frac{\Delta\theta}{\theta}\right)^2} \tag{3.9}$$

Prior to the measurements samples were thermostated in aluminium cans in which temperature and the humidity was controlled. This procedure is described in detail elsewhere [101]. The variation of the difference of the scattering length density in the chamber (neutron contrast) was achieved by adjusting the chamber atmosphere up to four different H_2O/ D_2O compositions (92/ 8, 80/ 20, 50/ 50 and 0/ 100, w/w) in order to facilitate the assignment of the phases [102]. The sample was equilibrated for 12 hours after each change of aqueous solution prior to the measurement.

The diffraction intensities of each sample were recorded either as $\theta - 2\theta$ -scan (high mosaicity samples), or as rocking scan (ω-scan), whereby the sample was rocked around the expected Bragg position θ, by $\theta \pm 2°$. Both ways allowed the collection of up to five orders of diffraction. Before the collection of the diffraction data, the rocking curve was checked. A Gaussian-type rocking curve is evidencing a one-dimensional crystal. Two examples are illustrated in Fig. 3-4, where the left rocking curve (A) belongs to a sample with low mosaicity, which is suitable for a rocking scan. Fig. 3-4B, on the other hand demonstrates a sample with high mosaicity, for which the diffraction intensity could only be recorded as $\theta-2\theta$ -scan.
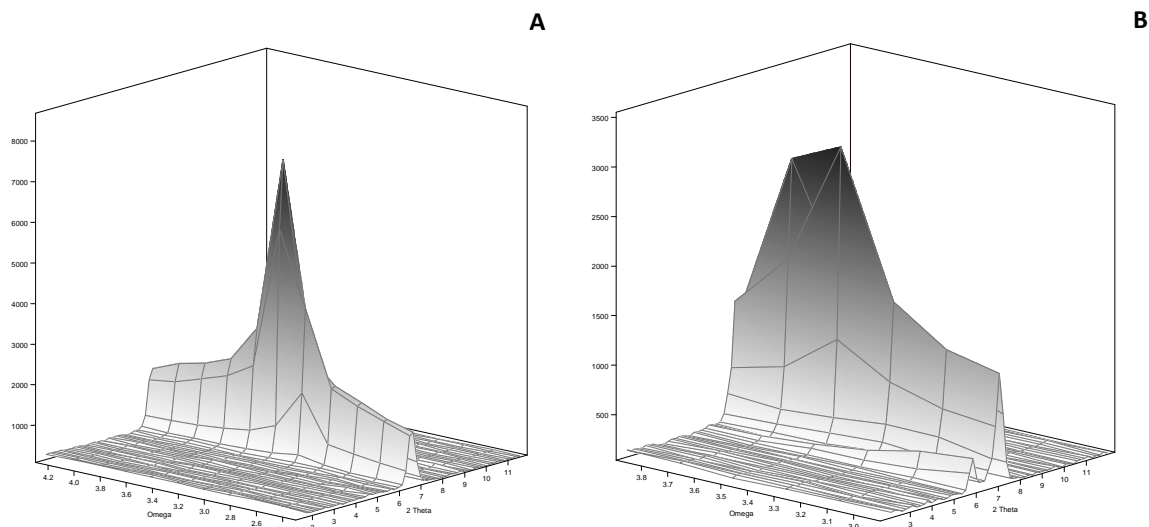
Fig. 3-4 Rocking curve around a fixed angle 2θ to verify the mosaicity of the sample.
A) Example for a sample with a low mosaicity which allowed recording of a rocking scan around the expected Bragg position.
B) Illustration of a sample with a high mosaicity for which the diffraction intensities could only be recorded as a $\theta - 2\theta$ -scan.

3.3.2   Evaluation of the neutron diffraction data

In the neutron diffraction patterns, the scattering intensity I (in arbitrary units, a.u.) was measured as a function of the scattering vector Q (in reciprocal Å), according to (3.8). The integrated intensities were calculated using Gaussian fits to the received Bragg

reflections. From the integrated peak intensity the absolute value of the structure factors (SF) was calculated as

$$\left| F_h \right| = A_h(\theta) \cdot \sqrt{h \cdot I_h}$$

(3.10)

with Lorentz correction h and absorption factor $A_h(\theta)$, whereby the absorption factors were calculated according to Eq. (3.11) [102]:

(3.11)

$$A_h(\theta) = \left[\frac{\sin\theta}{2\mu L} \cdot \left(1 - \exp\left(-\frac{2\mu L}{\sin\theta} \right) \right) \right]^{-\frac{1}{2}}$$

with μ being the linear absorption coefficient, calculated for $\lambda = 5.23$ Å to $\mu = 6.1$ cm^{-1} [28], and the thickness L of the lipid film, which amounts to $L = 7.5$ µm.

Bimolecular lipid membranes composed of two equal monolayers facing each other are centrosymmetric bilayers, for which the sign of the structure factor can be determined by isotopic substitution of H_2O by D_2O (contrast variation) [103] and assuming the penetration of water into the bilayer [104, 102]. For such symmetrical and hydrated bilayers it was shown, that the phase problem of the SF simplifies to the determination of the sign of + or − [102]. The sign of the structure factor was derived from the slope of the correlation of F_h against the D_2O content in water vapour as shown in Fig. 3-5.
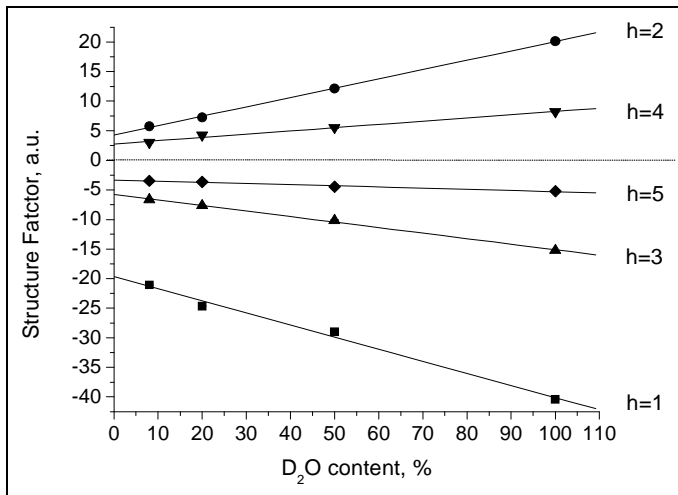
Fig. 3-5 Example of the dependency of the membrane structure factor F_h of the orders h=1, 2, 3, 4 and 5 on the D_2O content in water vapour a SC lipid system composed of CER[AP]/CHOL/ BA/ChS (57/24/9.5/9.5, w/w) at 20°C and 57% RH.

The nanostructure of the bilayer was conventionally analysed by the construction of the neutron scattering length density profile $\rho_s(x)$ across the bilayer as Fourier synthesis according to Nagle and Tristam-Nagle [105]:

(3.12)

$$\rho_s(x) = a + b \frac{2}{d} \sum_{h=1}^{h_{max}} F_h \cos\left(\frac{2 \cdot \pi \cdot h \cdot x}{d} \right)$$

whereby F_h stands for the scaled structure factor of the order h. The function $\rho_s(x)$ describes the distribution of the scattering length density (SLD) across the bilayer, whereby d expresses the length of the unit cell. The SLD across the bilayer $\rho_s(x)$ is calculated in arbitrary units due to the unknown values of *a* and *b* [105], consequently the profiles are presented in arbitrary units but on the same scale. The reason for this presentation is the large error which would result in using the absolute scaling method. The determination of the absolute scale (or more precisely the relative absolute scale as defined by Wiener and White [103]) relies on the knowledge of the number of water molecules per lipid. With this information the difference density of e.g. profile measurements at 8% D_2O and 50% D_2O can be placed on an absolute scale. In the case of the investigated stratum corneum model membranes the intermembrane space was determined to approx. 0.1 nm [28]. With a head group area of 0.3 nm^2 (between pure ceramide (0.25 nm^2) and cholesterol (0.37 nm^2)) the space for one water molecule can be calculated with a volume of 0.03 nm^3. But this estimation suffers from many obstacles such as the error to the intermembrane space of 30%, ranging from 0.7 nm to 1.3 nm, not well-defined area per lipid ranging from 0.4 nm^2 to 0.2 nm^2 (an estimation from Dahlen and Pascher [106]), and it is not well justified, if the water volume of 0.03 nm^3 or a smaller one more close to the van der Waals volume of 0.0146 nm^3 is used. Alternatively, it is possible to determine the water content gravimetrically. But with the low water content of ceramide-based membranes the difference in weight between a dry and a hydrated sample is very small. All together, the calculation of the absolute scale provides results with an exceedingly large error, which will render it useless.

3.3.3   Localisation of a deuterium label

The localisation of a specific deuterium label within a lipid membrane is reflected by the positive difference in the scattering length density (SLD) profile between samples containing the deuterated and protonated lipid. According to Eq. (3.13) the difference was calculated for each structure factor:

$$\Delta F_h^{deut} = F_h(\,deut\,) - F_h(\,prot\,) \qquad\qquad (3.13)$$

The difference SLD profile can be calculated by substituting the structure factor F_h by ΔF_h^{Deut} in Eq. (3.12) [107-109].

The SLD maxima resulting from the deuterated groups can be fitted using either one Gaussian function in case of one maximum or with two identical Gaussian functions using Eq.

(3.14), when two centrosymmetric maxima are present. Thereby the exact position of the deuterated label (x_1 and x_2) is available.

$$\rho^{sym}(x) = \frac{A}{\sqrt{2\pi\sigma}}\left\{exp\left[-\frac{1}{2}\left(\frac{x-x_1}{\sigma}\right)^2\right] + exp\left[-\frac{1}{2}\left(\frac{x-x_2}{\sigma}\right)^2\right]\right\}$$ (3.14)

3.3.4 Truncation errors of the Fourier synthesis

The full Fourier transformation from reversed space to direct space requires the knowledge of the structure factors for the diffraction orders h from zero to infinity. In the experiment only a limited number of diffraction peaks can be acquired resulting in a very limited set of structure factors. The application of such a limited number of summands in Eq. (3.12) causes the truncation errors in the application of Fourier transformation to the experimental data. The deviation of the calculated values of the scattering density from the real density distribution shows mainly two effects: the resolution is diminished and at the edges of a sharp density change additional oscillations as artefacts are produced. To estimate the influence of the truncation errors Kiselev and co-workers [110] compared a periodic step function $\rho(x)$ with its Fourier image $\rho_{im}(x)$. In this model calculation assumed relative variables have been used which are comparable to the variables available from the neutron diffraction experiment. Fig. 3-6 represents such a periodical step-function $\rho(x)$ and its Fourier image $\rho_{im}(x)$, which was synthesised on the basis of five structure factors ($h_{max} = 5$) as

$$\rho_{im}(x) = \frac{F_0}{d} + \frac{2}{d}\sum_{h=1}^{h=5} F_h \cdot cos\left(\frac{2\cdot\pi\cdot h\cdot x}{d}\right),$$ (3.15)

with the structure factors F_h given by:

$$F_h = \frac{d\cdot\Delta\rho}{\pi\cdot h}sin\left(\frac{\pi\cdot h}{2}\right)$$ (3.16)

and with

$$F_o = \frac{d\cdot\Delta\rho}{2}$$ (3.17)

whereby $\Delta\rho = 2$ and $d = 6$ are relative values used for the model calculation (see Fig. 3-6). As can be seen in Eq. (3.17) the amplitude of the harmonic functions is proportional to the value of $\Delta\rho$. Higher harmonics create the main part of the truncation errors near the sharp boundaries as seen in Fig. 3-6.
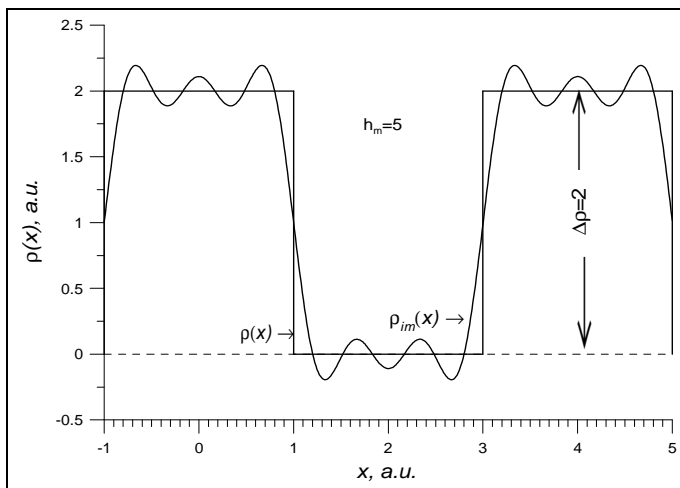
Fig. 3-6 Truncation errors of the Fourier synthesis based on 5 diffraction orders as described in Kiselev et al., 2006 [110]. The step function $\rho(x)$ is an example of neutron length density profile. The term $\rho_{im}(x)$ is the Fourier synthesis model of the periodic step function $\rho(x)$ based on 5 diffraction peaks.

The truncation errors were considered as the difference between the real $\rho(x)$ step-function and experimentally obtained scattering length density $\rho_s(x)$, which was obtained after the Fourier synthesis.

Limited space resolution allows distinguishing two different molecular groups in the experiment *only* if the distance Δx between these groups is equal or larger then:

$$\Delta_{FS} = \frac{3.8 \cdot d}{2\pi \cdot h_{max}} \approx 0.6 \frac{d}{h_{max}} \tag{3.18}$$

where Δ_{FS} is the space resolution of the Fourier synthesis and d is the membrane repeat distance [28]. The differences in the value of $\rho(x)$ and $\rho_s(x)$ at a given value of x are such truncation errors due to the limited number of diffraction peaks received in the experiment. The truncation errors near the sharp boundary are proportional to the value of the boundary density contrast $\Delta\rho$. In neutron diffraction experiments on hydrated lipid membranes, the value of $\Delta\rho$ (value of contrast) can be varied by increasing the D_2O content in the water vapour. Thus, increasing of the contrast could increase the value of truncation errors of the Fourier synthesis at a fixed space resolution.

3.4   Preparation of the SC lipid model membranes for the neutron diffraction experiment

The samples for the neutron diffraction experiment were prepared as a stack of oriented multilamellar membrane layers from lipid solution. In order to produce a lipid mixture with a total lipid concentration of 10 mg/ml the appropriate quantity of each lipid species was dissolved in a chloroform:methanol mixture (2:1, V/V). To create multilamellar SC

lipid membranes a volume of 1200 µl of this solution was spread over the surface of a quartz slide with the dimensions of 6.5 cm × 2.5 cm according to the procedure by Seul and Sammon [111]. After the depositing, the organic solvent was removed by evaporation firstly at atmospheric pressure, then under vacuum. Afterwards a subsequent heating (at 75°C) and cooling cycle at 100% relative humidity (RH) was applied to decrease the mosaicity of the samples.

This annealing procedure improved the signal-to-noise ratio in the neutron diffraction experiment and was essential for the further analysis of the received data. The benefit of the annealing procedure for the a model membrane based on CER[AP] is demonstrated in Fig. 3-7, whereby the rocking curve of the model membrane before the annealing procedure was performed is presented in Fig. 3-7A, while Fig. 3-7B displays the rocking curve of the same sample after the heating and cooling cycle was performed.

The main goal in the sample preparation is to create a one-dimensional liquid crystal with approximately 1600 membrane layers and a mosaicity about 0.1 degree. From such well oriented samples up to 4-5 diffraction orders are detectable in the neutron diffraction experiment, which allows the application of the Fourier analysis for the synthesis of the neutron scattering length density across the membrane. For many years this technique has been used for the characterisation of phospholipid membranes [104, 103].
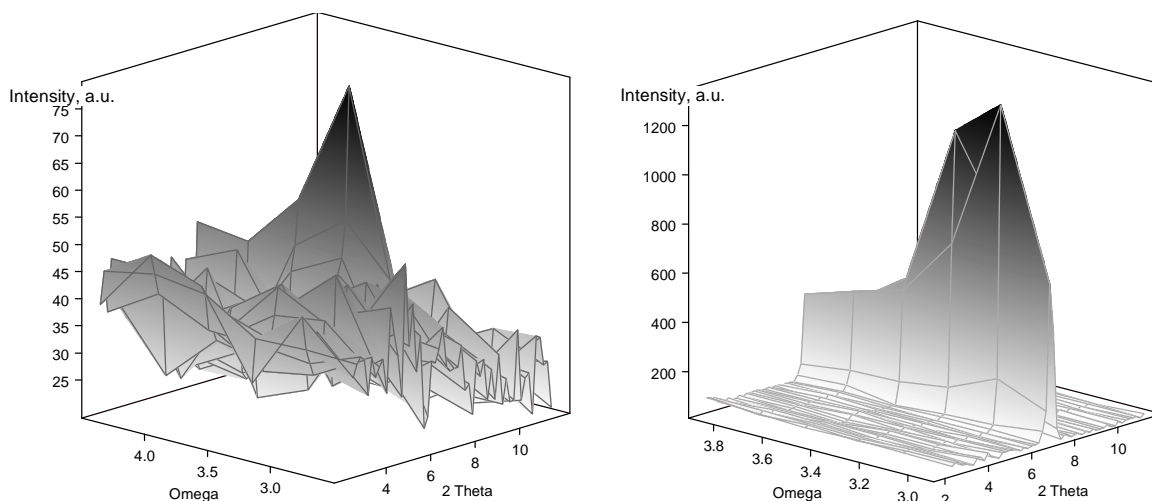
Fig. 3-7 Rocking curve around a fixed angle 2θ to verify the mosaicity of the sample composed of ceramide [AP]/ cholesterol/stearic-d$_{35}$-acid/cholesterol sulphate. The intensity scale is normalised to the intensity of the primary beam (50000 Monitor counts/ step).
(Right) Example for a sample with high mosaicity and low intensity before the annealing procedure was performed.
(Left) Illustration of the same sample after heating at 75°C and cooling at 100% RH.

4   The role of the free fatty acids in the structure of stratum corneum model membranes based on ceramide [AP]

4.1   Introduction

It is assumed, that the permeability of the SC intercellular lipid matrix is largely determined by the lipid organisation, which therefore depends to a great extent on the lipid composition [76, 112]. In particular, the influence of the free fatty acids (FFA) on the structural organisation is of interest, as the FFA have the only ionisable head group aside of small amounts of cholesterol sulphate, this may be important for the formation of lamellae. In addition, Bouwstra and co-workers found that inclusion of FFA in SC lipid model membranes composed of ceramides mixtures and cholesterol resulted in orthorhombic chain packing, whereas in their absence the chain were packed in a hexagonal subcell [70]. Further, the presence of FFA is also regarded to be crucial for the formation of the long-periodicity-phase (LPP) [71]. Therefore, it can be assumed that the FFA are an important determinant for the nanostructure of the SC intercellular lipid matrix.

The presented study describes the influence of the free fatty acids chain length to a SC model membrane composed of the main lipids found in the SC. The chain length of the FFA used ranged from stearic acid (SA) with 18 carbon atoms to cerotic acid (CA) with 26 C-atoms. The neutron and X-ray diffraction investigations were carried out on oriented multilamellar membranes. A model membrane system containing a realistic mixture of different FFA cannot give detailed information on the influence of *each* FFA species and does not provide any indication about the influence of the chain length of the FFA to the structure of such SC lipid model membranes. In experiments performed by Kiselev and co-workers unique information was obtained with model membranes based on CER[AP] containing palmitic acid [28]. Therefore, the variation of the FFA chain length in this model membrane can give precise information about structural role of *each* FFA used.

4.2   Materials and methods

4.2.1   Materials and sample preparation

The SC lipids used for the model preparation were ceramide [AP] (CER[AP]), stearic acid, docosanoic acid (further referred as behenic acid), tetracosanoic acid, hexacosanoic acid (further referred as cerotic acid), as well as cholesterol and cholesterol sulphate (see Appendix A). Quartz slides (Spectrosil 2000) were obtained from Saint-Gobain (Wiesbaden, Germany).

4.2.2   Sample Preparation

The SC model membranes were studied in four different compositions, however only the FFA was changed as shown in Table 4.1.

Table 4.1 Composition of the quaternary system for the SC model membrane based on CER[AP]. The SC model membrane was always composed of CER[AP]/CHOL/FFA/ChS. Only the FFA component was varied.

Mixture	Free fatty acid (FFA)	Component ratio (w/w) (CER[AP]/CHOL/FFA/ChS)
QuatSA	stearic acid (SA)	55/25/15/5
QuatBA	behenic acid (BA)	57/24/9.5/9.5
QuatTA	tetracosanoic acid (TA)	55/25/15/5
QuatCA	cerotic acid (CA)	55/25/15/5

The ratio of the lipids chosen was similar to the ratio of ceramide, cholesterol and FFA found in the native SC [61] and to the composition used by Wertz and co-workers [113] as well as Hatfield and Fung [114]. The preparation of each SC lipid model membrane was performed as described in Chapter 3.4.

4.2.3   X-Ray diffraction measurements

The X-ray diffraction patterns were collected using the Stoe Stadi MP Powder diffraction system (STOE & Cie GmbH, Darmstadt, Germany) in the Bragg-Brentano high resolution mode with a linear position sensitive detector. The samples were measured in vertical position at room temperature and room humidity.

4.2.4   Neutron diffraction measurements

In the experimental setup the diffraction intensities were recorded either as

   a) $\theta - 2\theta$ -scan (high mosaicity samples), or as

   b)   rocking scan (ω -scan), whereby the sample was rocked around the expected Bragg position, θ, by $\theta \pm 2°$. This allowed the collection of up to five orders of diffraction.

All measurements were carried out at T = (20 ± 0.1)°C and 57% relative humidity (RH) after 12 hours of equilibration in above mentioned thermostated chamber.

4.3   Results and discussion

4.3.1   SC lipid model membranes including behenic acid

The SC model membranes based on CER[AP] containing behenic acid (BA, 22 C-atoms) as the FFA component exhibit a mosaicity inferior to 0.11 degrees, which is similar to membranes based on palmitic acid (mosaicity 0.12 degree) [28]. Five orders of diffraction peaks could be collected. Fig. 4-1 represents the diffraction pattern of the SC model membrane containing behenic acid.
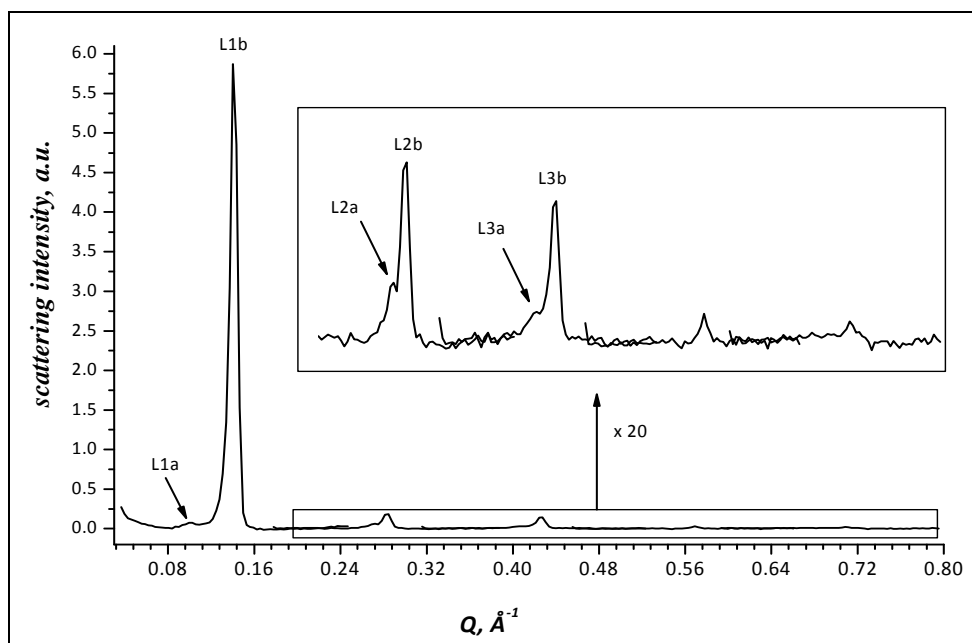
Fig. 4-1 Diffraction pattern for the quaternary SC model membrane composed of CER[AP]/CHOL/BA/ChS (57/24/9.5/9.5, w/w) measured at 5 different detector angles (6.7, 13.4, 20.1, 26.8, 33.5°), at 57% RH, 8% D_2O and 20°C. Up to 5 orders of diffractions are visible. The orders 2 to 5 are zoomed by a factor of 20 to the right intensity scale. For the small phase (a) and the main phase (b) the 1st, 2nd and 3rd diffraction orders have been indicated, respectively.

Membranes containing palmitic acid as the FFA component exhibit only one phase at 57% relative humidity (RH) and room temperature, a second phase appears at a temperature of 81°C and an increased relative humidity of 97% [28]. In contrast, the membranes containing BA, two phases already coexist at 20°C and 57% RH as seen in Fig. 4-1, where the first diffraction peak exhibits a small shoulder. The scattering intensity of the phases differed significantly, consequently, the notation of the phases was made according to their scattering intensity: left phase was labelled as small phase (smaller scattering intensity) and the second phase was assigned as main phase, because it exhibits the main scattering intensity. The membrane repeat distance d was determined for each phase from the position of the a series of equidistant peaks. For the small phase it amounts to d_1 = (45.5 ± 0.3) Å and for the main phase d_2 = (44.00 ± 0.02) Å.

For each phase the calculations of the scattering length density (SLD) profiles were done separately in order to make a comparison of the nanostructure and to analyse the differences between both phases. Fig. 4-2 represents the SLD profiles of the small phase at 8, 20, 50 and 100% D_2O, respectively. The left and right maxima in the profiles are related to the hydrophilic head groups of the bilayer.
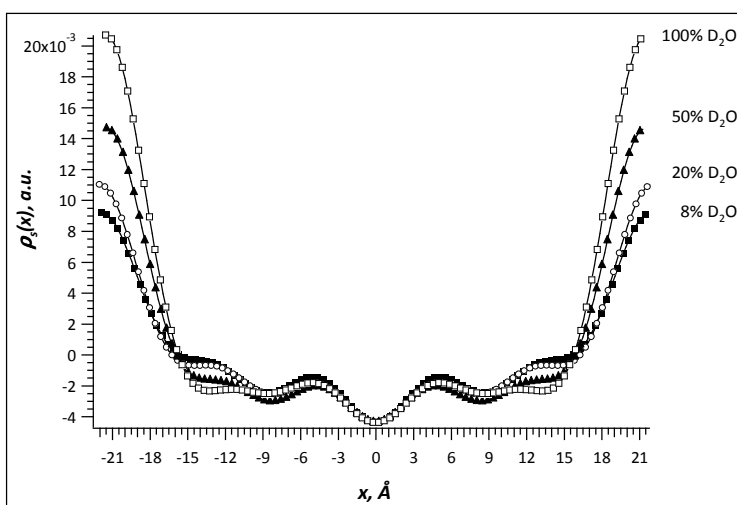
Fig. 4-2 The neutron SLD profiles of small phase of the SC model membrane composed of CER[AP]/ CHOL/BA/ChS (57/24/9.5/9.5) at different D_2O contents (8, 20, 50 and 100%), measured at 57% RH and 20°C.

The SLD in the region of the polar head groups increases with increasing D_2O concentration because the D_2O molecules are able to penetrate into the hydrophilic region. The lower values of $\rho_s(x)$ within the profiles resemble the hydrophobic inner part of the membrane, that is, the hydrocarbon chains of the lipids, which consist of methylen and methyl groups. The density profile in this region should not be influenced and the small changes see in Fig. 4-2 are due to truncation errors of the Fourier synthesis. Maximum truncation errors exist at 100% D_2O due to the greatest difference in the scattering density between the hydrated polar head groups and the hydrophobic region. The origin of this

problem is presented and explained in detail in Chapter 3.3.4. In contrast to the SLD profile of the small phase, the SLD profile of main phase (Fig. 4-3) does not show such pronounced truncation errors because the scattering intensity of the first order diffraction peak for the main phase is sufficiently larger relative to the small phase. The consequence is a better signal to noise ratio. Both profiles show no principal differences in the internal alignment of the lipid molecules.
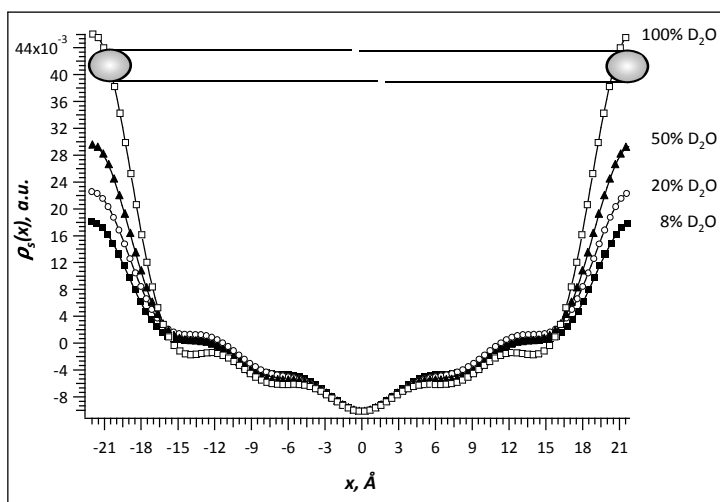
Fig. 4-3 The neutron SLD profile of main phase of the SC model membrane composed of CER[AP]/CHOL/BA/ChS (57/24/9.5/9.5) at different D_2O-contents (8, 20, 50 and 100%), measured at 20°C and 57% relative humidity. A pair of CER[AP] molecules has been added, for better orientation.

From the SLD data it is also possible to assign the position and orientation of the bilayer constituents. The model of the SC membrane structure based on polar head groups, CH_3 groups, hydrocarbon chain region, and the region of cholesterol location was proposed by Kiselev and co-workers [28]. For more precise determination of the position of the aliphatic groups, parts of the density profile were fitted by Gaussian functions. Four functions were used for the fitting and characterisation of the four different groups within the bilayer. For the position of the methyl group only one Gaussian function is required as this group is centred at $x = 0$. As those bilayers are centrosymmetric it is possible to fit the polar head groups and the methylen chains as well as the position of the cholesterol molecules in the bilayer using Eq. (3.14). The fit resembles the area A and the standard deviation σ.

In Fig. 4-4 the neutron SLD profile, in addition to the results of the fit for each group are displayed for the main phase.
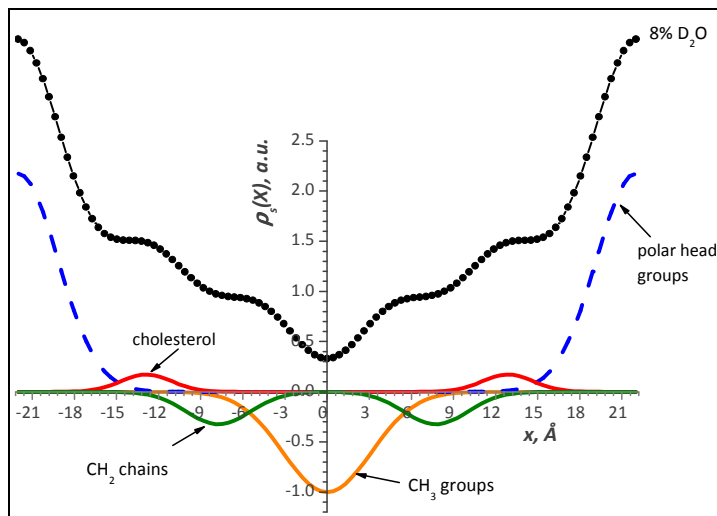
Fig. 4-4 Model calculations of the neutron SLD profile of main phase of SC lipid system containing behenic acid.

The fitted curves for each group are: polar head groups (blue dash); CH$_2$-groups (green), CH$_3$-groups (orange), cholesterol (red).

The thickness of the polar head group region equals $FWHH/2$, where full width at half height *(FWHH)* is given by Eq. (4.1) [115].

$$FWHH = 2 \cdot \sigma \sqrt{2 \cdot ln\, 2}$$

(4.1)

For the small phase the same fitting procedure of the SLD profile was applied (Appendix B, Fig. B 1).

For both phases the parameters taken from the fit differ only marginally due to experimental errors. As a consequence, although the small phase and the main phase show different repeat distances, the structural alignment of the lipids within both phases is similar. Therefore, the difference in the thickness of the membrane between small phase and main phase is due to a different composition of the lipids inside both phases.

In contrast to phospholipids, a SC lipid model membrane based on ceramide [AP] does not show a region of intermembrane space ,as described by Kiselev and co-workers [28]. As illustrated there, the membrane repeat distance d is equal to the distance between the two maxima of the polar head groups d_{PH}. Therefore, the polar head groups of the adjacent leaflets are arranged very close to each other. This is also the case for both phases of the model membrane containing behenic acid. The thickness of the intermembrane space of such membranes amounts to approximately zero at 57% RH. The region which is hydrated by the water molecules is very small, therefore the intermembrane space of such model membranes is not suitable for lateral water diffusion in addition to the lateral diffusion of drugs. This can be a reason for the low penetration rates of drugs through the stratum corneum. On the other hand, the results presented by Kiselev and co-workers on a similar system [28] show, that lamellar diffusion of water and water soluble drugs is preferred relative to lateral diffusion because hydration of the internal part of the bilayer appears to be very similar to that of phospholipids

The dependence of the SLD profile on the D_2O content in water vapour enables the calculation of the water distribution function ρ_w across the bilayer as the difference between the neutron SLD at high D_2O concentration (50 and 100%) and 8% D_2O in water vapour according to Eq. (4.2a) and (4.2b). For both phases calculation were done. The result for the main phase is presented in Fig. 4-5.

$$\rho_{w_1} = \rho_{100\% D_2O} - \rho_{8\% D_2O} \qquad (4.2a) \qquad \rho_{w_2} = \rho_{50\% D_2O} - \rho_{8\% D_2O} \qquad (4\text{-}2b)$$

In order to prove the accuracy of this method the difference between 100 and 8% D_2O was compared with the difference between 50 and 8% D_2O. The comparison of both calculated values gave an accuracy of 0.2 Å for the method used.
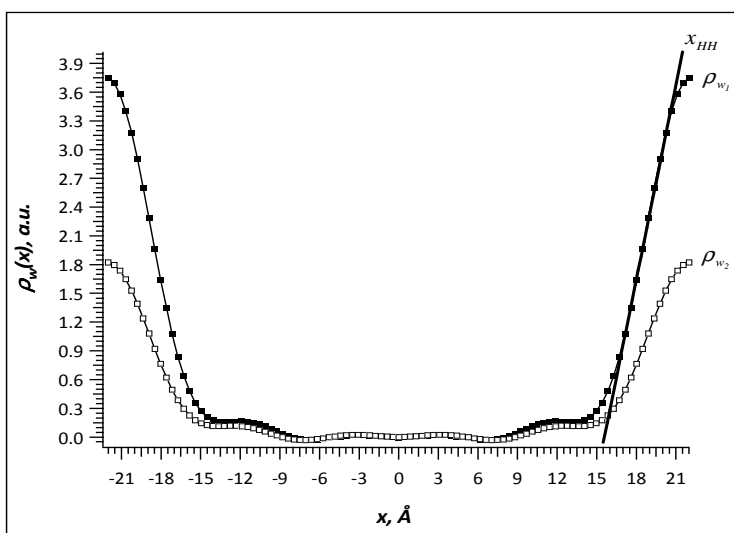
Fig. 4-5 Water distribution function $\rho_w(x)$ of main phase across the CER[AP]/CHOL/BA/ChS membrane. The *HH* boundary is determined via linear fit as demonstrated here.

Again, the small phase exhibits the same water distribution function as the main phase (Appendix B, Fig. B 2), which further underlines the conclusion, that both phase do not show a difference in the structural alignment of the lipids, but rather a different composition of the lipids.

A lipid membrane can be divided into two parts, namely the hydrophilic and hydrophobic region. Thus, the boundary between both regions can be described as hydrophilic-hydrophobic (*HH*) boundary and is located at the position x, where the water distribution function ρ_w deeply decreases to zero. The *HH* boundary determines the thickness of the hydrophilic part of the bilayer.

The position of the *HH* boundary, determined by extrapolation of a linear fit, is summarised in Table 4.2 for each phase.

Table 4.2 Structural parameters for each phase of the membrane containing behenic acid at 20°C, 8% D_2O and 57% RH.

Membrane with BA	$d = d_m$, Å	x_{PH}, Å	x_{HH}, Å	Thickness of hydro-phobic layer, Å	Thickness of hydro-philic layer, Å
small phase	45.5 ± 0.3	22.74	17.0 ± 0.3	34.0 ± 0.6	5.7 ± 0.3
main phase	44.0 ± 0.02	22.00	15.7 ± 0.3	31.4 ± 0.6	6.3 ± 0.3

d ... repeat distance, d_m ... membrane thickness, x_{HH} ... hydrophilic-hydrophobic boundary, x_{PH} ... position of polar head groups

4.3.2   Incorporation of stearic acid in a SC lipid model membrane

The model membrane containing stearic acid (SA) as the FFA component was also characterised by neutron diffraction. Comparable to the sample containing behenic acid the low mosaicity of this model membrane (0.10 degree) allowed the collection of 5 orders of diffraction peaks at a temperature of 20°C, 57% RH and a concentration of either 8, 20 or 50% D_2O in water vapour, respectively. As described for the membrane containing behenic acid, this membrane also shows a coexistence of two phases at 20°C. In contrast to the system based on behenic acid, the phase separation cannot be observed in the first diffraction peak, because the intensity of the first phase is substantially larger than that of the second phase. Again, for clarity each phase was labelled according to the extent of its scattering intensity: the first phase was assigned main phase, the other as small phase as it has a very small scattering intensity relative to the main phase. As described previously, the calculations were done independently for both phases in order to make a comparison of the structure. The membrane repeat distance d was determined for each phase from the position of the peak and amounts to $d_1 = (46.3 \pm 0.02)$ Å for the main phase and for the small phase to $d_2 = (45.3 \pm 0.2)$ Å. The presentation of the results will be limited to the main phase.

The neutron SLD profile $\rho_s(x)$ across the bilayer was calculated for each phase separately as Fourier synthesis (Appendix B, Fig. B 3 for the main phase). Similar to the membranes containing palmitic acid [28] or behenic acid, the membrane including SA does not show a region of intermembrane space, as the membrane repeat distance d is equal to the distance between the two maxima of the polar head groups d_{PH}. Therefore the thickness of the intermembrane space amounts to approximately zero at 57% RH, which corresponds to the organisation as described for the systems with palmitic [28] and behenic acid.

The calculation of the water distribution function across the bilayer produced similar results as described for the SC lipid model membrane containing behenic acid. No significant difference between main phase and small phase could be detected, which again proves the

assumption that there is no difference in the structural assembly of both phases. More detailed information about the internal structure was received by fitting the SLD profile as described before, the major results for the main phase are summarised in Table 4.3.

Table 4.3 Structural parameters for each fatty acid containing membrane at 20°C, 8% D_2O and 57% RH.

FFA component	$d = d_m$, Å	x_{PH}, Å	x_{HH}, Å	Thickness of hydro-phobic layer, Å	Thickness of hydro-philic layer, Å
stearic acid	46.3 ± 0.02	23.14	15.4 ± 0.2	30.9 ± 0.4	7.7 ± 0.2
behenic acid	44.0 ± 0.02	22.00	15.7 ± 0.3	31.4 ± 0.6	6.3 ± 0.3
tetracosanoic acid	43.4 ± 0.1	21.43	15.4 ± 0.3	30.8 ± 0.6	6.3 ± 0.3
cerotic acid	43.7 ± 0.1	21.85	16.3 ± 0.2	32.1 ± 0.4	5.4 ± 0.2

d – repeat distance, d_m – membrane thickness, x_{HH} – hydrophilic-hydrophobic boundary, x_{PH} – position of polar head groups

The results show that the membrane structure is not altered due to variation of chain length from C22:0 (BA) to C18:0 (SA). To further prove this fact, model membranes containing FFA with a longer chain were investigated in detail.

4.3.3   SC lipid model membrane containing tetracosanoic acid

The model system containing tetracosanoic acid (TA) showed a mosaicity which was to high to measure rocking curves, however it was possible to collect 5 orders of diffraction as a $\theta - 2\theta$-scan (see Fig. 4-6).
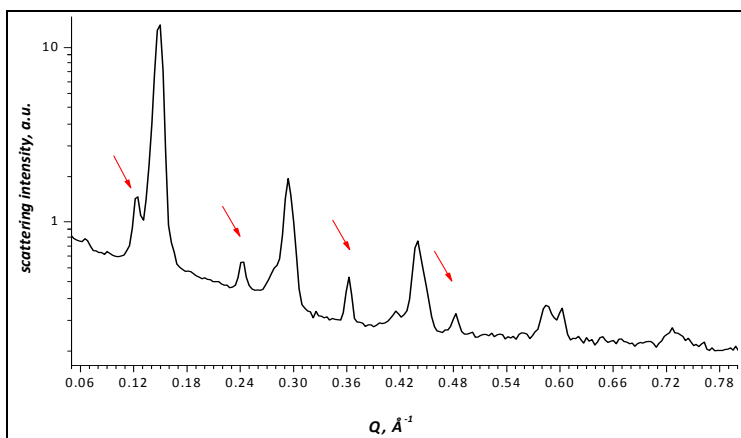
Fig. 4-6 $\theta - 2\theta$ scan of the membrane composed of CER[AP]/CHOL/TA/ChS (55/25/15/5, w/w) measured at 57% relative humidity, 50% D_2O and 20°C. The red arrows mark the clearly distinguishable small phase.

Again, this membrane exhibits a two phase system at 57% relative humidity and a temperature of 20°C. In contrast to the described model membranes containing either behenic or stearic acid, the scattering intensity of this additional phase was larger and clearly distinguishable from the main scattering intensity (see Fig. 4-6). This lead to the assumption that the tendency for phase separation increases with increasing FFA chain length. Once

more, the phases were labelled according to the extent of their scattering intensity: small phase and main phase (main scattering intensity). To gain more detailed structural information about this system the phases were regarded as independent phases for further analysis.

From the position of the diffraction peak the membrane repeat distance d was determined and amounts to $d_1 = (51.1 \pm 0.8)$ Å for the small phase and for main phase to $d_2 = (43.3 \pm 0.1)$ Å. Again, the neutron SLD profiles $\rho_s(x)$ were calculated independently for both phases (Appendix B, Fig. B 5, main phase). The calculation of the SLD $\rho_s(x)$ revealed no intermembrane region, the thickness of the intermembrane region amounts to approximately zero, as described for the model membranes containing either stearic or behenic acid. The structural parameters of the main phase received from the evaluation of the hydrophobic-hydrophilic boundary (x_{HH}) from the water distribution function are presented in Table 4.3 and show that no influence due to the increased chain length of the FFA occurred.

The comparison of the membrane repeat distance d_1 of the small phase with the lamellar spacing of membranes created from pure tetracosanoic acid showed, that the values are similar. Therefore, it can be assumed, that the small phase is mainly composed of phase separated tetracosanoic acid. To prove this point the electron density profile received from pure fatty acid membranes via X-ray diffraction was compared with the neutron SLD profile of small phase which is displayed in Fig. 4-7.
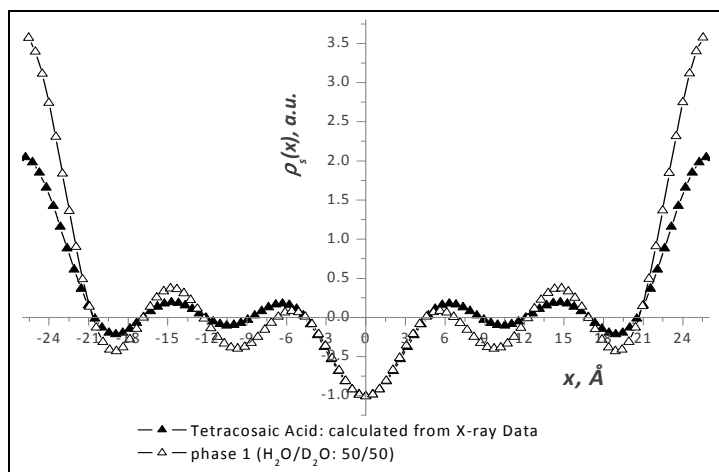
Fig. 4-7 Comparison of the neutron scattering length density profile of the small phase with the electron density profile of a membrane composed of pure tetracosanoic acid.

Note, that the structural differences are only minor between the profile taken from pure tetracosanoic acid membranes and that from the small phase. This is an evidence that the small phase is a tetracosanoic-rich phase. Therefore, it can be stated that the appearance of this separated phase in a SC model membrane based on CER[AP] and containing tetracosanoic acid is due to the decreased solubility of this long chain fatty acid inside this SC

model membrane. As the other model systems also shoed the phase separation tendency, it can be assumed, that these separated phases consist primarily of the respective FFA, too.

4.3.4   Study of a membrane containing cerotic acid as FFA

The longest free fatty acid used in this study was cerotic acid (CA) with 26 C-atoms. Again, 5 orders of diffraction peaks could be recorded as rocking curves, due to the low mosaicity of the sample.

As described for the membrane containing tetracosanoic acid (TA) this fatty acid also displays an additional, clearly separated phase with a longer periodicity. Therefore, it can be assumed that the inclusion long chain FFA causes an increased tendency for phase separation. Similar to the other described model systems, the phases were labelled as followed: small phase (smallest Q-value, longest periodicity) and main phase representing the main scattering intensity. Once more, similar to the membrane with TA, small phase is related to the diffraction from the CA-rich phase.

The membrane repeat distance d was determined for each phase from the position of the peaks and amounts to $d_1 = (56.2 \pm 0.3)$ Å for the small phase and for the main phase main the value was determined to $d_2 = (43.70 \pm 0.07)$ Å. The calculated SLD profiles (Appendix B, Fig. B 5, main phase) revealed, as for all the other FFA used in this study, that this model membrane does not exhibit an intermembrane region. The results of the main phase of the CA-containing membrane received from evaluation of the *HH* boundary form the water distribution function are summarised in Table 4.3. Yet again, they do not show remarkable differences when compared to the model membranes containing one of the other FFA used in this study.

4.4   Conclusion

The results of the neutron diffraction experiment revealed that the internal nanostructure of the SC lipid model membrane based on ceramide [AP] is not altered by the increase of the chain length of the FFA from stearic (C18:0) to cerotic (C26:0) acid.

The obtained nanostructure for each FFA-containing model membrane investigated in this study is similar to that of the membrane containing palmitic acid (C16:0) [28]. It was observed, that an *increase* in the FFA chain length resulted in a *decrease* of the membrane

repeat distance d, which is demonstrated in Fig. 4-8. On the other hand, the lamellar spacing of the small phase increases with the chain length of the FFA (see Fig. 4-9).
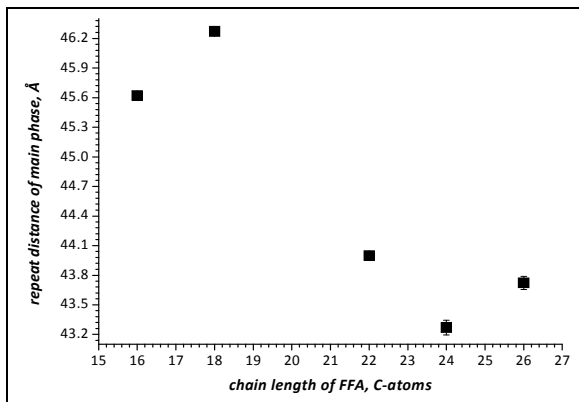
Fig. 4-8 Membrane repeat distance dependency on the FFA chain length. Plotted is the main phase of the different FFA-containing model membranes.
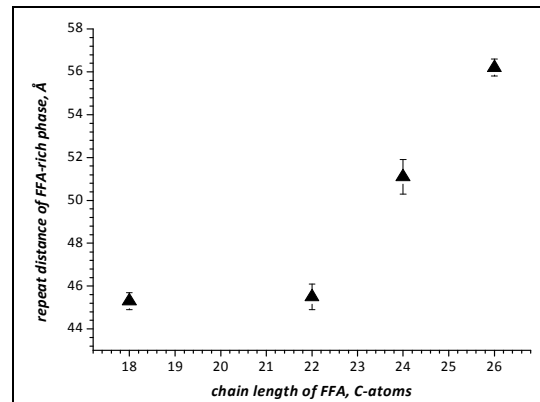
Fig. 4-9 Repeat distance of the small phase (FFA-rich phase) in dependence of the FFA chain length.

This unexpected dependency can be explained by a partial interdigitation of the FFA chains. This interdigitation behaviour results from the tendency of the FFA to "fit" into the membrane size created by ceramide [AP]. The presented results, show that ceramide [AP] creates a superstable nanostructure, which is not influenced by the alteration of the FFA chain length. The interdigitation of the FFA follows this stability of the membrane. On the other hand this interdigitation creates some free space as shown in Fig. 4-10. To fill this free space the FFA "pull" the membrane together. This need to minimise the free volume inside of the membrane can explain the reduction of the membrane thickness when the chain length of the FFA is increased.
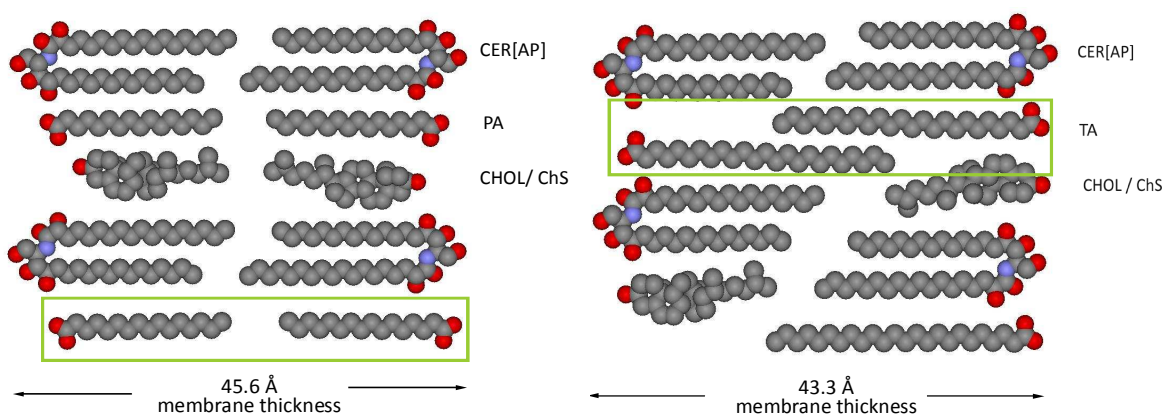
Fig. 4-10 Proposed schematic presentation of the structural assembly of the SC model matrix. To demonstrate the influence of the longer chained fatty acids a model for the membrane based on palmitic acid (left) is compared to the matrix based on tetracosanoic acid (right).
CER[AP] … ceramide [AP], CHOL … cholesterol, PA … palmitic acid, TA … tetracosanoic acid

The term "interdigitation" has been used to describe a phenomenon found for phospholipids, whereby pure phospholipids with unequal fatty acid chain length. There, the methyl groups of the leaflet with longer fatty acids protrude into the acyl chains of the opposing leaflet [116, 117]. The use of especially long chain FFA this SC model membrane is comparable to phospholipids with unequal fatty acid chains, therefore this phenomenon can be conveyed to the SC model membranes discussed here.

Another finding obtained from this study is that the long chain FFA, form a new " free-fatty-acid-rich phase". This finding can be explained by the decreased solubility of the long chain FFA within the SC model membrane based on ceramide [AP]. This could be substantiated by the investigation of pure fatty acid membranes using X-ray diffraction. The small phase has a similar periodicity to the lamellar spacing of the pure fatty acid membranes (Table 4.4). Furthermore, the structural comparison of the pure fatty acid membrane with either phase1 also revealed an alikeness of both membranes (see Fig. 4-7). In addition, the membrane repeat distance of the separated phase increased along with the increase of the FFA as depicted in Fig. 4-9.

Table 4.4 Comparison of the repeat distance d of a pure fatty acid membrane with the repeat distance d of the small phase of the SC lipid model membrane containing either tetracosanoic or cerotic acid.

Fatty acid	d of pure fatty acid membrane (X-ray), Å	d of the small phase (neutron diffraction), Å
tetracosanoic acid	52.6 ± 0.2	51.1 ± 0.8
cerotic acid	56.5 ± 0.2	56.2 ± 0.3

To conclude this investigation it can be summarised, that the very polar short chain phytosphingosine-type ceramide [AP] dictates structure of the main phase of this SC lipid model membrane. The interactions created by the ceramide [AP] molecules are the main forces which determine the stability of this SC model membrane. Therefore, the ceramide obligates the long chain FFA to either arrange inside this phase or separate as a small phase. Further, the appearance of a "fatty-acid-rich phase" indicates that the longer chained FFA tend towards the formation of a separated phase.

5   Evidence of the interdigitation of the free fatty acids in ceramide [AP] based membranes

5.1   Introduction

This study is a continuation of the investigation described in Chapter 4. The aim of this research was to further contribute to the role of the free fatty acids (FFA) in stratum corneum lipid model membranes based on ceramide [AP]. The presented results demonstrate the direct experimental evidence of the interdigitation of the FFA, which was already concluded in Chapter 4. For that purpose specifically deuterated behenic and cerotic acid have been used as the FFA component in neutron diffraction experiments. This allowed visualising the precise location of the deuterated label of the FFA within the lipid model systems.

5.2   Materials and methods

The stratum corneum (SC) lipid model membranes were used in the component ratio of CER[AP]/CHOL/FFA/ChS (55/25/15/5, w/w), whereby only the deuterated FFA was exchanged (see Fig. 5-1). The model membranes used in this study were prepared as described in Chapter 3.4.

Behenic-d$_{22,22,22}$ Acid   *Cerotic-d$_{12,12,13,13}$ Acid*
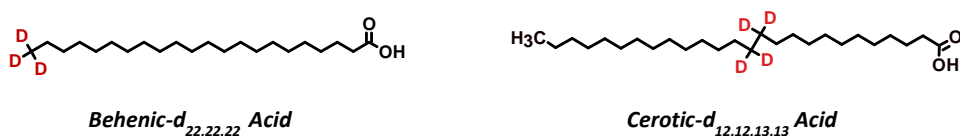
Fig. 5-1 Chemical structures of the deuterated fatty acids used in this study.

The nanostructure of the bilayers was analysed by calculating the neutron scattering length density (SLD) profiles $\rho_s(x)$ as described in Chapter 3.3.2.

The localisation of the specific deuterium label within the lipid membrane is reflected by the positive difference in the SLD profile between samples containing the deuterated and protonated FFA. The details are described in Chapter 3.3.3.

5.3   Results and Discussion

5.3.1   Deuterated terminal methyl group of behenic acid

In this approach the FFA behenic acid (BA) in the SC model membrane composed of CER[AP]/CHOL/BA/ChS was deuterium labelled at the terminal methyl group in order to identify the exact position of the label within this lipid model membrane. As the model membranes show a tendency towards phase separation, the application of partially deuterated FFA can also prove that the separated phase is a FFA-rich phase by determining the (relative) concentration of deuterium in the two phases, respectively.

The quality of the sample allowed the collection of five diffraction orders as rocking curves. Fig. 5-2 represents the diffraction pattern of the SC model membrane containing deuterated BA. The two present phases were assigned as FFA-rich phase (smaller Q-value and scattering intensity) and main phase (main scattering intensity), respectively.
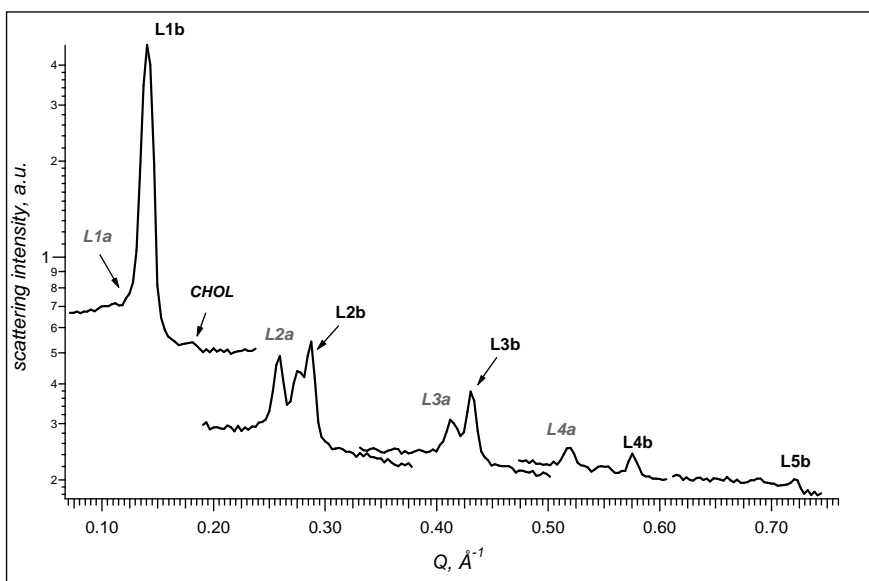
Fig. 5-2 Diffraction pattern of the sample containing deuterated behenic acid (CER[AP]/CHOL/d$_{22}$BA/ChS (55/25/15/5, w/w) measured as rocking scans at 57% RH, 50% D$_2$O and 20°C. Up to 5 orders of diffractions are visible. For the FFA-rich phase diffraction orders 1 to 4 and the diffraction orders 1 to 5 for the main phase (b) have been indicated. The abbreviation CHOL indicates the [010] diffraction peak from phase separated cholesterol crystals.

The lamellar repeat distance amounts to $d_I = (47.4 \pm 0.8)$ Å for the FFA-rich (BA-rich) phase and $d_{main} = (44.1 \pm 0.2)$ Å for the main phase, respectively. For orientation, the diffraction orders 1 to 4 of FFA-rich phase as well as diffraction orders 1 to 5 of the main phase have been indicated in Fig. 5-2. Small amounts of phase separated cholesterol crystals could be identified from the [010] reflection located at Q = 0.18 Å^{-1} and representing the diffraction from the triclinic crystal with the lattice parameters a = 14.172 Å, b = 34.209 Å,

c = 10.481 Å, and α = 96.64°, β = 90.67°, γ = 96.32° [118]. The crystalline CHOL does not influence the multilamellar lipid organisation as described in other studies [119, 120, 72, 121] and has no effect for the further reconstruction of the Fourier analysis by calculating the structure factor (SF) from the integrated peak intensity.

The neutron scattering length density (SLD) profiles $\rho_s(x)$ for both phases were calculated independently according to Eq. (3.12) in order to compare the deuterated with the protonated membrane [105]. Fig. 5-3 presents the neutron SLD profile of the FFA-rich phase containing either protonated BA or the deuterated species (d_{22}BA), with the deuteration located at the terminal methyl group. In the neutron SLD profile the midplane of the lipid bilayer is centred at zero, while the hydrophilic head groups are positioned at the outer edges, contributing the maxima at the edges of the neutron SLD profile [28]. The SLD profile of the FFA-rich phase of the deuterated sample clearly reflects a distinct maximum at the centre of the membrane, which corresponds to the position of the deuterated methyl groups of d_{22}BA as can be seen in Fig. 5-3.
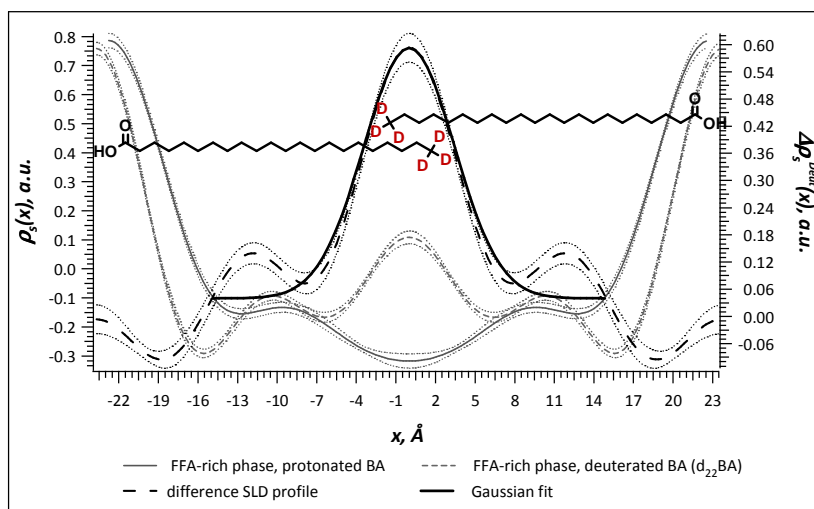
Fig. 5-3 BA acid membrane, FFA-rich phase. Neutron SLD profiles of the membrane containing either deuterated d_{22}BA (dashed line) or protonated BA (solid line). Dotted lines: corresponding errors. Long dash: difference SLD profile. Fat solid line: fit of the difference SLD profile by a Gaussian function (deuterium distribution). The measurements were carried out at 57% RH, at 8% D_2O and 20°C

The difference SLD profile $\Delta\rho_s^{Deut}(x)$ was calculated as described in Chapter 3.3.3 applying Eq. (3.13) and (3.12) to exactly localise the position of the deuterated methyl groups. The small differences in the thickness between the protonated and the deuterated sample is not significantly and does not affect the calculation of the difference SLD profile (see Fig. 5-3). Such a SLD difference profile $\Delta\rho_s^{Deut}(x)$ of the BA-rich phase is presented in Fig. 5-3. The maximum corresponds to the deuterium atoms, which are situated in the central part of the bilayer, indicating that the deuterated methyl group of BA molecule is positioned at the centre. The position was fitted by a Gaussian function and the centre was determined at $x_{C_{22}D_3}$ = (0.01 ± 0.04) Å. The fact, that the deuterated behenic acid could be identified within

the smaller phase shows, that this phase is made up not solely, but to a certain amount of the FFA behenic acid and verifies its assignment as FFA-rich phase. Furthermore, to underline this experimental result the following model should be applied:

The estimated repeat distance d of a bilayer created by two adjacent behenic acid molecules amounts to approximately 55 Å, assessed by the values of 1.5 Å for a CH_3-group and 1.25 Å for a CH_2-group [122]. As the repeat distance d for the FFA-rich phase amounts to $d_1 = (47.4 \pm 0.8)$ Å a difference of approximately 7.6 Å to the theoretical BA membrane occurs. Therefore, this difference can be compensated by the interdigitation of the terminal butyl (5.25 Å) or pentyl (6.5 Å) residues of the behenic acid chain. This minor interdigitation of the terminal butyl residue accounts for the broadness of the maximum in the difference SLD profile as seen Fig. 5-3.

The neutron SLD profile of the main phase is displayed in Fig. 5-4. Further, this figure presents the comparison of the neutron SLD profiles of the protonated and deuterated membrane. Additionally, the difference SLD profile $\Delta\rho_s^{Deut}(x)$ of the protonated and deuterated main phase is included. Here, two overlapping maxima are visible, which resemble the distribution of the deuterium atoms. Therefore, two Gaussian functions according to Eq. (3.14) were used to fit the difference SLD profile $\Delta\rho_s^{Deut}(x)$ in order to identify the position of the label. The centre of each Gaussian function was determined at $x_{C_{22}D_3} = (4.08 \pm 0.02)$ Å and (-4.08 ± 0.02) Å, respectively.

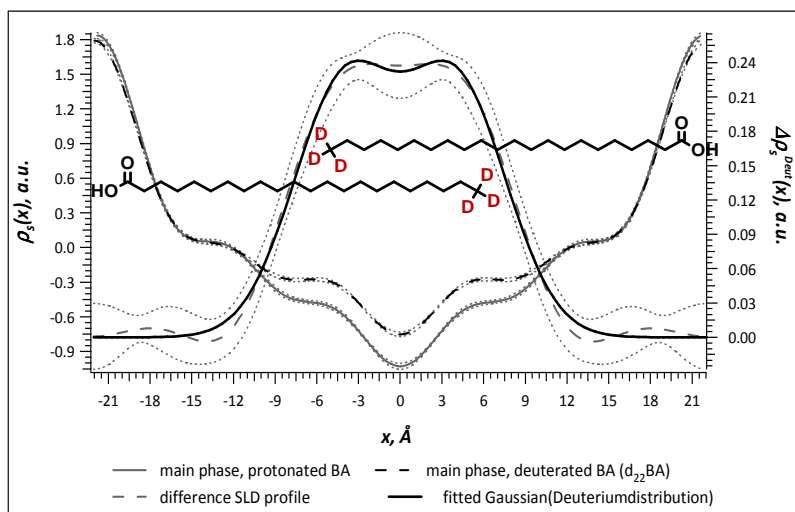**Fig. 5-4** BA membrane, main phase. neutron SLD profiles of the membrane containing either deuterated $d_{22}BA$ (*dashed line*) or protonated BA (*solid line*). Dotted lines: corresponding errors. Long dash: difference SLD profile. Fat solid line: fit of the difference SLD profile by two Gaussian functions (deuterium distribution). The measurements were carried out at 57% RH, at 8% D_2O and 20°C

43

This result shows, that the terminal methyl group of the specifically deuterated behenic acid $d_{22}BA$ is not positioned at the centre of the membrane as demonstrated for the FFA-rich phase of this membrane. This is due to the chain interdigitation of the behenic acid in this phase. Again, the theoretical BA bilayer can be used to confirm this result. In this case a difference of the repeat distances between the hypothetical BA bilayer and the main phase amounts to approximately 10.9 Å, as the d-value for the main phase was calculated to d_{main} = 44.1 Å. A compensation of this difference can be accomplished by the interdigitation of the terminal heptyl (9 Å) or octyl (10.25 Å) residues of the behenic acid molecules.

5.3.2   Deuteration of the methylen groups

The longest free fatty acid investigated in this study was cerotic acid (CA) specifically deuterated at the C-atoms C12 and C13 in order to further proof that the long chain free fatty acids need to interdigitate into the membrane size dictated by the short chain ceramide [AP]. The diffraction pattern of the sample containing the deuterated CA , recorded as $\theta - 2\theta$-scan is presented in Fig. 5-5.
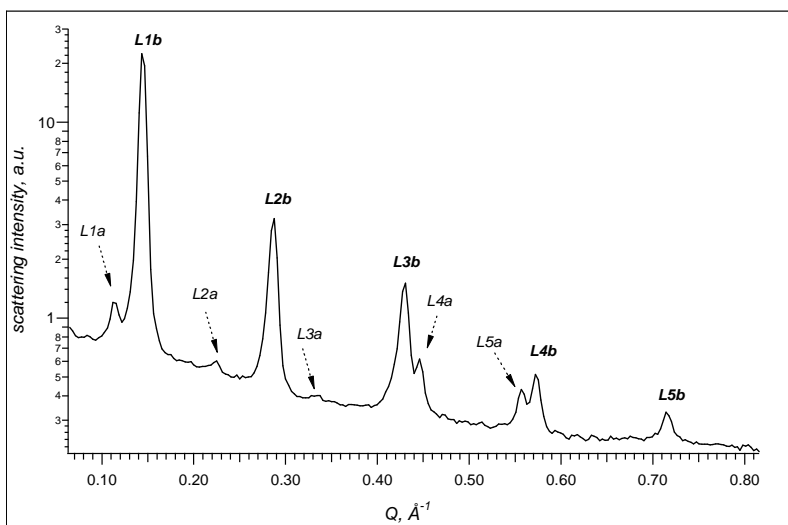
Fig. 5-5 Neutron diffraction pattern of the sample containing the deuterated cerotic acid (CER[AP]/CHOL/ $d_{12}CA$/ChS, 55/25/15/5, w/w) measured as $\theta - 2\theta$-scan at 57% RH, 8% D_2O and T = 20°C. The two phases have been indicated:
$L1a - L5a$ indicate the 5 diffraction orders of the FFA-rich phase, while $L1b - L5b$ indicate the 5 diffraction orders for the main phase, respectively.

The repeat distance d was determined to d_1 = (56.3 ± 0.6) Å for the FFA-rich phase and to d_{main} = (43.8 ± 0.4) Å for the main phase. The neutron SLD profile of the FFA-rich (CA-rich) phase containing the specifically deuterated CA showed two distinct maxima (see Fig. 5-6A).
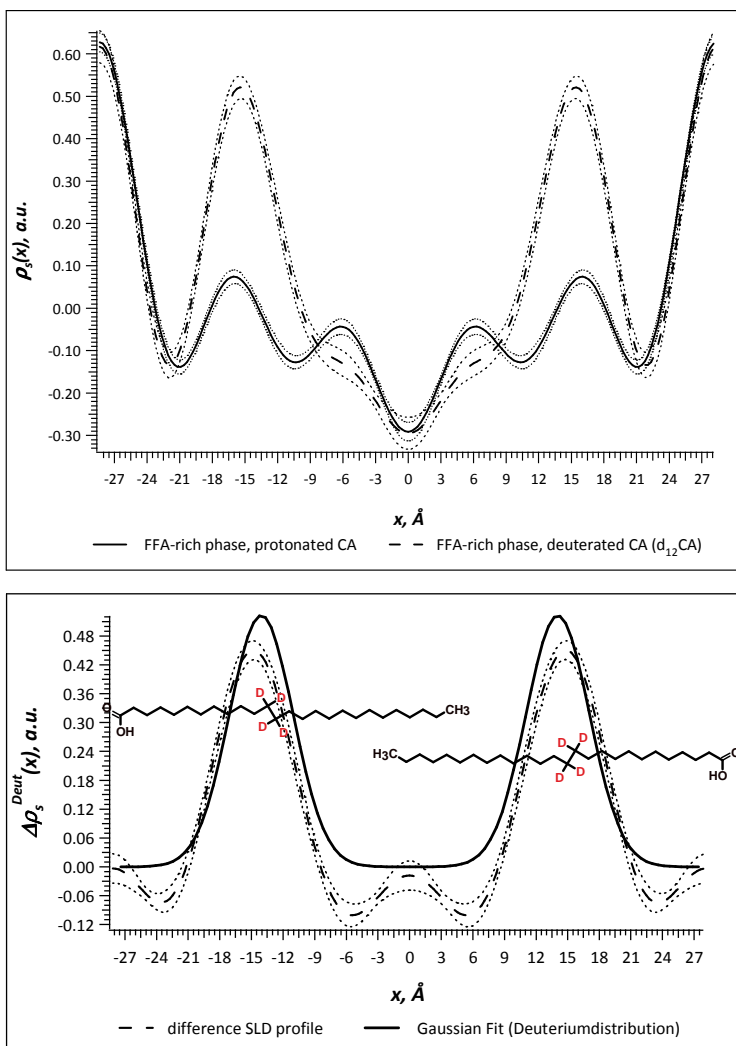
Fig. 5-6 Neutron scattering length density profile of the FFA-rich phase of the sample containing cerotic acid.

(A) Comparison of the neutron SLD profile of the sample containing the deuterated CA (long dash) with the model membrane containing the protonated FA (solid line).

(B) Cerotic acid, FFA-rich phase. Difference SLD profile for CA specifically deuterated at positions 12,12,13,13 (− − −). Dotted lines: corresponding errors. Fat solid line: fit of the difference SLD profile by two Gaussian functions (deuterium distribution).

The difference SLD profile $\Delta\rho_s^{Deut}(x)$ of the protonated and the deuterated FFA-rich phase together with the corresponding fit of the difference profile by two Gaussian functions are presented in Fig. 5-6B. The results of the fitting procedure of $\rho_s^{Deut}(x)$ by two Gaussian functions $\rho^{sym}(x)$ according to Eq. (3.14) are summarised in Table 5.1 and give the exact position of the CD$_2$-groups within the CA-rich phase. The CD$_2$-groups of the deuterated cerotic acid d$_{12}$CA are situated inside this phase at $x_{C_{12}D_2C_{13}D_2}$ = (14.05 ± 0.08) Å and (-14.05 ± 0.08) Å, respectively. The appearance of the deuterated label of CA directly proves, that indeed the separated phase is separated CA.

Table 5.1 Lamellar repeat distance d and the position x of the deuterated label of the FFA inside one lipid leaflet for each deuterated FFA containing membrane at 20°C, 8% D_2O and 57% RH

Phase of membrane	d , Å	Position x of label, Å
d_{22}BA: FFA-rich phase	47.4 ± 0.8	CD_3-groups +/- 0.01 ± 0.04
d_{22}BA: main phase	44.1 ± 0.2	CD_3-groups +/- 4.08 ± 0.02
d_{12}CA: FFA-rich	56.5 ± 0.6	CD_2-groups +/- 14.05 ± 0.08
d_{12}CA: main phase	43.8 ± 0.4	CD_2-groups +/- 5.4 ± 0.04

Once more, the theoretical fatty acid membrane model can be employed. Here, two opposing CA-molecules have an estimated repeat distance d of approximately 65.5 Å. The difference to the d_1-value of the FFA-rich phase of the SC model membrane amounts to approximately 9.2 Å, which can be compensated by the interdigitation of the terminal heptyl residues of the CA chains. From the full width at half height (FWHH) it can be deduced, that the CH_2-groups region represents the largest region inside the membrane [28]. Assuming that the relevant maxima of the $\Delta\rho_s^{Deut}(x)$ correspond to the region of $C_{12}D_2$-$C_{13}D_2$ with the centres x at 14.05 Å and -14.05 Å, respectively, the FWHH (7.37 Å) comprises the region with the highest density of deuterium atoms. This region can be calculated as 14.05 ± ½ FWHH (± 10.36 Å to ± 17.74 Å). In this hypothetical cerotic acid bilayer, the position of label at C_{12} and C_{13} can be estimated as $x_{C_{12}D_2-C_{13}D_2}$ = +16.5 Å and -16.5 Å, respectively. Related to the fitted position at 14.05 Å, this would be inside these error margins.

In case of the main phase of this SC lipid model membrane the calculation of the difference SLD $\Delta\rho_s^{Deut}(x)$ resulted in two broad maxima overlapping each other, as shown in Fig. 5-7. As the deuterated CD_2-groups of the CA are detectable in this model membrane based on CER[AP] it can be stated that some amount of this long chain FFA is incorporated into this phase. The fitting of two Gaussian functions $\rho^{sym}(x)$ of the difference SLD profile $\Delta\rho_s^{Deut}(x)$ revealed the position of the label of CA. Therefore, it can be concluded, that CA protrudes through the adjacent layer in order to fit into the membrane size created by CER[AP] (see Fig. 5-7). The results received from the fitting are summarised in Table 5.1.

Fig. 5-7 Cerotic acid, main phase. Difference SLD profile of CA specifically deuterated at positions 12,12,13,13 (- - -). Dotted lines: corresponding errors. Fat solid line: fit of the difference SLD profile by two Gaussian functions (deuterium distribution).
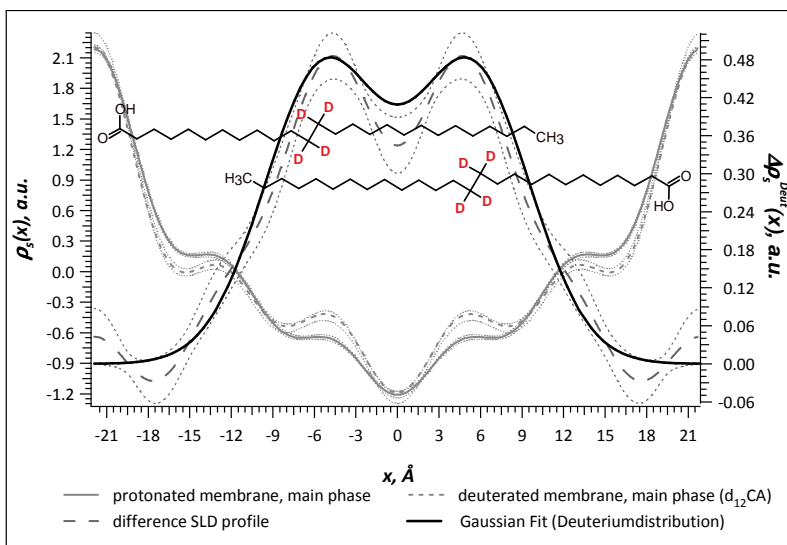
Applying the theoretical CA bilayer model yet again as described above a difference to the d_{main}-value of approximately 21.7 Å occurs, which can only be compensated by the interdigitation of the last 15 to 16 CH_2 groups and the terminal methyl group of the CA chain.

5.4   Conclusion and Summary

The application of the specifically deuterated free fatty acids behenic and cerotic acid supplied *direct* experimental evidence that long chain free fatty acids incorporated into a stratum corneum lipid model membrane based ceramide [AP] need to protrude into the adjacent layer in order to arrange in the membrane size dictated by this ceramide. Therefore, the free fatty acids are forced by ceramide [AP] to occupy the bilayer thickness determined by ceramide [AP]. Furthermore, the use of the deuterated free fatty acids confirmed the coexistence of free fatty acid rich phase and main phase. The formation of this free fatty acid rich phase is a result of the decreased solubility of the longer chained free fatty acids within the membrane created by the ceramide. The main forces which constrain the free fatty acids to either interdigitate in the membrane or to separate as the free fatty acid rich phase are caused by the very polar short chain phytosphingosine-type ceramide [AP] molecules, which therefore determine the stability of this stratum corneum lipid model membrane. The presented results support the phenomena of the *armature reinforcement model* of stratum corneum lipid model membranes based on ceramide [AP] proposed by Kiselev [110] and presented in Chapter 2.4. Furthermore they show the importance of this short chain ceramide for the nanostructure of such model membranes.

6   Structural organisation of stratum corneum lipid model membranes based on the artificial ceramides [NP]A and [NP]B

Submitted to: *Biophysical Journal, 2009*

6.1   Introduction

This Chapter presents information about the influence of the artificial ceramides [NP] type A and type B to the spatial organisation of SC lipid model membranes containing also cholesterol, a free fatty acid and cholesterol sulphate. As these ceramides chemically differ only slightly from the already discussed CER[AP], this study can contribute to the analysis of the structure-function-relationship of ceramides. For that purpose, the SC lipid model membranes were investigated with neutron diffraction to describe the impact of such lipids to the nanostructure by analysing the corresponding scattering length density profiles. Furthermore, the addition of CER[AP] to SC model systems containing the artificial ceramides CER[NP]A or B and its role in the structural assembly is discussed.

6.2   Materials and methods

The artificial ceramides used for this study are ceramide [NP] type A (*N*-Lineoyl-phytosphingosine, CER[NP]A) and ceramide [NP] type B (*N*-Oleoyl-phytosphingosine, CER[NP]B). Their chemical structures are depicted in Fig. 6-1.
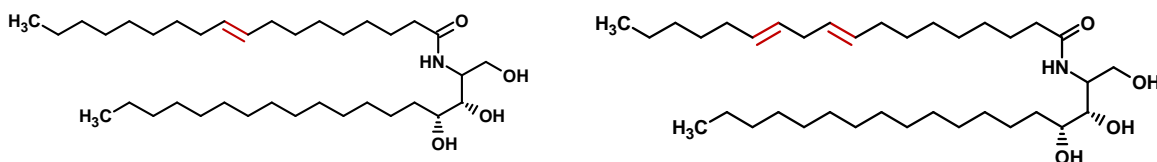
Fig. 6-1 Chemical structures of the phytosphingosine type ceramide analogues CER[NP] type A (right) and CER[NP] type B (left).

Table 6.1 shows the composition of the quaternary SC lipid model membranes used for the investigation.

Table 6.1 Composition of the SC lipid model systems containing the artificial CER[NP]A or CER[NP]B.

Mixture	Components	Component ratio (w/w)
Quat[NP]A	CER[NP]A/CHOL/palmitic acid (PA)/ChS	55/25/15/5
Quat[NP]B	CER[NP]B/CHOL/PA/ChS	55/25/15/5
Quat[NP]A_[AP]	CER[NP]A/CER[AP]/CHOL/PA/ChS	27.5/27.5/25/15/5
Quat[NP]B_[AP]	CER[NP]B/CER[AP]/CHOL/PA/ChS	27.5/27.5/25/15/5

The ratio of the lipids were chosen in order to compare the system containing the synthetic ceramide analogues to the already described SC model membranes based on ceramide [AP] discussed in the previous Chapters 4 and 5. The multilamellar lipid membranes for the neutron diffraction experiment were prepared as described in Chapter 3.4.

The structure of the bilayers is analysed by construction of the neutron scattering length density (SLD) profiles $\rho_s(x)$ as described in Chapter 3.3.2.

For the temperature scan the sample was heated in 5 K steps until the temperature of 70°C was reached. After attaining each temperature step the sample was equilibrated for one hour, after which the scattering intensity I of the first diffraction order was recorded as function of the scattering vector Q. The temperature-depending experiment was performed at 57% relative humidity (RH) and 8% D_2O.

6.3   Results and discussion

6.3.1   Model membranes based on CER[NP] type B

In Fig. 6-2 the diffraction pattern of the SC lipid model membrane composed of the artificial ceramide [NP] type B (CER[NP]B), cholesterol (CHOL), palmitic acid (PA) and cholesterol sulphate (ChS) (55/25/15/5, w/w) is displayed. As can be seen, this model membrane exhibits a three phase system at 20°C and 57% relative humidity (RH). All three phase show a high scattering intensity for the first diffraction order, indicating that all phases are more or less equally present in the membrane. From the overall scattering intensity of the first diffraction order the fraction of each phase was evaluated and amounts to 46.2% for phase C, 41.1% for phase B and 12.6% for phase A, respectively.
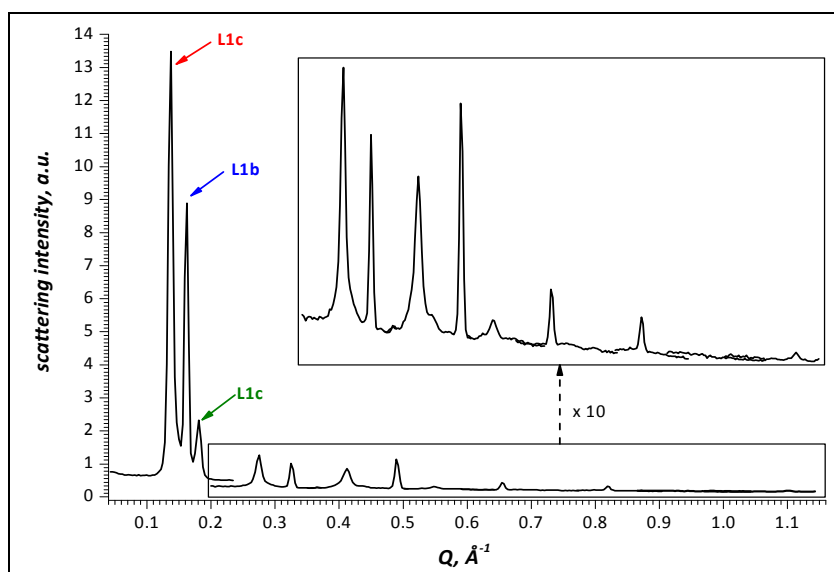
Fig. 6-2 Neutron diffraction pattern for the CER[NP]B/CHOL/ BA/ChS (55/25/15/5, w/w) at 57% RH, 8% D_2O and T = 20°C. The three phases of the model membrane have been indicated: L1a, L1b and L1c represent the first diffraction order of phase A, B and C, respectively.

From the position of equidistant peaks the lamellar repeat unit d for each phase was calculated as described in Chapter 3.3.2; the results are listed in Table 6.2. The artificial ceramide [NP]B is chemically very similar to the naturally existent ceramide [NP], only the additional double bound in the acyl residue of CER[NP]B marks the difference between both molecules (see Fig. 6-1). Therefore, a comparison to the natural CER[NP] can give information to understand the role of the artificial ceramide, in particular its chemical alteration. Consequently, the solid states of the natural CER[NP] were compared to the lamellar phases detected in the SC lipid model membranes. Raudenkolb and co-workers reported for CER[NP] three solid states, which all exhibit lamellar crystalline structure and which were assigned as phase α, β and δ based on X-ray diffraction and FT-infrared data [123]. The corresponding spacings are listed in Table 6.2.

Table 6.2 Lamellar repeat distance of the SC lipid model membranes based either on CER[NP]B or CER[AP] compared with the lamellar spacings of pure CER[NP] received from X-ray experiments.

	Repeat distance, Å	
CER[AP] membrane [#]	*CER[NP]B membrane*	*pure CER[NP]**
45.68 ± 0.05	phase A: 34.24 ± 0.28	α-phase: 36.9 ± 0.05
	phase B: 38.24 ± 0.01	β-phase: 39.5 ± 0.05
	phase C: 45.74 ± 0.16	δ-phase: 44.9 ± 0.05

[#] data obtained from Kiselev et al. [28], * data from Raudenkolb et al. [123]

Interestingly, the SC lipid model membrane based on CER[NP]B showed almost equivalent lamellar repeat units. Thus, it can be assumed, that the pseudo CER[NP] type B exhibits the same polymorphism as the natural species. The introduced double bond therefore, has no influence to the conformational properties of the ceramide molecules.

Accordingly, the three phases of the SC lipid model membrane were assigned as: phase A corresponds to the α-phase of the pure CER[NP], while phase B corresponds to the β-phase, as phase C to the δ-phase found in pure CER[NP]. However, for the natural CER[NP] only one conformation exists at fixed conditions, while in SC model membranes with CER[NP]B all three conformations are present under the same experimental conditions. One explanation for this finding is, that the phase transition to one conformational state is not completed, because it is a time consuming process. On the other hand, it seems more likely, that the other lipids present in the SC lipid system such as CHOL and PA influence the phase behaviour of the ceramide. Both PA and CHOL are probably stabilising the different conformations of the ceramide molecules.

Raudenkolb and co-workers [123, 124] concluded from X-ray diffraction that the lamellar spacings detected correspond to the following conformation of the CER[NP] molecule: α-phase: V-shape, β-phase also V-shape with a smaller angle between the hydrocarbon tails and for the δ-phase the fully extended (FE) conformation, where the hydrocarbon chains are directed oppositely. These conformations were also found for the α-hydroxy-phytosphingosine ceramide [AP] as stated in Chapter 2.4. Conferring this information to the artificial ceramide [NP]B, it can be concluded that this ceramide can also exist in these conformations (see Fig. 6-3).
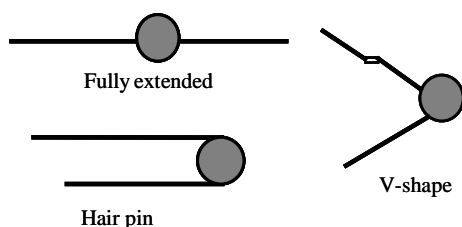
Fig. 6-3 Proposed conformation of the artificial ceramide [NP]B based on the X-ray diffraction data for natural CER[NP] [123, 124].

Comparing the repeat distances to the SC lipid model matrix composed of ceramide [AP]/CHOL/PA/ChS (55/25/15/5, w/w) showed that phase C exhibits a similar lamellar spacing (see Table 6.2). Therefore, it can be assumed that both ceramides also show the same conformation, which is either the fully extended (FE) or the hairpin (or one-sided) conformation.

In Fig. 6-4 the neutron scattering length density (SLD) profiles of the three phases are displayed. The comparison demonstrates that not only the d-spacing of the phases differs, but also the structural alignment of the lipids.
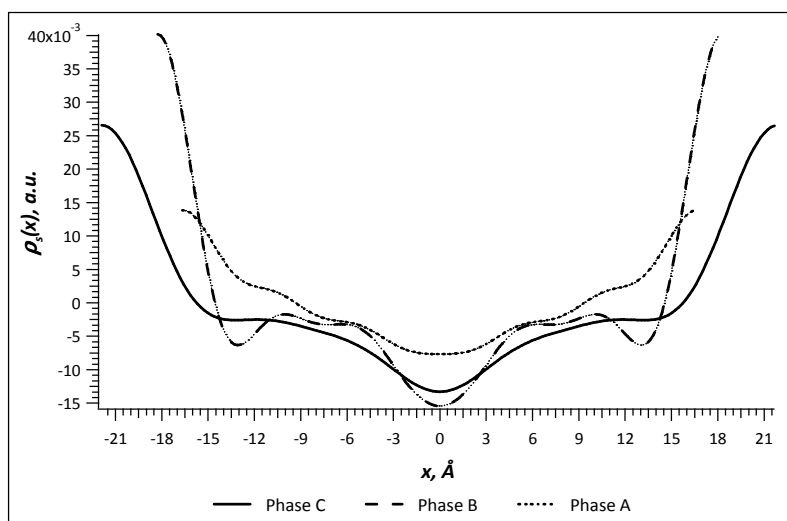
Fig. 6-4 Neutron SLD density profiles of the three phases present in the SC model membrane based on the artificial CER[NP]B measured at 57% RH, T = 20°C and 8% D_2O.

The conformational state of the CER[NP]B molecules has a significant effect to the structural assembly of the SC lipid model membrane (see Fig. 6-4). In phase C the CER[NP]B molecules are most likely in the full extended conformation; the two maxima correspond to the polar head groups, while the centre of the membrane is occupied by the CH_3 residues of the acyl chain, which are responsible for the minimum located there. As the CER[NP]B molecules change to the V-shape conformation of phase B the repeat distance is reduced. Further, the SLD at the centre of the membrane increases as well as the SLD in the polar head group region when compared to phase C. The explanation again can be found in the conformation of the CER[NP]B molecules: when the FE conformation is favoured this creates some free space in the centre, while some amount of the CH_2 groups close to the polar head groups penetrate into the polar head group region, thereby decreasing the SLD.

In the SLD profile of phase A the maxima belonging to the polar head groups have a significant smaller scattering length density as detected for the phase C and B. Further, the minimum at the centre of the membrane is much less pronounced. One explanation for this phenomenon could be, that the amount of phase A is smaller when correlated to the phases B and C. Another explanation for both differences can be derived again from the different conformations of the ceramide molecule. Raudenkolb and co-workers explained the different lamellar repeat units of phases α and β with an increase of the angle between the hydrocarbon chains [124]. In case of the artificial ceramide [NP]B based model membrane this explanation is not satisfactory. Such a conformation would result in an arrangement similar to phase B, only with a smaller repeat unit. Even taking into account the smaller scattering intensities in respect to both other phases does not suffice to explain the alignment of the lipids within phase A. It cannot explain, that the minimum at the centre of the membrane is less pronounced as for phase C and B. Such a reduction can only result from

the penetration of the hydrocarbon chain through the centre of the membrane, whereby CH_2-groups are located in the CH_3-group region. As the CH_2-groups have larger scattering length density compared to the CH_3-groups, the minimum is reduced. The CH_2-group region is on the other hand not altered and is similar to both other phases. Therefore, it can be assumed that the acyl chains of the CER[NP]B molecules penetrate into the opposing layer, creating thereby an interdigitated phase. As mentioned in Chapter 4 the phenomenon of interdigitation was described for uneven chained phospholipids [116, 117] and as well as for the long chain free fatty acids in model membranes based on CER[AP].

In order to receive information about the influence of the artificial CER[NP]B to the structural assembly, the model system was compared to the already described CER[AP] based SC model membranes (discussed in detail in Chapters 4 and 5).

As described for CER[NP] and the artificial CER[NP]B the α-hydroxy-phytosphingosine CER[AP] can also exist in three different conformations, the V-shape, FE and hairpin conformation [125]. Only the FE and the hairpin conformation comply with the neutron SLD profiles established for SC lipid model membranes composed of CER[AP]/CHOL/FFA/ChS as discussed by Kiselev and co-workers [28] and in Chapter 4. There, it was found that in contrast to the lipid model membrane based on CER[NP]B the polymorphism of CER[AP] does not create a phase separated system.

The comparison of the SLD profile of the SC lipid model membrane based on CER[AP] with the SLD profile of phase C of the membrane based on the artificial CER[NP]B is depicted in Fig. 6-5.
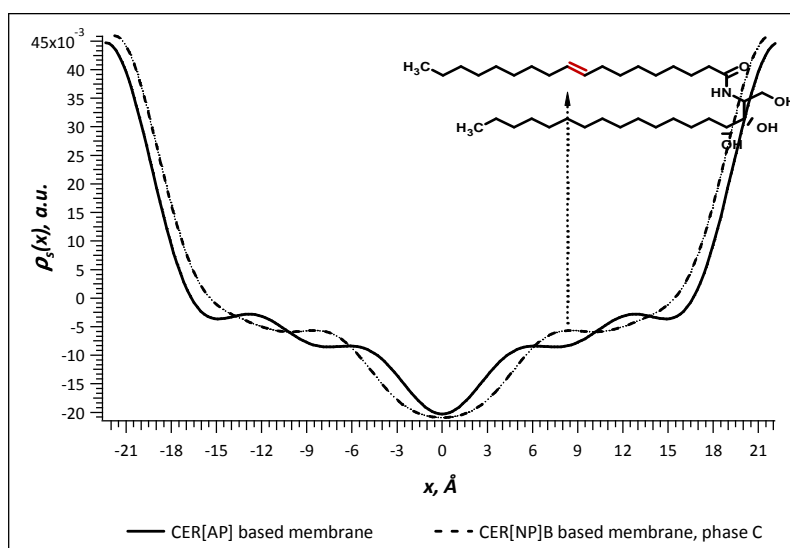
Fig. 6-5 SLD profile of the SC model membrane based on CER[AP] composed of CER[AP]/CHOL/PA/ChS (55/25/15/5, w/w) compared to phase C of the SC model matrix made up of CER[NP]B/CHOL/PA/ChS (55/25/15/5, w/w). Both measurements were per-formed at 8% D_2O, T = 20°C and 57% RH. For better understanding a CER[NP]B molecule has been added.

In general the structural alignment of the lipids in both membranes is similar as is the lamellar spacing (see Table 6.2). Nevertheless, it is possible to distinguish the characteristics

of the artificial ceramide in the neutron SLD profile. Chemically both ceramides belong to the group of phytosphingosines, whereby CER[AP] has an additional hydroxyl group. In the SLD profile the additional OH-group can be detected as the polar head group region of the CER[AP] based membrane has a slightly larger scattering length density in comparison to the CER[NP]B-based membrane. Furthermore, in the artificial ceramide the phytosphingosine backbone is connected to the unsaturated fatty acid oleic acid. This accounts for the small maxima visible in the CH_2 group region. As demonstrated in Fig. 6-5 these two maxima clearly correspond to the position of the double bound within the CER[NP]B molecule.

The correlation of the SLD profiles of the CER[AP] based membrane with phase B of the CER[NP]B based membrane is depicted in Fig. 6-6. As discussed above, the differences visible in the SLD profile between the membrane based on CER[AP] and phase B of the membrane based on the artificial ceramide are due to the conformational differences of CER[NP]B. As stated previously, CER[NP]B adopts here the V-shape conformation. The higher values in the polar head group region of phase B of the CER[NP]B-based membrane can be attributed to the V-shape conformation. In contrast, CER[AP] molecules can also exist in the FE conformation, whereby CH_2 groups are positioned in the polar head group region, thereby reducing the scattering length density as demonstrated in Fig. 6-6. As mentioned for phase C, the double bond of the oleic acid moiety is again detectable in the neutron SLD profile.
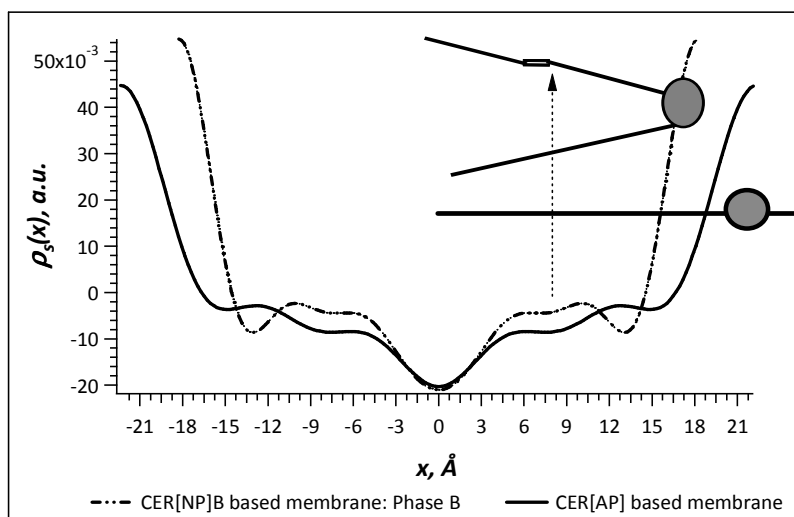
Fig. 6-6 SLD profiles of the reference membrane based on CER[AP] in comparison to the model system composed of CER[NP]B/CHOL/PA/ChS (55/25/ 15/5, w/w). Both measurements were carried out at 57% RH, 20°C and 8% D_2O. A sketch of the CER molecules have been added in the respective conformation (V-shape for CER[NP]B and FE for CER[AP].

Summarising, it can be stated that the artificial CER[NP] type B showed the same polymorphism as the natural CER[NP], with three different conformations. In respect of this, the introduction of the double bound into the molecule did not alter the conformational properties.

In mixtures with other prominent SC lipids the artificial CER[NP] type B is able to form multilamellar structures. However, when compared to the SC model system based on

CER[AP], it does not create a homogeneous layer, but rather a three phase system, whereby each phase is defined by one conformation of CER[NP]B. This is an interesting result, as model membranes containing CER[AP] exhibited only one phase, although CER[AP] also shows the same polymorphism.

The presence of the artificial CER[NP]B in the natural stratum corneum might also cause the creation of a multiphase system, thereby perturbing the barrier function of the SC.

6.3.1.1   Temperature dependence of model membranes based on CER[NP]B

In Fig. 6-7 the dependence of the membrane repeat distance d on temperature is depicted for all three lamellar phase. As can be seen, the temperature dependence of the lamellar spacing differs for all three phases: the repeat distance of phase C, d_C shows no significant decrease up to a temperature of 50°C, after which d_C increases from (45.71 ± 0.12) Å (50°C) to (47.73 ± 0.32) Å (65°C). At 70°C however, phase C disappears completely. In case of phase B no significant change in the d_B-value could be observed, this phase could be detected up the final temperature of 70°C. For phase A also no decrease in the repeat distance could be observed; the phase was stable until a temperature of 50°C is reached, after which it disappears completely. Furthermore, at 50°C a new phase could be detected with a repeat distance between the values of phase C and B ((42.22 ± 0.30) Å). The repeat distance of the new phase showed the typical decrease upon on temperature increase (from (42.22 ± 0.30) Å at 50°C to (40.59 ± 0.02) Å at 70°C), which can be attributed to the melting of the hydrocarbon chain. A more detailed study of the temperature behaviour of the SC lipid membranes on the basis of Differential scanning calorimetry, Raman spectroscopy and neutron diffraction is described in Chapter 8.
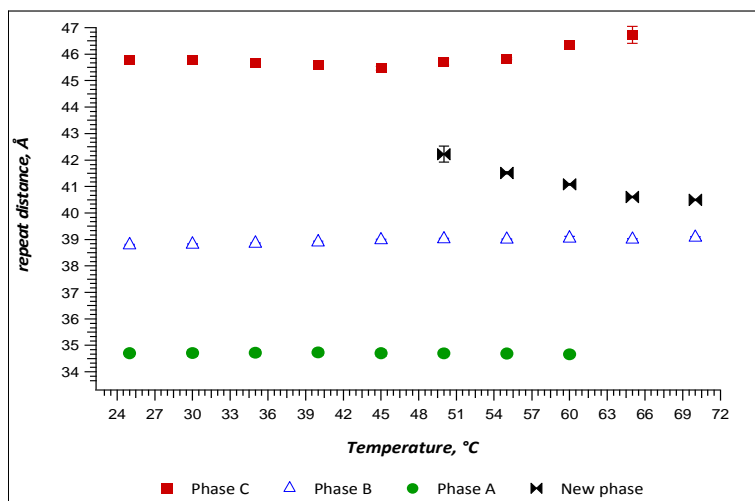
Fig. 6-7 Temperature-dependence of the repeat distances d_A to d_C of the three phases measured at 57% relative humidity and 8% D_2O. Note, at 50°C a new phase appears.

Combining the results, it can be assumed that increase of the temperature leads to restructuring of the membrane lipids, whereby the three phases merge into this new phase. These findings are consistent with the results obtained from the heating experiment of pure CER[NP]. There, a phase transition from phase δ to β-phase occurred at a temperature of 84°C, after which the β-phase persisted until its melting at 123°C [123]. Therefore, at elevated temperatures only one conformation, the V-shape conformation is favoured. Although, small amounts of phase B can be detected at 70°C it can be assumed that the new phase and phase B are structurally similar and that they differ only in the lipid composition. To prove this point a rocking curve at fixed 2θ-positions was recorded at 70°C. The corresponding diffraction pattern in presented in Fig. 6-8.
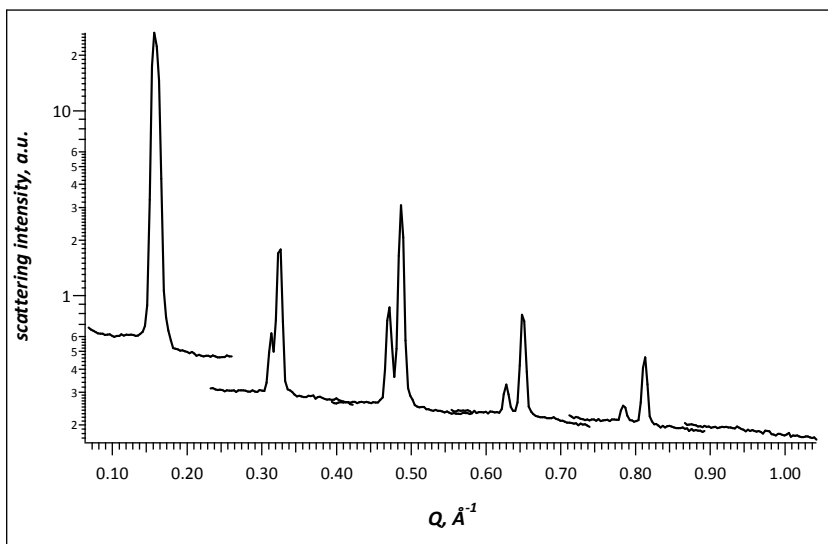
Fig. 6-8 Neutron diffraction pattern of the sample composed of CER[NP]B/CHOL/PA/ChS (55/25/15/5, w/w) at 57% RH, 8% D_2O and a temperature of T = 70°C.

The neutron SLD profiles for phase B and the new phase at 70°C are presented in Fig. 6-9. As can be seen, the structural alignment of the lipids within both phases is very similar, confirming the assumption that in both phases the CER[NP]B molecules adopt the V-shape conformation and that the small variations are due to compositional differences resulting from the reordering of the lipids.
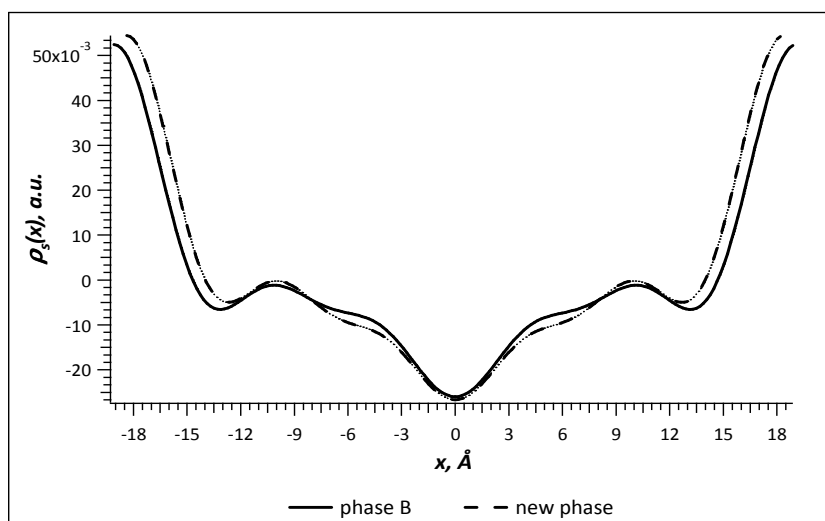
Fig. 6-9 Neutron SLD profiles for phase B and the new phase at a temperature of 70°C.
The measurement was performed at 8% D_2O and 57% RH.

6.3.2   Addition of CER[AP] to model membranes based on CER[NP] type B

Another aspect of this investigation was to identify the influence of the artificial CER[NP]B to the structural assembly of model membranes based on CER[AP]. As concluded in Chapters 4 and 5 very polar short chain phytosphingosine CER[AP] molecules force the long chain free fatty acids (FFA) to either arrange inside a lamellar phase created by CER[AP] or separate as a FFA-rich phase. Consequently, the interactions created by the CER[AP] molecules are the main forces which determine the stability of this SC model membrane.

The question which needs to be answered is, whether the influence of CER[AP] exceeds the influence of CER[NP]B for the formation of the lamellae, when both ceramides are present. Therefore, a system composed of CER[AP]/CER[NP]B/CHOL/BA/ChS with the component ratio of 27.5/27.5/25/15/5 (w/w) was investigated. Fig. 6-10 displays the corresponding diffraction pattern. Interestingly, the three phase system discussed above could not be observed when CER[AP] was included in the model system. The SC model membrane containing both ceramides favours only one conformation. It can, therefore, be assumed that the forces of the more polar CER[AP] outweigh those of CER[NP]B.
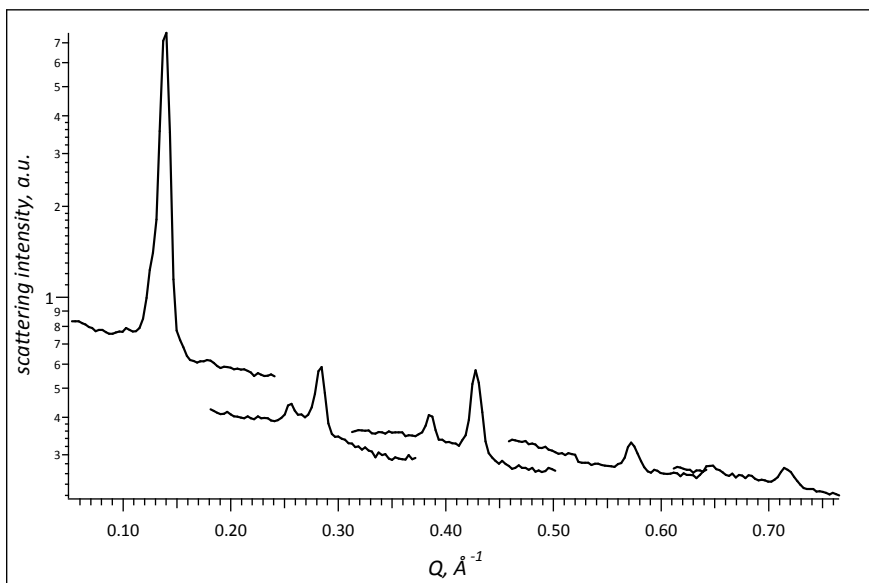
Fig. 6-10 Diffraction pattern of the sample composed of CER[AP]/CER[NP]B/ CHOL/BA/ChS (27.5/ 27.5/25/ 15/5, w/w) measured at 8% D_2O, 57% RH and 20°C.

As can be seen in the diffraction pattern, peaks belonging to a second phase are present. It was found to be the FFA-rich phase, which is formed due to the decreased solubility of long chain FFA in model membranes based on CER[AP]. Substituting behenic acid by the terminally deuterated species confirmed this assumption (Appendix C, Fig. C 1).

From the neutron SLD profile and the correlation to the model system composed of CER[AP]/CHOL/BA/ChS (55/25/15/5, w/w) it was concluded, that in mixtures with CER[AP] the artificial CER[NP]B needs to adopt the same conformation as CER[AP] (see Fig. 6-11). As the repeat distance d amounts to $d = (43.48 \pm 0.04)$ Å it was further presumed, that CER[NP]B needs to be in fully extended conformation because this spacing corresponds to the spacing found for the δ-phase of pure CER[NP] (see Table 6.2).
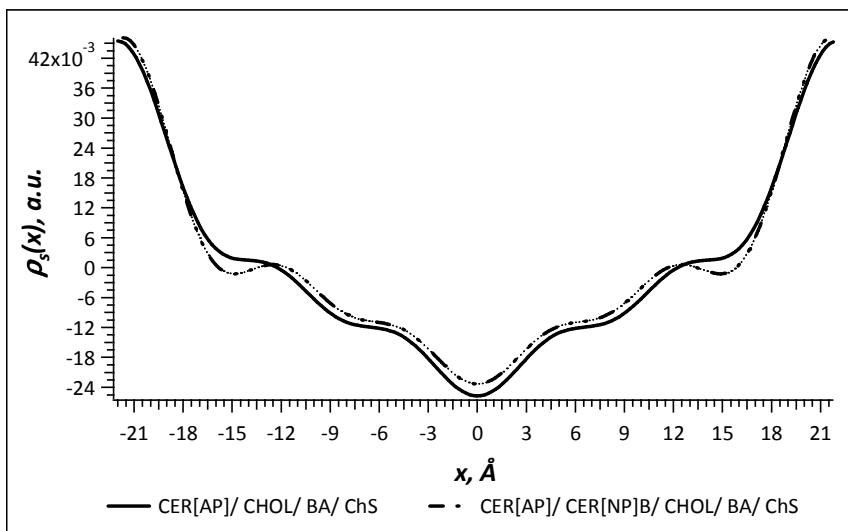
Fig. 6-11 Comparison of the neutron SLD profile of the SC lipid model membrane based solely on CER[AP] and the matrix containing both CER[AP] and CER[NP]B.

From the SLD profile presented in Fig. 6-11 it can be deduced that the inclusion of CER[NP]B does not affect the structural alignment of the membrane based on CER[AP].

As discussed in Chapter 4 membranes based on CER[AP] are very stable to compositional influences such as the increase in the FFA chain length. In this approach it was demonstrated, that also the addition of another phytosphingosine-type ceramide did not influence the structure determined by CEP[AP]. This is a further support of the *armature reinforcement model* presented in Chapter 2.4.

6.3.3   Effect of CER[NP] type A to SC lipid model membranes

The artificial ceramide [NP] type A is a derivative of ceramide [NP], two conjugated double bonds have been introduced (see Fig. 6-1).

The diffraction pattern of the SC lipid model membrane composed of CER[NP]A/CHOL/PA/ChS (55/25/15/5, w/w) is depicted in Fig. 6-12. In contrast to the membrane based on CER[NP] type B this model system exhibited only one phase. This is in accordance to findings on pure CER[NP]A [126].

The SC lipid model membrane based on CER[NP]A displayed a poor lamellar ordering, it was not possible to characterise the nanostructure via Fourier synthesis. From the peak position only the repeat distance could be evaluated, it amounts to d = 43.14 Å.
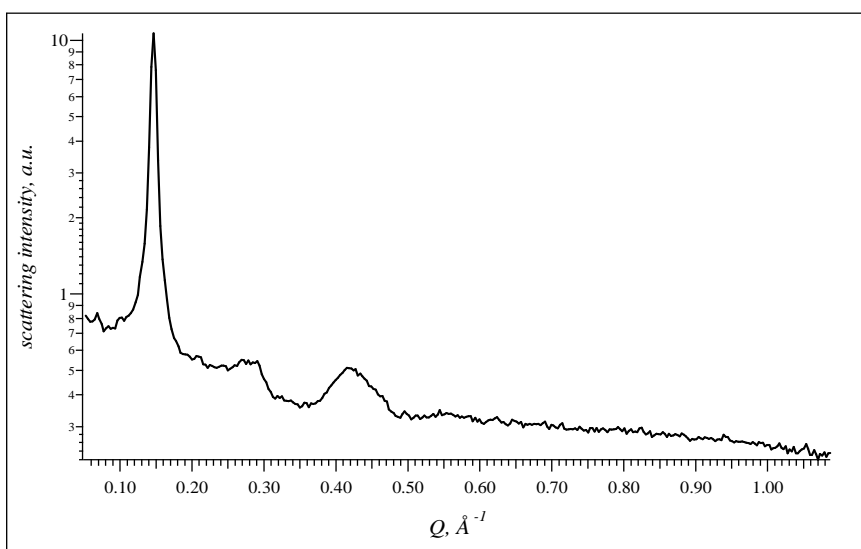
Fig. 6-12 Neutron diffraction pattern of the membrane composed of CER[NP]A/ CHOL/PA/ChS (55/ 25/15/5, w/w) at 8% D_2O, 20°C and 57% RH.

The presence of two double bonds in the CER[NP]A molecule effects the geometrical structure, causing a kink in the hydrocarbon chain of the CER[NP]A molecule. This disturbs the ordered array of the membrane lipids and thereby increasing the fluidity of the SC lipid model membranes [127]. Such an effect to the natural SC would result in an increased permeability

for substances. The question, which now needs to be answered is whether CER[NP]A can act as a penetration enhancer in the SC. For that purpose a model membrane composed of CER[AP]/CER[NP]A/CHOL/BA/ChS (27.5/27.5/25/15/5, w/w) was investigated. In Fig. 6-13 the corresponding diffraction pattern is presented.
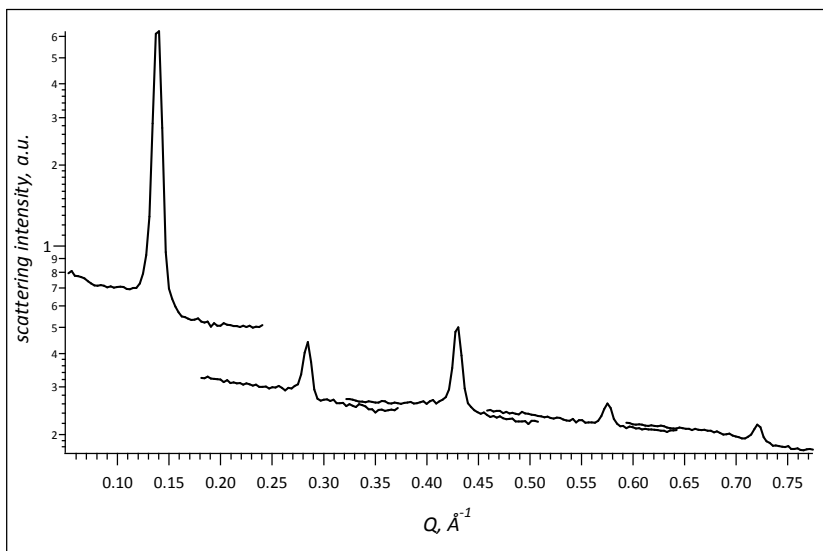
Fig. 6-13 Diffraction pattern of the model membrane with the following constituents: CER[AP]/CER[NP]A/CHOL/BA/ChS (27.5/27.5/25/15/5, w/w). The measurement was carried out at 57% RH, 20°C and a D_2O content of 8%.

Interestingly, the addition of CER[AP] to the system described above resulted in the formation of a well ordered lamellar system due to the stabilising effect of CER[AP]. This is in accordance with the *armature reinforcement model* ([82] and Chapter 2.4), where it was proposed, that the CER[AP] molecules act as an anchor and thereby providing the basis for the adhesion of the polar head groups of adjacent bilayers. Further, as can be seen from the neutron diffraction pattern depicted in Fig. 6-13 this system does *not* exhibit a FFA-rich phase. This phase was found to form in SC lipid model membranes based on CER[AP] and long chain FFA due to the mismatch of the hydrocarbon chain length as discussed in Chapters 4 and 5. It can therefore, be assumed that CER[NP]A acts as an solubiliser for the long chain FFA behenic acid (BA). To substantiate this finding BA was replaced by the longer chained FFA cerotic acid (CA) with 26 C-atoms. The corresponding diffraction pattern is presented in Fig. 6-14 in comparison with the sample containing only CER[AP] as ceramide fraction (CER[AP]/CHOL/BA/ChS, 55/25/15/5, w/w). As can be seen the diffraction peaks belonging to the FFA-rich phase are much less pronounced in the membrane containing CER[NP]A. Consequently, it can be concluded that indeed CER[NP]A acts as a solubiliser for the long chain FFA.
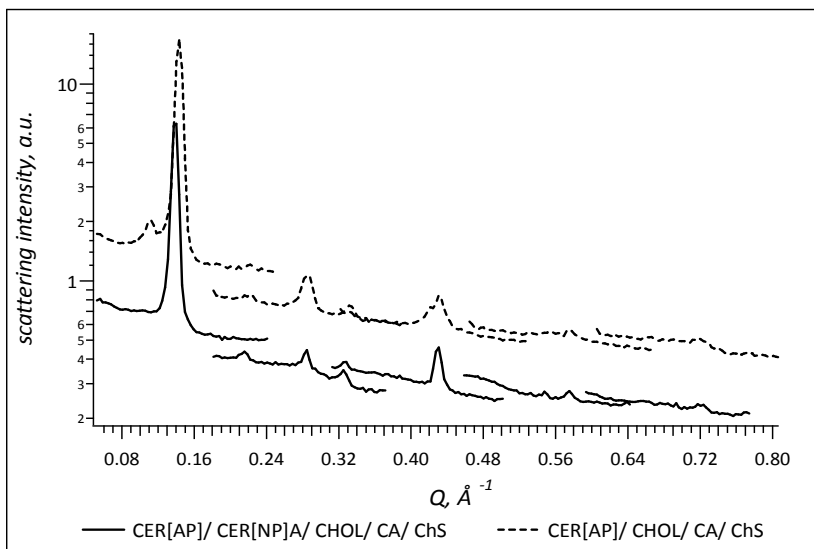
Fig. 6-14 Comparison of the neutron diffraction pattern of the membrane containing only CER[AP] (dashed line) and the system containing CER[AP] and CER[NP]A (solid line). The measurements were carried at 20°C, 57%RH and 8% D_2O.

In order to clarify the internal nanostructure the neutron SLD profile was calculated according to Eq. (3.12) for the system composed of CER[AP]/CER[NP]A/CHOL/BA/ChS and is presented in Fig. 6-15. It can be clearly seen, that there are no significant differences in the structural alignment between the membrane containing exclusively CER[AP] and the membrane consisting of the mixture of CER[AP] and CER[NP]A. The only slight difference between both SLD profiles originates from the double bonds of the CER[NP]A molecules. Their presences causes a small increase in the scattering length density in the CH_2-group region as indicated in Fig. 6-15.
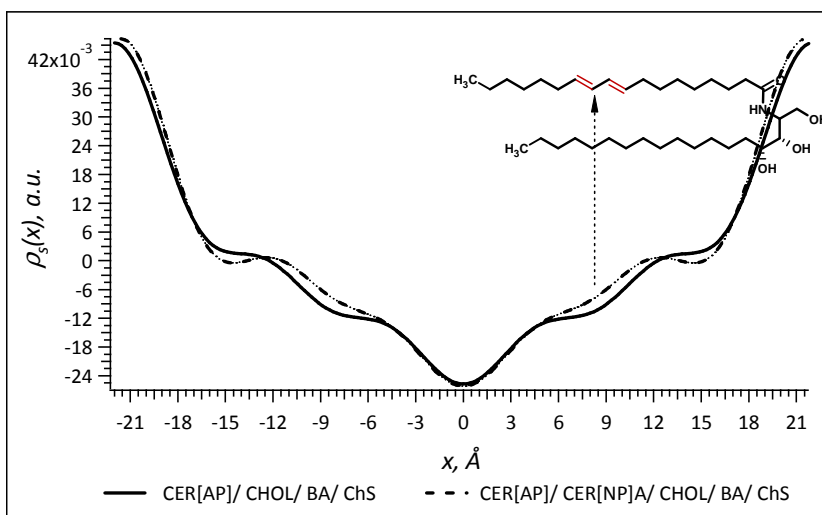
Fig. 6-15 Comparison of the neutron SLD profiles of the SC lipid model membranes containing either CER[AP] or the 1:1 mixture of CER[AP] and CER[NP]A as ceramide fraction.
The measurements were carried out at 8% D_2O, 57% RH and 20°C.

6.4   Summary and conclusion

In summary, it can be stated that the introduction of a double bond (or in case of CER[NP]A two double bonds) has a significant effect for the structural assembly of SC lipid model membranes.

In case of CER[NP]B the SC lipid membrane exhibited a three phase system in which the CER[NP]B molecules adopt different conformations, either the fully extended or V-shape conformation. Interestingly, all conformation coexist at defined conditions such as temperature and humidity, in contrast to pure CER[NP] where the conformations were found at different temperatures [125]. A phase separated membrane is a defective system in the sense of barrier function. Therefore, it can be assumed that CER[NP]B could act as an penetration enhancer as phase separation can increase the permeability of the SC lipid barrier.

Ceramide [NP]A-based model membranes on the other hand displayed a poor lamellar ordering, due to the two double bonds in the CER molecules. These double bonds can disturb the ordered structure of the SC lipids, therefore, the membrane fluidity is increased. An increased fluidity of the SC lipids causes an increased permeability of the intercellular lipid matrix of the SC. The insertion of CER[NP]A might disturb the natural barrier of the SC lipids, thereby acting also as an penetration enhancer. This question still needs to be answered.

Independently of the artificial CER[NP]-species the addition of CER[AP] resulted in well-oriented membranes in which the structural assembly is dictated by CER[AP]. The phase separated CER[NP]B-system disappeared, while mixtures of CER[NP]A and CER[AP] resulted in well-oriented lamellar membranes. Consequently, the driving forces for the assembling process are realised by the CER[AP] molecules.

The findings of this investigation further support the *armature reinforcement model* presented in Chapter 2.4.

7 Nanostructure of stratum corneum lipid matrices based on ceramides [EOS] and [AP]

7.1 Introduction

The intention of this study was to investigate SC lipid model membranes based on CER[EOS]/CER[AP]/CHOL/FFA, therefore containing the most relevant lipids in a near natural ratio. The corresponding SLD profile was used to describe the internal membrane nanostructure. Further, the influence of single defined lipid species on the membrane assembling process is discussed. To receive additional information concerning the position of a molecule within the lipid layer, specifically deuterated molecules were applied. Finally, the influence of hydration on the structure of this SC lipid model membrane shows to substantiate the creation of a superstable structure dictated by CER[AP].

7.2 Materials and methods

The stratum corneum (SC) lipid model membranes were studied in two different compositions as detailed in Table 7.1, whereby only the FFA component was changed. The preparation of the multilamellar lipid membranes is described in Chapter 3.4.

Composition	Ratio % (w/w)
CER[EOS]/CER[AP]/CHOL/palmitic acid	23/10/33/33
CER[EOS]/CER[AP]/CHOL/behenic acid	23/10/33/33

Table 7.1 Composition of the SC lipid model membranes.

All samples were measured in thermostated aluminium cans at the fixed temperature of 32°C and either 57% or 98% relative humidity (RH). The nanostructure of the bilayers was analysed by calculating the neutron scattering length density (SLD) profiles $\rho_s(x)$ as described in Chapter 3.3.2.

The localisation of a specific deuterium label within the lipid membrane is reflected by the positive difference in the SLD between samples containing either deuterated or protonated FFA. The detailed description can be found in Chapter 3.3.3.

7.3   Results and Discussion

7.3.1   Finding of an appropriate stratum corneum lipid matrix model

In this approach, the already by Kessner and co-workers [81] described ternary system CER[EOS]/CER[AP]/CHOL (33/22/45, w/w) was completed by a free fatty acid (FFA). Therefore, a lipid system composed of all three main constituents resembles the native SC lipid matrix to a high extent and can give more precise information concerning its properties.

The first step was to add the rather short chain FFA palmitic acid (PA) to the ternary SC lipid matrix because its chain length is in the range of the short chain ceramide [AP]. The diffraction patterns of the CER[EOS]/CER[AP]/CHOL/BA membrane showed reflections resulting from phase separated CHOL-crystals and phase separated PA (see Fig. 7-1).
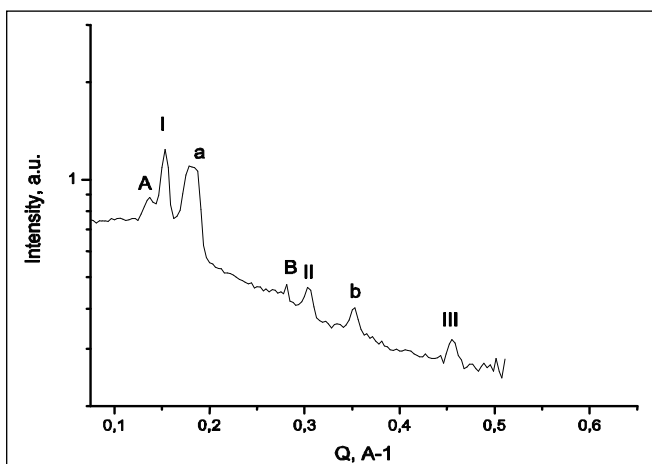
Fig. 7-1 Neutron diffraction pattern of the CER[EOS/CER[AP]/CHOL/PA membrane (23/10/33/33, w/w) at 57% RH, 50% D_2O and T = 32°C. The roman numbers indicate the 1st, 2nd and 3rd order diffraction peaks for the model membrane, the small letters assign the [010] and [020] diffraction peaks from pure CHOL crystals and capital letters indicate the diffraction of a PA-rich phase.

The characterisation of the internal membrane nanostructure could not be performed due to the strong phase separation (three different phases with low intensities). Only the lamellar repeat distance with d = 42.2 Å could be evaluated. In the next step, the FFA palmitic acid was substituted by the longer chained behenic acid (22:0). In the native SC the fraction of FFA mainly contains FFA with chain length in the region between C24 and C26 [54, 55]. Therefore, the use of long chained FFA in such SC model systems will resemble more closely the natural SC lipid matrix. For the mixture of CER[EOS]/CER[AP]/CHOL/behenic acid (BA), diffraction patterns were received as demonstrated in Fig. 7-2.
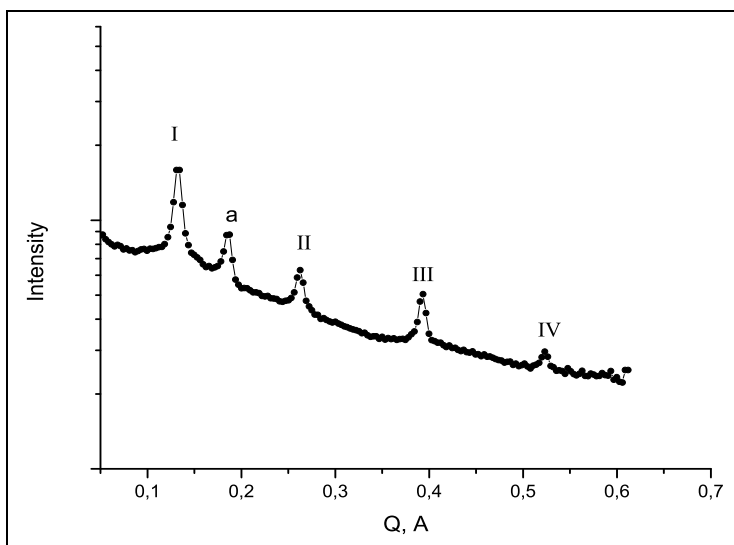
Fig. 7-2 Neutron diffraction pattern for the CER[EOS]/CER[AP]/ CHOL/BA membrane (23/10/33/ 33, w/w) at 57% RH, 50% D_2O and T = 32°C. The roman numbers indicate the 1st, 2nd, 3rd, and 4th order diffraction peaks for the model membrane and the small letter indicates the [010] diffraction peak from pure CHOL crystals.

These patterns exhibit a one-phase multilamellar membrane with only a small fraction of phase separated cholesterol crystals. The presence of small amounts of crystalline CHOL does not influence the multilamellar lipid organisation as described in other studies [119, 128, 72, 121].

A system composed of a long chain and a short chain ceramide combined with a long chain FFA as it is typical for the SC lipid matrix causes a reasonable miscibility of the lipids and a good solubility of cholesterol inside the model matrix. Interestingly, the amount of CER[AP] in this SC model system could be reduced upon addition of BA to the ternary system [81]. In order to characterise the internal membrane nanostructure, the neutron scattering length density profile (SLD) was calculated.

7.3.2 Discussion of the membrane profile

From the peak position the membrane repeat distance d was calculated to $d = (48.3 \pm 0.1)$ Å. Additionally, phase separated cholesterol crystals were present in the model membrane which can be deduced from the [010] reflection located at Q = 0.18 Å^{-1}, representing diffraction from the triclinic crystal as stated before [118]. In spite of the presence of the long chain ceramide CER[EOS], the long-periodicity phase, the LPP was *not* detected. In fact, a periodicity of approximately 48 Å indicated the presence of a bilayer in the range of two opposing CER[AP] molecules. This is consistent with the ternary system described by Kessner and co-workers [81].

A similar SC lipid model system composed of CER[AP]/CHOL/PA/ChS was described in detail previously [28] and was used as reference system. The comparability of the lamellar

repeat distances of the reference system ($d = 45.6$ Å) and of the presented system ($d = 48.3$ Å) allows the parallel presentation of both SLD profiles as demonstrated in Fig. 7-3.
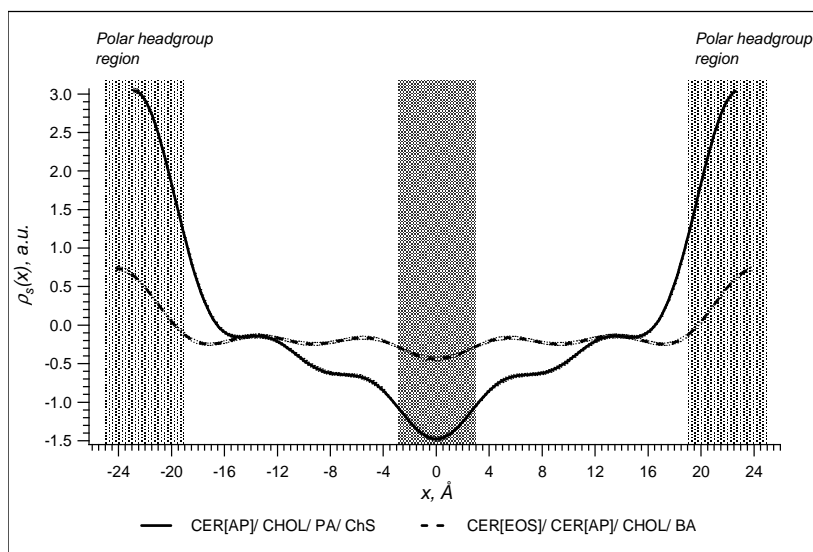
Fig. 7-3 Neutron SLD profile across the CER[EOS]/CER[AP]/CHOL/ BA membrane (23/10/33/ 33, w/w) at 57% RH, 8% D_2O and T = 32°C and the SLD profile of the CER[AP]/CHOL/PA/ChS (55/25/15/5, w/w) membrane measured under the same conditions.

In accordance to the observations for the ternary system based CER[EOS]/CER[AP]/CHOL the major results taken from the comparison of the SLD profiles of presented SC lipid model matrix with the reference membrane (CER[AP]/CHOL/PA/ChS) are the following:

(i)   The smaller scattering length density at the position of the polar head group region of the CER[EOS]/CER[AP]/CHOL/BA membrane is caused by the CH_2 groups of the CER[EOS] molecules, which protrude into the adjacent layer in order to fit into the membrane size created by CER[AP]. The negative scattering length density of the CH_2 groups ($-3.0 \times 10^9 cm^{-2}$) at the polar head group region leads to a reduction in the SLD of the polar head group region, while in the reference system the CH_2 groups are not present in this area and cannot produce such a reduction of the SLD.

(ii)   The minimum in the centre of the bilayer representing the CH_3 groups is less pronounced when compared to the reference system. This is an evidence, that also in the centre of the membrane CH_2 groups are present. Therefore, it can be stated again, that the long hydrocarbon chains of the CER[EOS] molecules protrude through the bilayer. This leads to an increase of the SLD because the CH_2 groups show a higher SLD compared to the CH_3 groups.

Taking both experimental results into account, it can be concluded that the arrangement of CER[EOS] inside the lipid matrix is similar to the already described ternary system [81]: CER[EOS] is positioned inside a phase with a short-periodicity by spanning a bilayer and extending into adjacent layer. In contrast to the ternary system, the presented SC lipid model matrix was completed by the inclusion of the long chain FFA behenic acid.

Furthermore, due to this FFA addition the amount of CER[AP] could be reduced from 22 to 10% (w/w), which is close to the fraction of CER[AP] found in human SC (4-7%) [129, 48].

In order to estimate the exact position of behenic acid inside this SC lipid model membrane partially deuterated behenic acid was applied.

7.3.3   Identification of the exact position of behenic acid inside the lipid matrix

To identify the exact position of the FFA in SC lipid model membranes based on the ceramides [EOS] and [AP] two membranes have been investigated, each contained partially deuterated BA. The exact composition is listed in Table 7.2.

Table 7.2 Composition of the model SC lipid system. Only the deuterated FFA component was varied.

CER[EOS]/CER[AP]/CHOL/d_7BA: EOS_d_7BA (23/10/33/33, w/w)	
CER[EOS]/CER[AP]/CHOL/d_{22}BA: EOS_d_{22}BA (23/10/33/33, w/w)	
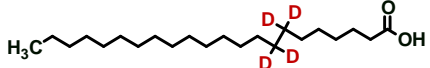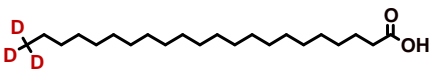
The calculated SLD profiles of the samples containing specifically deuterated BA revealed distinct differences when compared to the sample containing the protonated FFA. In Fig. 7-4 the comparison of the SLD profiles of the membrane containing either protonated BA (CER[EOS]/CER[AP]/CHOL/BA, EOS_BA) or deuterated BA (CER[EOS]/CER[AP]/CHOL/d_{22}BA, EOS_d_{22}BA) with the deuteration at the terminal methyl group is illustrated. The SLD profile of the deuterated SC model matrix shows a distinct maximum in the centre of the membrane (CH$_3$-group region), which is related to a high scattering length density of the terminal CD$_3$ groups of behenic acid.
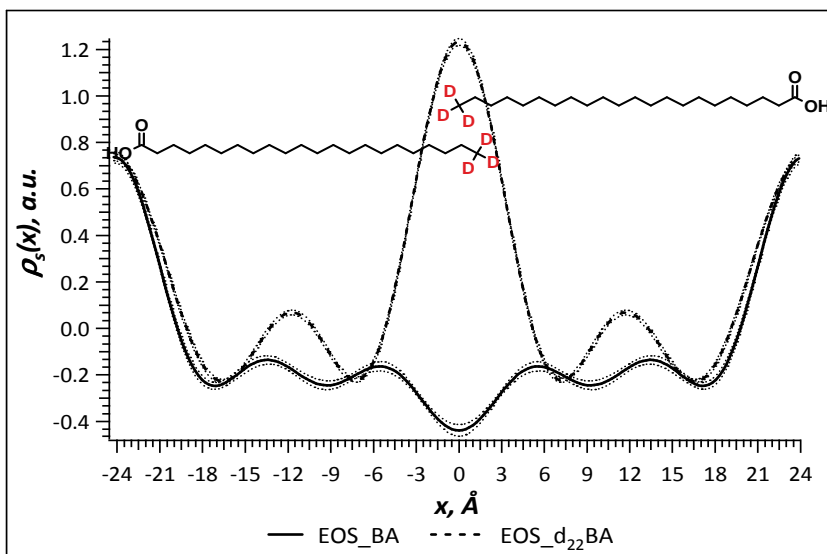
Fig. 7-4 Comparison of the neutron SLD profiles of a membrane composed of CER[EOS]/CER[AP]/CHOL/ and either protonated BA (EOS_BA, *solid line*) or deuterated d_{22}BA (EOS-d_{22}BA, *dashed line*) at T = 32°C, 57% RH and 8% D_2O. Dotted lines: corresponding errors. To visualise the proposed arrangement the molecular structure of d_{22}BA was introduced.

To further identify the exact position of the label within the membrane, the difference SLD profile $\Delta\rho_s^{Deut}(x)$ was calculated according to Eq. (3.13) and (3.12) and then fitted by a Gaussian function as can be seen in Fig. 7-5.
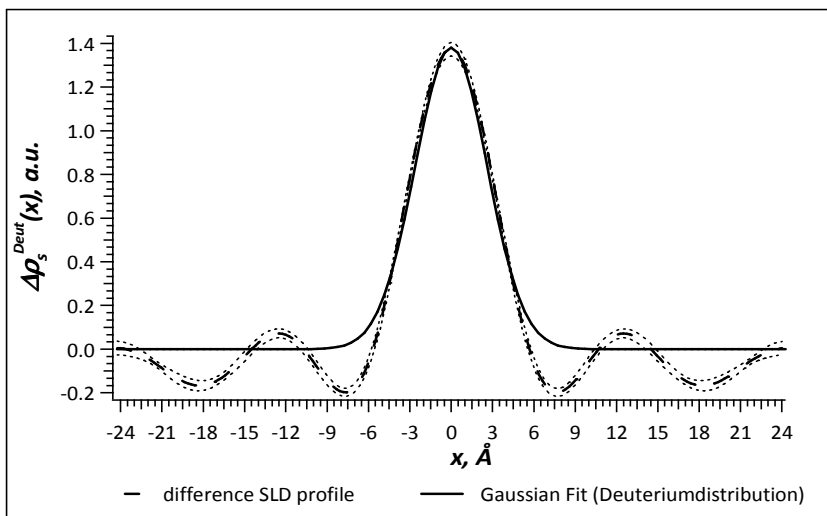
Fig. 7-5 Difference SLD profile for CER[EOS]/ CER[AP]/CHOL/d_{22}BA membrane (– – –). Dotted lines: corresponding errors to the difference SLD profile. Fat solid line: fit of the difference SLD by a Gaussian function (deuterium distribution)

The result of this fit is presented in Table 7.3. For this maximum with a fixed centre at x_0 = 0 Å, the full width at half height (FWHH) parameter equals approximately 6 Å (region from -3 to 3 Å). The latter comprises the membrane region in which the terminal alkyl groups interdigitate and therefore, a high density of deuterium atoms appears. The maxima at the edges of the profile are attributed to the polar head group region [28]. The high scattering length at approximately -15 and 15 Å corresponds to the position of cholesterol [57].

Table 7.3 Lamellar repeat distance d and the position x of the deuterated label of the FFA inside one lipid leaflet for each deuterated FFA containing membrane at 32°C, 8% D_2O and 57% RH.

SC lipid model membrane	d , Å	Position x of label, Å
EOS_d_{22}BA	48.52 ± 0.27	CD_3-group: 0.00 ± 0.09
EOS_d_7BA	48.28 ± 0.08	CD_2-groups ±: 16.10 ± 0.09

The same procedure was applied to the sample containing BA specifically deuterated in the methylene group region (CER[EOS]/CER[AP]/ CHOL/ d_7_BA; EOS_d_7BA). The comparison of the SLD profiles of the protonated and deuterated sample as well as the difference SLD $\Delta\rho_s^{Deut}(x)$ of both are presented in Fig. 7-6 and Fig. 7-7, respectively.
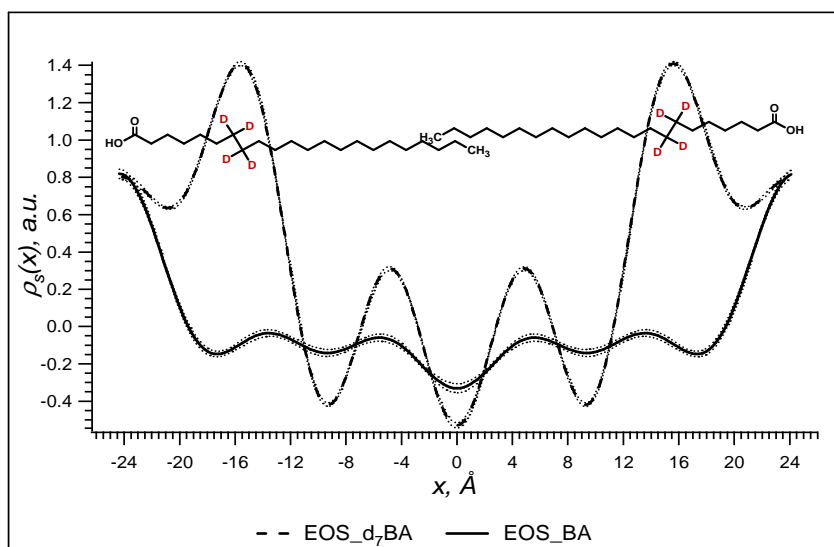
Fig. 7-6 Comparison of the SLD profiles of the membrane composed of CER[EOS]/CER[AP]/CHOL/ and either protonated BA (EOS_BA, *solid line*) or deuterated d_7BA (EOS_d_7BA, *dashed line*) at T = 32°C, 57% RH and 8% D_2O. Dotted lines: corresponding errors. To visualise the proposed arrangement the molecular structure of d_7BA was introduced.

Next to the two maxima belonging to the polar head groups, the membrane profile of CER[EOS]_d_7BA shows two additional maxima which were assigned to the labelled CD_2-groups with a high density of deuterium atoms and with positive coherent scattering length density. After the calculation of the difference SLD profile (see Fig. 7-7) both maxima have been fitted by a Gaussian function and the centre of both Gaussian function was determined at $x_{C_7D_2,C_8D_2}$ = 16.10 and -16.10 Å, respectively (see also Table 7.3)
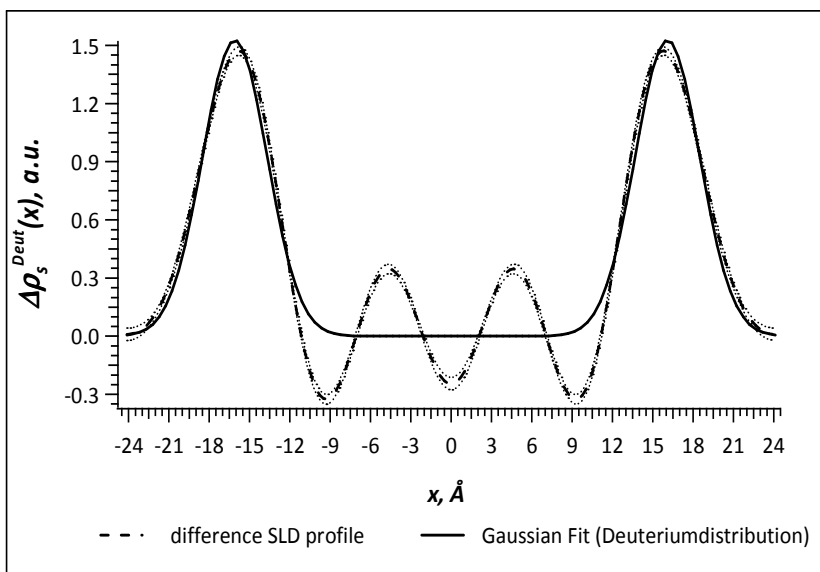
Fig. 7-7 Difference SLD profile for CER[EOS]/ CER[AP]/CHOL/d_7BA membrane (− − −). Dotted lines: corresponding errors to the difference SLD profile. Fat solid line: fit of difference SLD by two Gaussian functions (deuterium distribution).

To visualise this result, the following model was applied: A bilayer, formed by two opposing BA-molecules reveals a repeat distance d of approximately 55 Å, estimated by the values of 1.5 Å for a CH_3-group and 1.25 Å for one CH_2-group [122]. When this hypothetical BA-bilayer is compared to the SC lipid model system which exhibits a d-value of approximately 48 Å, a difference of about 7 Å occurs. It was supposed that this difference between both hypothetical and real membrane is compensated by the interdigitation of the terminal butyl (5.25 Å) or pentyl (6.5 Å) residues of the behenic acid chain in the SC lipid membrane. The relevant maxima of the deuterium distribution $\Delta\rho_s^{Deut}(x)$ correspond to the region of C_7D_2-C_8D_2 with the centre x at 16.1 Å and -16.1 Å, respectively (see Fig. 7-6). From the full width at half height (FWHH) it can be deduced, that the CH_2-groups region represents the largest region within such a membrane [28]. Therefore, the FWHH (5.67 Å) comprises the region with the highest density of deuterium atoms. This region can be calculated as 16.10 ± ½ FWHH (± 13.27 Å to ± 18.94 Å). In the hypothetical behenic acid bilayer, the position of C_7 and C_8 may be estimated as $x_{C_7H_2-C_8H_2}$ = +18 Å and -18 Å, respectively. Related to the fitted position at 16.10 Å, the difference of approximately 1.9 Å would indicate only an interdigitation of the terminal propyl-residue. Consequently, a shift of the position of C_7D_2-C_8D_2 from 18 Å to 13 Å would be inside these error margins for the case of an interdigitation of terminal butyl residues in the centre of the membrane. Due to truncation errors of the applied Fourier synthesis, the centre of the membrane profile cannot be taken into account.

The evidence of a stretched, gel-like conformation of the BA molecule arises from the condensing effect of cholesterol on acyl chains [58, 60]. Cholesterol forces the *trans* conformation of the chains and decreases the tilt angle. In a recent study it is suggested that short chain ceramides, may have, like cholesterol a similar ordering effect themselves [130].

Summarising, the study of the SC lipid model matrices composed of CER[EOS]/CER[AP]/CHOL/ containing either protonated or deuterated BA showed the arrangement of the FFA inside the bilayer. The application of specific deuterated BA-derivatives caused different local contrasts and therefore, the labelled molecular regions could be identified inside the membrane profile.

7.3.4 Influence of hydration on the membrane structure

In order to deepen our knowledge about the SC model systems based on the ceramides [EOS] and [AP] the influence of hydration on the membrane structure was studied. In the work of Raudenkolb and co-workers it was concluded that the SC lipids, in particular the ceramides show only a small tendency to bind water [131].

The model system CER[EOS]/CER[AP]/CHOL/BA (23/10/33/33, w/w) was measured at 57% relative humidity (RH) and 98% RH, respectively (see Appendix D). From the peak position the lamellar repeat distances d were calculated and amount to d = 48.3 Å at 57% RH and 48.4 Å at 98% RH, respectively. Because of the almost identical values of the periodicities, a minimal influence of the degree of humidity on the hydration behaviour of the lipids as well as on the membrane structure was concluded. From the calculated neutron scattering length density profiles several membrane parameters were determined by applying a fit-procedure as described in the work of Kiselev and co-workers [28]. The results are summarised in Table 7.4.

Table 7.4 Membrane parameters as taken from the neutron scattering length density profile

EOS_BA, humidity	molecular group	X_0, Å[*]	σ, Å	FWHH, Å[†]
57% RH	Polar head groups	24.15	2.43 ± 0.03	5.49 ± 0.06
98% RH	Polar head groups	24.20	2.36 ± 0.03	5.78 ± 0.14

($^*x_0 = \dfrac{d}{2}$ is fixed; †FWHH= $2\sigma\sqrt{2\,ln\,2}$)

As pointed out already in Chapter 4 the dependence of the SLD on the D_2O content in water vapour enables the calculation of the water distribution function ρ_w across the bilayer according to Eq. (4.2b). In order to compare the water distribution across the bilayer at the different relative humidities the water distribution function was calculated for the EOS_BA membrane at 57% RH and at 98% RH, respectively. Fig. 7-8A and B show ρ_w across the membrane at 57% RH (A) and at 98% RH (B), respectively. The minima and maxima in the centre of the membrane are due to truncation errors.
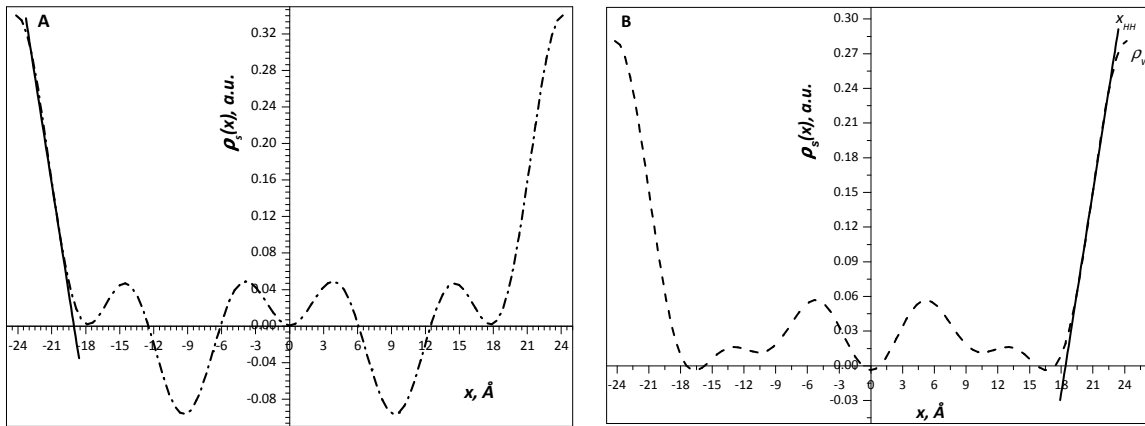
Fig. 7-8 Water distribution function $\rho_w(x)$ across the CER[EOS]_BA membrane at 57% RH (*A*) and 98% RH (*B*), respectively. The *HH* boundary is determined via linear fit as demonstrated here.

As described in Chapter 4, the hydrophilic-hydrophobic (*HH*) boundary determines the thickness of the hydrophilic as well as lipophilic part of the bilayer. The position of the *HH* boundary for the SC lipid model membrane at each humidity as well as the thickness of the hydrophobic and hydrophilic layer are summarised in Table 7.5. From those results it can be concluded, that although the value for the thickness of the hydrophilic layer is slightly higher at 98% RH, there are no significant changes due to the hydration process.

Table 7.5 Structural parameters of the membrane containing behenic acid at 32°C and 8% D_2O at different humidities.

EOS_BA, humidity	d , Å *	x_{PH} , Å †	x_{HH} , Å ‡	Thickness of hydro-phobic layer, Å	Thickness of hydro-philic layer, Å
57% RH	48.3 ± 0.1	24.15	19.0 ± 0.5	38.1 ± 0.9	5.1 ± 0.5
98% RH	48.4 ± 0.1	24.20	18.4 ± 0.6	36.8 ± 1.2	5.8 ± 0.6

* d ... repeat distance, $^+$ x_{PH} ... position of polar head groups, ‡ x_{HH} ... hydrophilic-hydrophobic boundary

As it was described by Kiselev et al. 2005, SC lipid model membranes based on CER[AP] do not show a region of intermembrane space at 57% RH [28]. From the neutron SLD profile it can be derived, that the present model matrix, EOS_BA and the reference system share an extremely small intermembrane hydration of approximately 1 Å. This value was received as difference between the d -spacings at 57% RH and at water excess in the work of Kiselev and co-workers [28]. Consequently, the head groups of the neighbouring leaflets are positioned close to each other. The distance between the two adjacent maxima of the head groups d_{PH} is equal to the membrane repeat distance d_m. Therefore, the position of the polar head groups x_{PH} is determined by $d_m/2$, whereby the x_{PH} -value increases with increasing hydration. From that fact it can be deduced, that the hydration of the polar head groups

increases. This theory is drawn upon the increasing value of the FWHH, indicating an enhancement of the area per head group at 98% RH. The low intermembrane space does not allow the calculation of the thickness of the water layer d_w as $d_W = d - d_m$ as the space resolution according to $0.6 \cdot d / h_m$ (h_m = number of diffraction orders) was calculated to 5.8 Å [28]. In the presented work, a difference of 0.1 Å was observed between the periodicities of the membrane measured at 57% RH and at 98% RH, respectively. This distinction could be inside certain error margins, indicating that no significant influence of hydration on the membrane assembling process occurs. On the other hand, based on the membrane parameters taken from the SLD profiles $\rho_s(x)$, a slight increase of the hydration of the head groups at higher humidity may be supposed.

7.4   Summary

Summarising, it can be stated that the SC lipid model system composed of CER[EOS]/CER[AP]/CHOL/BA (23/10/33/33, w/w) represents a reasonable model of the native lipid matrix. The composition comprises the three major lipid classes in an appropriate ratio. Inside the ceramide fraction, the model contains the ceramide [EOS] which is attributed to be crucial for the proper skin barrier function, in particular for the formation of the long-periodicity-phase [23, 24]. Behenic acid represents the most abundant subtype of the skin's free fatty acids [2]. The presented quaternary system forms multilamellar oriented bilayers and supplies reasonable good diffraction patterns in the neutron experiments. By analysing the neutron scattering length density profiles, the arrangement of all lipid components inside the lipid matrix was concluded as visualised in Fig. 7-9.
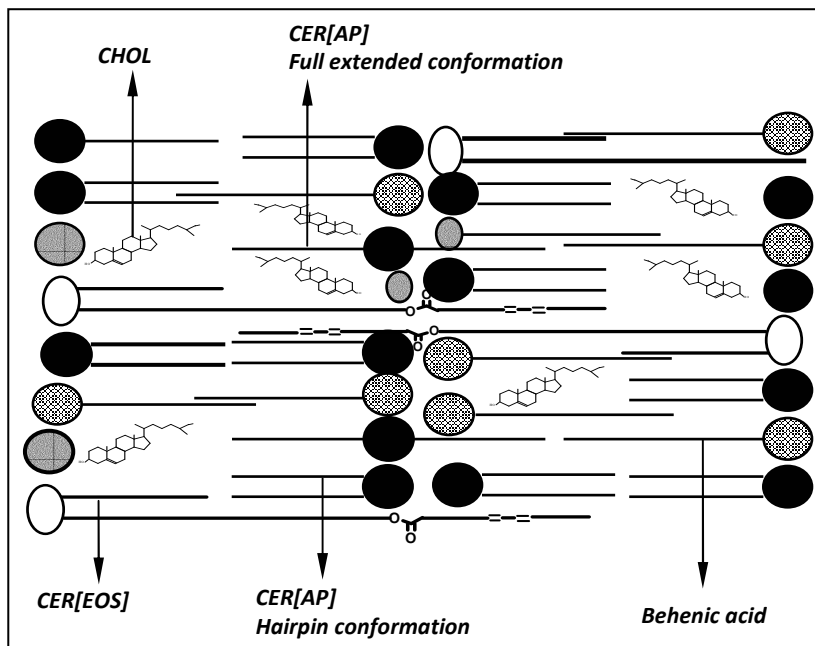
Fig. 7-9 Schematic presentation of the CER[EOS]/CER[AP]/CHOL / BA (23/10/33/33, w/w) model matrix.

Numerous former studies proclaimed the co-existence of two lamellar phases in the SC, the short-periodicity-phase (SPP) of approximately 60 Å and the long-periodicity-phase (LPP) of approximately 130 Å [20, 77, 25]. The latter is particularly associated with the presence of ceramide [EOS], which therefore, is regarded to be a prerequisite for proper barrier functions. The existence of the LPP including its organisation and the inducing or preventing conditions for its formation are currently a matter of debate [69, 68]. From X-ray diffraction patterns of ceramide [EOS] as bulk substance at hydrated state, the formation of a phase with a periodicity of approximately 130 Å could be proven [132]. But in mixtures with other prominent SC lipids, in particular with ceramide [AP], a multilamellar membrane based on ceramide [EOS] only exhibits the formation of a short-periodicity phase. In Chapters 4 and 5 As it was reasoned that this characteristic phase is predominantly induced by the short chain ceramide [AP], which is characterised by a distinct head group polarity. Therefore, it can be concluded that the influence of the head group polarity exceeds the influence of the chain length in terms of the membrane assembling, which is in accordance with previously reported results [81].

8   Phase state and structure of stratum corneum model membranes based on ceramide [AP]

8.1   Thermotropic phase behaviour of SC lipid model systems and phase separation of behenic acid in multilamellar SC lipid layers

Submitted to: *Chemistry and Physics of Lipids (as Part I)*

8.1.1   Introduction

In order to understand the driving forces of lipid self-organisation, to get insights into the process of annealing of the stratum corneum lipid model membranes, the formation of different phases and segregation effects, thermal analysis such as differential scanning calorimetry can provide information. Further information on molecular dynamics is available for the analysis of Raman spectroscopy data. In addition to above mentioned studies, the application of neutron diffraction directly enables the analysis of the thermotropic phase behaviour of a lamellar organisation. The presented study should contribute to elucidate the miscibility and the phase separation of the free fatty acids in multilamellar stratum corneum lipid layers

8.1.2   Applied methods

8.1.2.2   Preparation of SC lipids membranes

For the differential scanning calorimetry (DSC) and Raman spectroscopy measurements the lipids were dissolved in the appropriate ratio (CER[AP]/CHOL/BA/ChS, 55/25/15/5, w/w) in a chloroform:methanol mixture (2:1, V/V) after which the solvent was removed by evaporation at room conditions. The samples were kept at room conditions thereafter for one day prior to the DSC or Raman spectroscopy measurement.

For the neutron diffraction experiment the SC model membrane composed of the same composition was prepared as described in Chapter 3.4.

8.1.2.3   Differential scanning calorimetry

The quaternary SC lipid mixture as well as the solitary lipids were measured with the Netzsch DSC 200 differential scanning calorimeter (Netzsch Gerätebau, Selb, Germany) in the temperature range from 20 to 120°C with a scan rate of 5 K min^{-1}.

8.1.2.4   Raman spectroscopy

The Raman spectra were recorded by means of a Bruker Fourier transform (FT) Raman spectrometer RFS 100/S (Bruker Optics, Ettlingen, Germany). The source of excitation was a diode pumped Nd:YAG laser with an operating wavelength of 1063 nm. The spectra were acquired typically with 200 scans and a laser power of 350 mW at the sample location. For spectra with a resolution of 4 cm^{-1} the interferograms were apodised with a Blackman-Harris four term function and Fourier transformed. The samples were placed in X-ray capillaries and sealed airproof. For the temperature-dependent measurement the samples were studied in the range from 25 to 98°C. After each temperature step, the sample was equilibrated for 5 minutes to stabilises the temperature within the sample. The manipulation and evaluation of the Raman spectra were carried out using the Bruker OPUS software, whereby the Raman intensities were determined as integrated band intensities.

8.1.2.5   Temperature scan in the neutron diffraction experiment

The temperature scan was performed in 5 K steps until the temperature of 65°C (at 57% RH) or 55°C (at 98% RH), respectively was reached. Following each temperature step the sample was equilibrated for one hour, after which the scattering intensities I of the first diffraction order was recorded as described in detail in Chapter 3.3.1. The temperature scan at 57% RH was measured at 100% D_2O, whereas the scan at 98% RH was performed at 8% D_2O. In order to get information about the phase transitions and structural changes the absolute value of the structure factor (SF) for each temperature point was calculated according to Eq. (3.10).

8.1.3   Result and Discussion

8.1.3.1   Differential scanning calorimetry of a SC lipid mixture

Fig. 8-1 demonstrates the thermograms of the SC lipid model system composed of CER[AP]/CHOL/BA/ChS acquired during the first and second heating scan in comparison with the thermograms of the pure constituents.
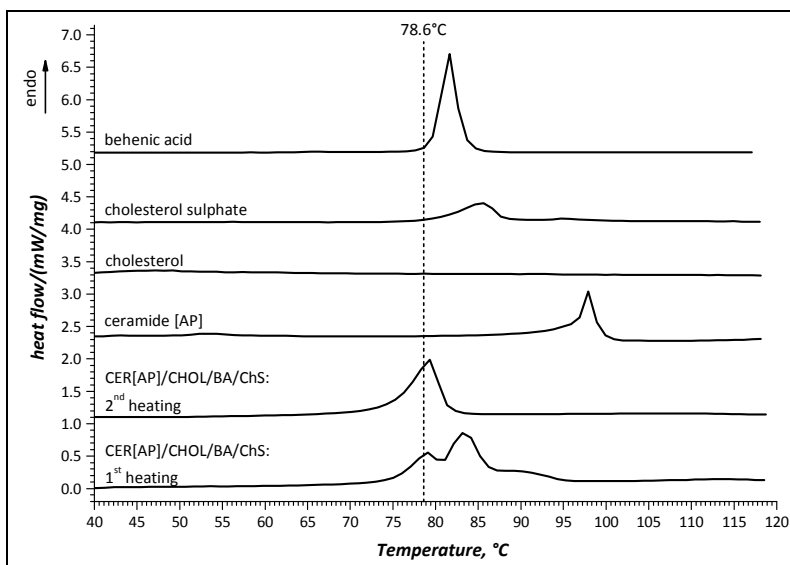
Fig. 8-1 DSC curves of the SC lipid model membrane composed of CER[AP]/CHOL /BA/ChS (55/25/15/5, w/w) acquired during first and second heating in comparison with the pure constituents.

The thermograms of this mixture show two endothermic phase transition peaks positioned at 78.6 and 83.5°C, respectively at first heating scan. As both peaks cannot be assigned to one of the peaks belonging to the pure constituents, it can be assumed that some sort of mixing of the lipids occurred, but that the lipids are not completely mixed. During the second heating scan these two peaks merge into one relatively sharp endothermic peak at 79.1°C, indicating that now all lipids participate at the main phase transition process. This mixing effect is persistent even when the sample is cooled down and heated for a third time, which proves that now the lipids are mixed in one phase and that the new created lipid mixture is stable (see Fig. 8-2). Presumably, the peak acquired during the second heating scan represents the main phase transition of the lipid mixture from gel to liquid crystalline phase, connected with the decrease of hydrocarbon chain order. This is consistent with results described previously for similar SC lipid mixture [133].
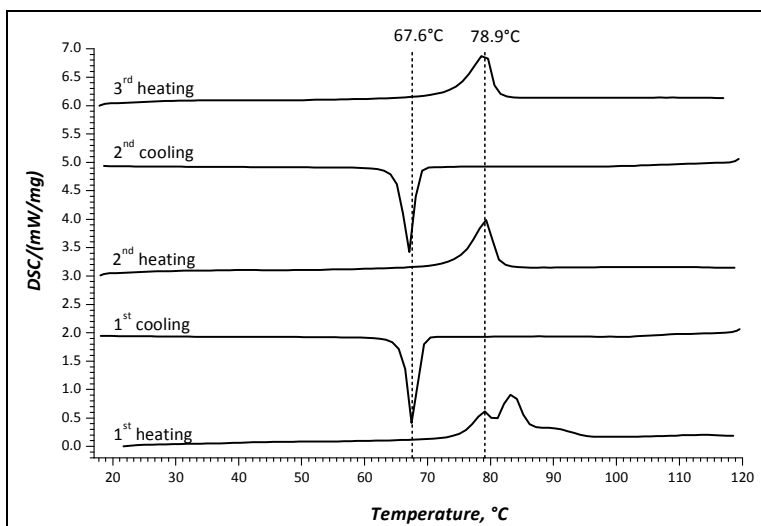
Fig. 8-2 DSC scans of the quaternary SC lipid mixture recorded during the first to third heating (top) and first to second cooling (bottom) process.
Scan rate: 5 K/min

When the heating and cooling scans are compared as demonstrated in Fig. 8-2 the SC lipid mixture shows a pronounced hysteresis of approximately 10°C. Such an effect was already reported for systems like phospholipids [134-136]. The appearance of a hysteresis upon cooling the sample from liquid crystalline indicates a delayed reformation of the ordered phase due to the very slow kinetics for the formation of the gel phase as described in literature [134-136]. The transformation occurring during the first heating scan are not reversible, indicating that the new system is more stable. On the other hand, the transformations taking place after the first heating are completely reversible as demonstrated by the third heating scan, which show the same thermotropic phase behaviour then during the second heating process.

The presented results from the DSC experiment underline the necessity of the annealing procedure described in Chapter 3.4. The lipids need to be ideally mixed, before oriented multilamellar SC lipid membranes necessary for the neutron diffraction experiment can be created.

8.1.3.2   *Raman spectroscopic investigation of quaternary SC lipid mixtures*

In general, hydrocarbon chains in crystalline state are in a highly ordered "zig-zag" structure which contains a high number of *trans* conformers with small amounts of conformational perturbation, by *gauche* conformers. As the temperature increases the chain disorder increases accordingly and the number of *gauche* conformers grows. With a decreased chain order the flexibility of the chain is increased.

Raman spectroscopy is a well established method for analysing the chain packing of lipids, the order/ disorder behaviour and the population of *trans* and *gauche* conformers. In Fig. 8-3 a typically FT-Raman spectra of the SC lipid system composed of CER[AP]/CHOL/BA/ChS is displayed at selected temperatures. The relevant Raman modes have been indicated.
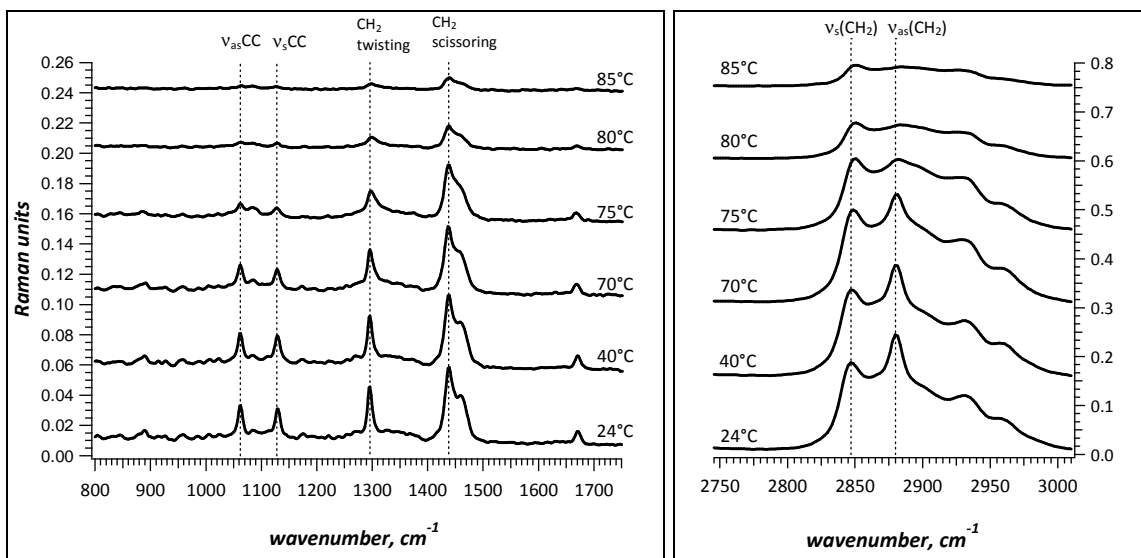
Fig. 8-3 FT-Raman spectra of CER[AP]/CHOL/BA/ChS (55/25/15/5, w/w) as a function of temperature in the spectral interval 800 – 1750 cm^{-1} (left) and in the CH$_2$ stretching region from 2750 – 3000 cm^{-1} (right). The regions for the C-C stretching ($\nu_{as/s}(CC)$), CH$_2$ twisting and CH$_2$ scissoring have been highlighted.

It is generally accepted, that the degree of the alkyl-chain order is elucidated by the band position of the symmetric CH$_2$ stretching wave number $\nu_s(CH_2)$ and by the intensity ratio of the asymmetric to the symmetric CH$_2$ stretching vibration [137]. The lower the value for the band position of the symmetric CH$_2$ stretching vibration, the higher the content of *trans* conformers and the degree of order [94, 95, 90]. The thermotropic response of the CH$_2$ symmetric stretching vibration $\nu_s(CH_2)$ of the CER[AP]/CHOL/BA/ChS mixture is provided in Fig. 8-4. The low value of the $\nu_s(CH_2)$ of 2847.2 cm^{-1} (25°C) indicates a high number of *trans* conformers in the alkyl-chain region [138, 139]. As the temperature increases the wave number of $\nu_s(CH_2)$ increases continuously, indicating that also the order of the chains in the quaternary system decreases. Between 70 and 75°C the wave number drastically shifts of approximately 1 cm^{-1} to 2850.1 cm^{-1}, representative for the beginning of the melting process of the hydrocarbon chains. This is consistent with the data received from the DSC experiment, where the melting process was evaluated to start also around 70°C (onset temperature of first and second heating, respectively.) Furthermore, the increase in the $\nu_s(CH_2)$ is also in accordance with results received from the analysis of hydrated SC and extracted SC lipids [140, 141].
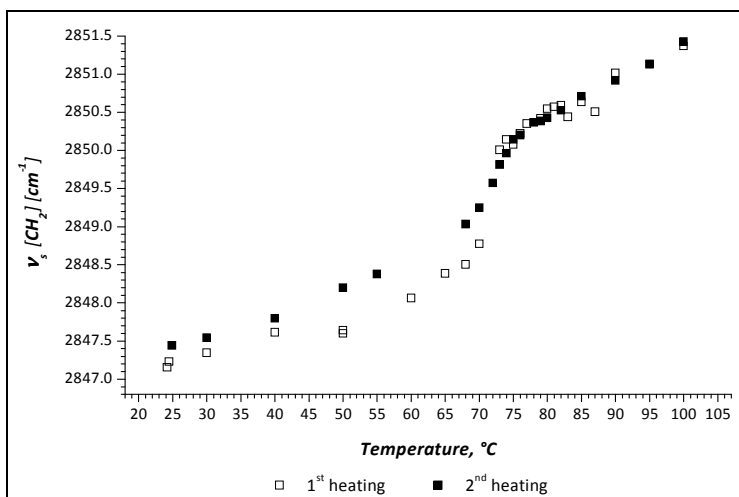
Fig. 8-4 Peak position of symmetric CH_2 stretching mode $\nu_s(CH_2)$ in dependence of the temperature.

The relative population trans/gauche is calculated as the ratio of the integral intensity of the asymmetric and symmetric CH_2 bands:

$$I_{\nu_{as}/\nu_s} = \frac{\int \nu_{as}(CH_2)}{\int \nu_s(CH_2)} \qquad (8.1)$$

Fig. 8-5 demonstrates the temperature-dependent intensity ratio of symmetric and asymmetric CH_2 stretching mode. During the heating process a continuous increase of *gauche* conformers can be observed as the decrease of the intensity ratio. In the range of the phase transition, between 65°C to 83°C the intensity ratio drops down by 0.3, as observed with the DSC measurement. There, the second heating is also different from the first heating process. The intensity ratio starts at a lower level when the second heating is performed. This indicates, that the amount of *gauche* conformations is increased, compared to the initial state.
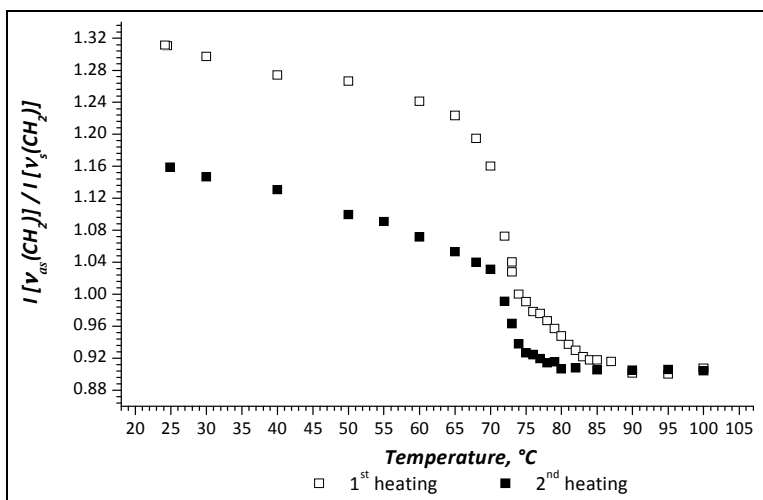
Fig. 8-5 Temperature dependence of the intensity ratio the SC lipid model system composed of CER[AP]/CHOL/ BA/ChS (55/25/15/5, w/w).

Information about the lateral packing of the lipids of this mixture can be obtained by analysing the region of the CH_2 scissoring bands. There, no factor group splitting could be

observed, indicating that the alkyl chains of this SC lipid mixture are packed in a hexagonal subcell (see Fig. 8-6). In contrast, Bouwstra and co-workers [24] stated, that in equimolar mixtures of human ceramides (HCER), cholesterol and free fatty acids (FFA) the lipids are mainly packed in an orthorhombic subcell, while equimolar mixtures of HCER and cholesterol have a hexagonal arrangement. They therefore concluded, that the FFA are crucial for the formation of the orthorhombic chain packing [52, 142]. A reason for this discrepancy could be, that the mixture under investigation contains only one ceramide and one FFA species, and in the before mentioned studies mixtures of isolated HCER and different FFA were used. Another reason may be, that the amount of behenic acid used in this study was *only* 15% (w/w), while in the investigations by de Jager and co-workers equimolar mixtures of HCER, cholesterol and different FFA were used. Therefore, it can be assumed that the amount of FFA in the presented study was not sufficient for the formation of the orthorhombic chain packing. As depicted in Fig. 8-6 (right) behenic acid alone shows the factor group splitting indicative for the orthorhombic chain packing of the alkyl-chains. Consequently, it was concluded, that a higher fraction of FFA in the mixture can superimpose its lateral chain packing to the other participants.
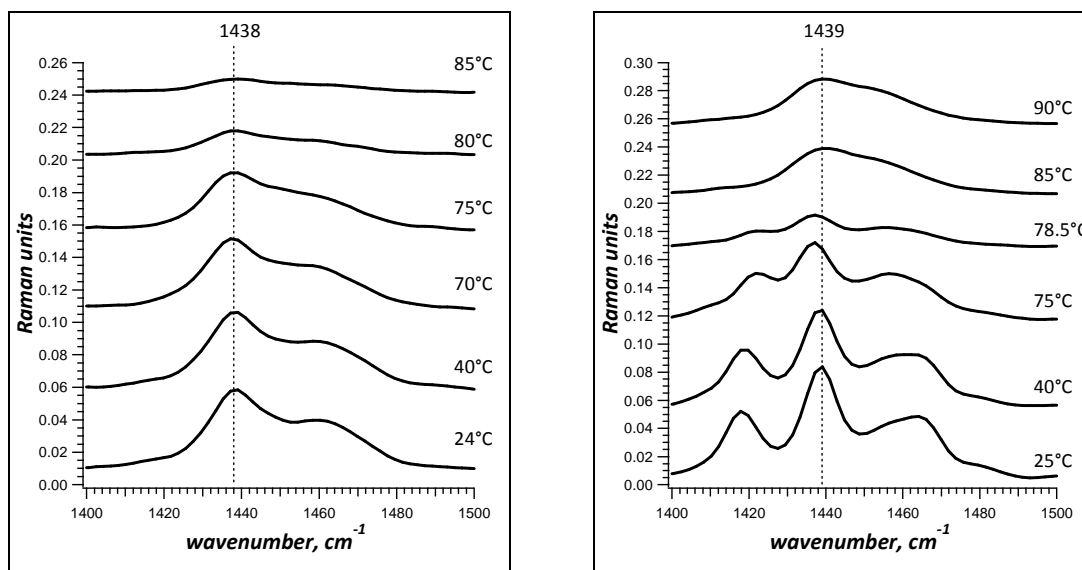
Fig. 8-6 FT-Raman spectra of CER[AP]/CHOL/BA/ChS (55/25/15/5, w/w) (left) and of behenic acid (right) as a function of temperature in the spectral interval 1400 – 1500 cm^{-1}
The respective regions for the CH$_2$ scissoring mode are indicated.

Both DSC and Raman spectroscopy provide no information on the lamellar organisation of the SC lipid membrane. Furthermore, no information on the solubility of the fatty acid within the lamellar phase created by CER[AP] is available. For that purpose the lipid model system was investigated as oriented multilamellar membrane with neutron diffraction.

81

8.1.3.3   Thermotropic investigations with Neutron diffraction

As described in Chapter 4 two phases coexist in SC model membrane. Accordingly, the phases were assigned as BA-rich phase (small scattering intensity) and main phase (main scattering intensity).

The dependence of the membrane repeat distance d on the temperature is depicted in Fig. 8-7 for both phases at two different humidities, 57% RH (*A*) and 98% RH (*B*), respectively. Independently of the relative humidity, both phases show a decrease in the repeat distance d as the temperature the increases. The respective decrease of the lamellar spacings are listed in Table 8.1.

Table 8.1 Temperature and humidity dependence of the membrane repeat distance of the respective phase, retrieved from the peak positions using Eq. (3.6). The highest temperature at 57% RH was 65°C, whereas 55°C at 98% RH.

Relative humidity	BA-rich phase		main phase	
	d_1, Å at 20°C	d_1, Å at 65°C / 55°C	d_2, Å at 20°C	d_2, Å at 65°C / 55°C
57%	44.6 ± 0.04	43.2 ± 0.01	46.9 ± 0.9	45.6 ± 0.4
98%	46.1 ± 0.02	43.2 ± 0.06	48.5 ± 0.6	46.1± 0.3
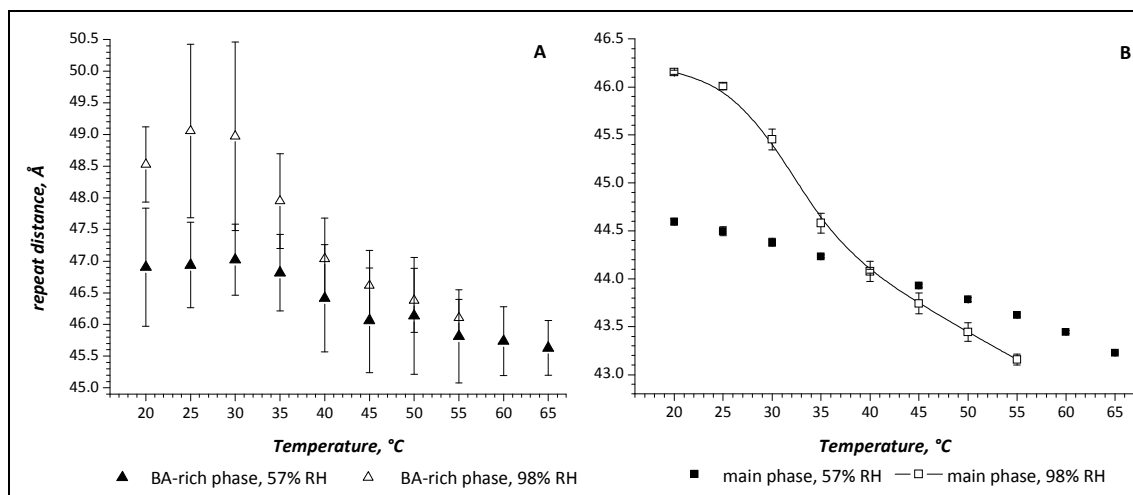
Fig. 8-7 Temperature dependence of the repeat distance d. Both phases show a decrease of d at increasing temperature.
A: BA-rich phase at 57% RH (closed triangles) and at 98% RH (open triangles).
B: main phase at 57% RH (closed squares) and at 98% RH (open squares).

This decrease in the repeat distance can be explained by the partial chain melting of the lipids at higher temperature and with the resulting increase in membrane disorder. These SC lipid model membranes do not show a region of intermembrane space in contrast to phospholipids [28], therefore, the head groups of adjacent bilayers are very closed to each

other. The thickness of the intermembrane space amounts to approximately zero at 57% RH, the region which is hydrated by the water molecules is very small. Consequently, changes in the thickness of the intermembrane space cannot be the reason for the decrease in the membrane repeat distance. A reasonable explanation for this behaviour at increasing temperatures can, therefore, only be the melting of the chains along with the increase of surface area per lipid molecules under hydrocarbon chain disorder. This is in accordance with the results received from the Raman spectroscopic investigations.

The comparison of the temperature-dependent change in the lamellar spacing at low humidity (57% RH) with the alterations occurring at high humidity (98% RH) is also depicted in Fig. 8-7 for the main phase. There, the swelling of the membrane due to the higher hydration level at 98% RH up to the temperature of 40°C is apparent. This is a typical property of a multilamellar lipid membrane [143]. In contrast to the almost linear decrease at 57% RH, the main phase shows at 98% RH not a gradual reduction of the repeat distance, but a region of phase transition in the range from 30°C to 40°C. This region of phase transition could be explained by the chain transformation from highly ordered *trans*-conformation to the lower ordered *gauche*-conformation. The appearance of a temperature-interval of 30-40°C instead of a sharp phase transition can be explained by the fact that the SC lipid system is composed of different types of lipids. These lipids have all different phase transition temperatures which cause the "overlapping" detected as temperature-interval.

As stated before, this phase transition interval cannot be observed at the lower humidity of 57% RH. The phenomenon can be explained by the fact that high humidities decrease the phase transition temperature, because the larger amount of water molecules between the head groups cause a greater space among the neighbouring lipids, therefore the transition energy needed is lower [144-146].

To receive information about the solubility of behenic acid within the main phase, the temperature-dependent changes of the percentage of the BA-rich phase were evaluated. For that purpose, the fraction of the BA-rich phase was determined by analysing the ratio of the intensity of the first order diffraction peak of the BA-rich phase in relation to the overall intensity (the overall intensity is the sum of the BA-rich phase and the main phase and equals 100%). It was found, as expected, that the fraction of the BA-rich phase is temperature and humidity dependent. The result is depicted in Fig. 8-8 for both humidities (57% RH and 98% RH, respectively). A marked tendency for the portion of the BA-rich phase in this system can be detected at both humidities: at 57% RH, the fraction of the BA-rich phase first starts from 18.2% (20°C) to decrease to 12.9% at 45°C, where a minimum is situated. After reaching this temperature, the amount of BA-rich phase increases almost linearly to 21.5% till 65°C. At

higher humidity (98% RH) the fraction of the BA-rich phase shows a similar behaviour: as soon as the temperature begins to rise, the amount of BA-rich phase decreases accordingly from 18.9% (20°C) to 13.9 % at 30°C, after which the amount of the BA-rich phase increases again to reach the value of 33.4% at the final temperature of 55°C.

The decrease of the BA-rich phase fraction at temperatures below of either 45°C (57% RH) or 35°C at 98% RH can be attributed to increased solubility of the BA within the main phase at higher temperatures. In accordance with published results it can be presumed that below this critical temperature of either 45°C (57% RH) or 35°C (98% RH) the chains of the lipids are in a crystalline phase separated into different domains [147]. Above this temperature a transformation into gel phase should occur, increasing the membrane fluidity and miscibility of the lipids.

A further increase of the temperature on the other hand, promotes phase separation, the amount of the BA-rich phase drastically increases. At 98% RH this increase is even more pronounced, when compared to the results at lower humidity. An explanation for this finding could be that at higher humidities the SC lipid model system is less stable to temperature alterations, therefore, the lipids start to separate and to reorganise. As stated above, the space among the neighbouring lipids is increased at high humidity, therefore, the lipids have more "room" for reorganisation. When the temperature is increased the lipids can start to form a more perfect lamellar phase, the same procedure happening during the annealing process. To prove this point, the sample was measured again after cooling back down to 20°C. As can be seen in Fig. 8-8, the amount of BA-rich phase is decreased after the heating procedure is finished and the sample is cooled back down to 20°C, indicating a higher amount of BA inside the main phase.
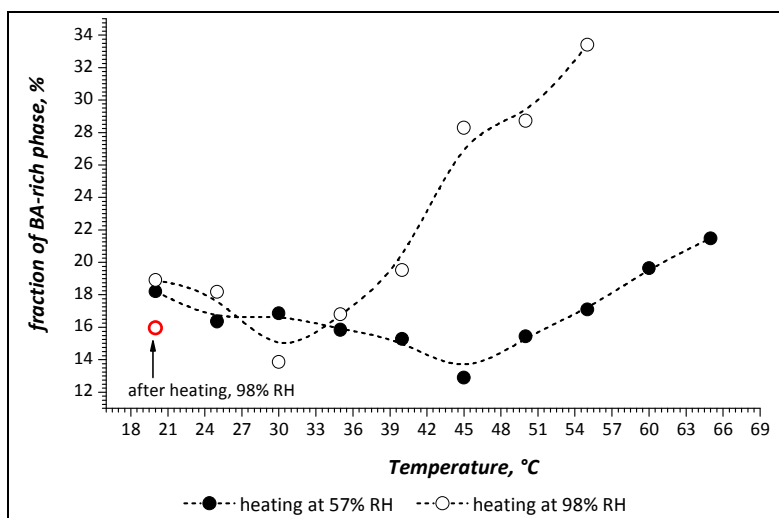
Fig. 8-8 Dependence of the fraction of the BA-rich phase on the temperature at two different humidities, 57% and 98% RH.
After the heating experiment that SC model membrane was measured again.

The existence of lamellar phases and in particular of the BA-rich phase cannot be measured with Raman spectroscopy, making the temperature dependent neutron diffraction experiment indispensable for the study of the thermotropic phase behaviour of such oriented multilamellar SC lipid model membranes.

The phase transition temperature could not be exactly determined from Fig. 8-7. Nevertheless, it is possible to estimate the phase transition as a temperature region of 30°C – 45°C. As discussed, the repeat distance characterises only the common membrane geometry. The structure factors (SF) on the other hand, are looking to the inside of the membrane. The first order SF, for example, gives mainly information about the region of the polar head groups and bilayer hydration, therefore characterising the alterations in the internal membrane structure. Temperature-dependent changes of the SF of the first diffraction order are presented in Fig. 8-9 (BA-rich phase) and Fig. 8-10 (main phase), respectively. The temperature scan at 57% RH was performed at 100% D_2O, while at 98% RH the measurements were carried out at 8% D_2O. These experimental conditions allow collecting the diffraction patterns with maximum information related to the internal structure of the bilayer. At low humidity the 100% D_2O vapour increases the signal from the water penetration inside the bilayer. At high hydration it is necessary to decrease signal from water, the scattering length density (SLD) of water is zero at 8% D_2O concentration in water vapour, therefore no signal from the water distribution is present. The SF was calculated from the integrated intensities as described (see Chapter 3.3.2).
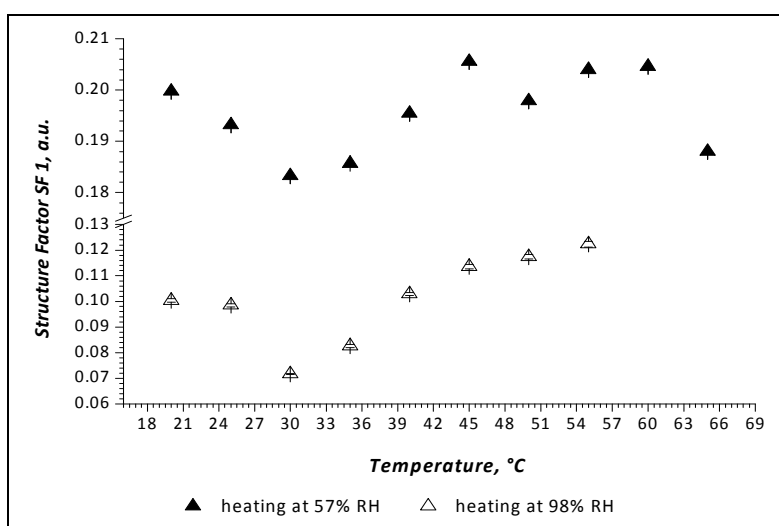
Fig. 8-9 Dependence of the first order SF of the BA-rich phase on the temperature either 57% RH (100% D_2O) or 98% RH (8% D_2O).

Temperature alterations for both phases are strongly connected with each other. In case of the BA-rich phase, the SF exhibits a local minimum at 30°C independently of the humidity (see Fig. 8-9). This finding indicates that this phase transition of the BA-rich phase is not sensitive to the hydration level. At temperatures above 30°C the SF increases

continuously. The minimum at 30°C could be interpreted as a minimum in the hydration of the polar head group region, originated from changes in the lipid bilayer structure. The increase of the SF at temperatures above 30°C demonstrates the increase of the content of water molecules in the polar head group region of the BA-rich phase accompanied by respective structural changes in this region. The described experimental results are an evidence that structural phase transition at approximately 30°C is not related to the chain melting as shown in Fig. 8-7A.
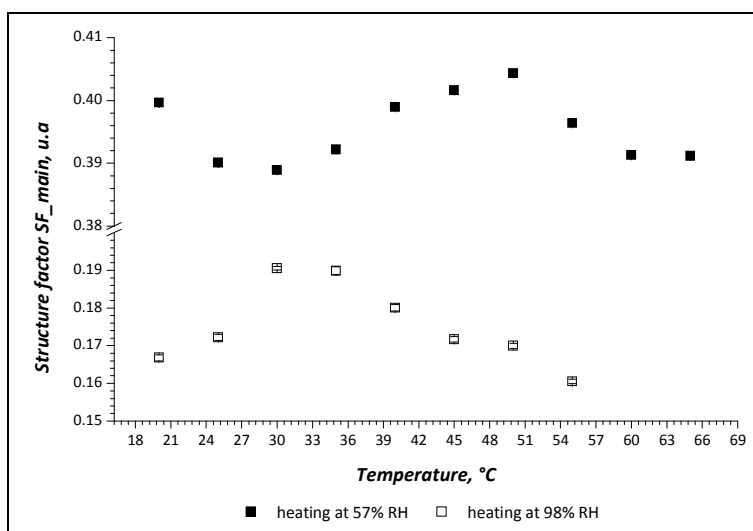
Fig. 8-10 Dependence of the first order SF of the main phase on the temperature at either 57% RH (100% D_2O) or 98% RH (8% D_2O).

The lower values for the first SF (SF1) at 98% RH are due to the fact, that this temperature scan was performed at a lower D_2O content. From the actual value of SF1 it is not possible to receive important information. The position of the local minimum and maximum is more important for the interpretation.

Important changes in the value of the first SF (SF_main) for the main phase under temperature alteration are presented in Fig. 8-10. The temperature dependence measured at 57% RH is completely different from the results obtained at 98% RH. At a relative humidity of 57%, the first order structure factor of the main phase decreases until the temperature of approximately 30°C is reached, after which the SF gradually increases with increasing temperature, until a maximum at approximately 50°C is approached. After reaching this temperature, the value for SF_main decreases again. In contrast to the BA-rich phase, SF_main shows a different behaviour at higher humidity (98% RH). In this case, the SF1 of the main phase first increases, up to the temperature of 30°C, after which SF_main decreases again. This finding is of great importance, as the maximum of SF_main at 30°C was measured at zero SLD of water and maximum relative humidity and therefore, originates from the maximum of the SLD of lipids in the region of polar head groups. The maximum in SLD could be explained by membrane density fluctuations, which is a property of the phase transition.

It is known that the phase transition temperature of phospholipids membranes decrease at the increase of the membrane hydration [148, 149, 28]. For now it seems to be a common property of the hydrated lipid membranes. This behaviour confirms that structural changes in the BA-rich phase and main phase are similar at low humidity, therefore, both phases are alike in the structure. This was already demonstrated in Chapter 4.

The presented method allows one to improve the accuracy in the determination the phase transition temperature. The conventional determination of the phase transition temperature from the decrease of the membrane repeat distance (see Fig. 8-7) results in a broad 30 - 40°C temperature interval for the phase transition. Based on the SF analysis, the phase transition was determined at $33.9°C \pm 0.1°C$ from the centre of the maximum in Fig. 8-10 at 98% RH for the main phase, while for 57% the phase transition was evaluated at about 50°C ($47.3°C \pm 0.2°C$) from the centre of the maximum in Fig. 8-10. As mentioned for the BA-rich phase, the reduction of the hydration level results in an increase in the phase transition temperature.

Phospholipids exhibit an abrupt decrease of the repeat distance at the phase transition temperature due to the chain melting, corresponding with a decrease of the membrane thickness [85]. As mentioned, the studied SC model membrane has a repeat distance approximately equal to the membrane thickness [28]. The presented experimental results demonstrate in contrast to phospholipids, that chain melting occurs at a broad temperature region. Thus, chain melting is not an appropriate phenomenon to characterise phase transition numerically for the case of SC lipid model membranes containing different species of lipids. Nevertheless, the structural phase transition could be determined by abrupt changes in the structure or position of the polar head groups. This structural phase transition is not directly connected to the temperature at which chain melting occurs.

This method of determination of the phase transition temperature is more appropriate for a complex lipid system, relative to conventional thermodynamic methods such as the DSC, as only a broad interval of phase transition is obtained with DSC [133] and furthermore, only the main phase transitions are visible as stated before. Both methods use the integral parameter of the membrane: enthalpy or repeat distance.

The advantage of the presented approach is the information about cooperative changes in a limited area of the bilayer (within the region of the polar head groups). Whereas differential scanning calorimetry and differential thermal analysis are methods which are related to transformations inside the region of the hydrocarbon chains, this is not supportive for complex mixtures of lipids with different chains length.

8.1.4 Conclusions

After merging into one phase the investigated stratum corneum lipid mixture showed a transition from the gel to the liquid crystalline phase at the temperature of 79°C. Further, the FT-Raman spectroscopy measurements illustrated, that this lipid system exhibits at low temperature (25°C) a highly ordered structure with a high amount of *trans* conformers. As the temperature increases the population of *gauche* conformers increases accordingly, therefore, the disorder of the membrane is increasing. Moreover, it could be demonstrated that the alkyl chains of the lipids are packed in a hexagonal packing subcell.

The temperature-dependent neutron diffraction investigation revealed the heating caused a restructuring of the membrane lipids, which resulted in a better oriented lamellar layer, as the amount of phase-separated behenic acid was reduced. Furthermore, the phase transition of such membranes is dependent on the humidity, at a high humidity the phase transition temperature is reduced. The analysis of the first-order structure factor showed a phase transition at either 47.7 Å (57% RH) or at 33.9 Å (98% RH) as an abrupt change in the structure of the polar head groups.

The combination of DSC with Raman spectroscopy and furthermore, with neutron diffraction revealed new and more detailed insights to the thermotropic phase transition properties of SC lipid model membranes. Especially the application of neutron diffraction can supply changes of structural data in the limited area of a bilayer.

8.2   Nanostructural phase transitions in lamellar SC model membranes

8.2.1 Introduction

This Chapter presents further insights into the thermotropic phase behaviour of SC lipid model membranes with the focus placed on the lamellar nanostructure. Here, the application of neutron diffraction enabled to *directly* monitor changes occurring in the nanostructure of a bilayer upon temperature alteration.

8.2.2 Materials and Methods

Sample preparation and data collection

The SC model membranes were used in three different compositions as listed in Table 8.2. Each sample was prepared as described in Chapter 3.4.

Mixture	Free fatty acid (FFA)	Component ratio (w/w) (CER[AP]/Ch/FFA/ChS)
QuatBA	behenic acid (BA)	57/ 24/ 9.5/ 9.5
QuatTA	tetracosanoic acid (TA)	55/25/15/5
QuatCA	cerotic acid (CA)	55/25/15/5

Table 8.2 SC model membrane composition All investigated systems were consisted of CER[AP]/CHOL/ FFA/ChS, whereby only the FFA was varied.

The sample was heated to the appropriate temperature after which the sample was again equilibrated for one hour. The measurements of the scattering intensities I were carried out at 57% RH and at 8% D_2O, except the for the sample containing BA, which was measured at 100% D_2O. The nanostructure of the bilayer was analysed by the construction of the neutron scattering length density profile $\rho_s(x)$ (in arbitrary units, a.u.) across the bilayer according to Eq. (3.10).

8.2.3 Results and Discussion

As discussed in the preceding part the quaternary SC lipid model membrane (CER[AP]/CHOL/BA/ChS) exhibits a decrease in the membrane thickness upon temperature increase. The SC lipid model membranes containing either tetracosanoic (TA) or cerotic acid (CA) as free fatty acid (FFA) component showed a similar behaviour at increased temperature. This decrease can be explained by the melting of the lipid chains as explained in detail in the preceding Chapter 8.1. The respective decreases are listed in Table 8.3. After cooling the TA

containing membrane back to 20°C the repeat distance of the main phase is restored to the initial value.

Table 8.3 Temperature-dependence of the membrane repeat distance of SC lipid model membranes containing FFA with increasing chain length.

Temperature, °C	d of CER[AP]/CHOL/*TA*/ChS, Å	d CER[AP]/CHOL/*CA*/ChS, Å
30	43.8 ± 0.09	43.6 ± 0.06
50	42.8 ± 0.02	42.8 ± 0.01
80	41.4 ± 0.03	41.3 ± 0.06

In Fig. 8-11 the diffraction pattern of the sample containing TA at two different temperatures is compared.
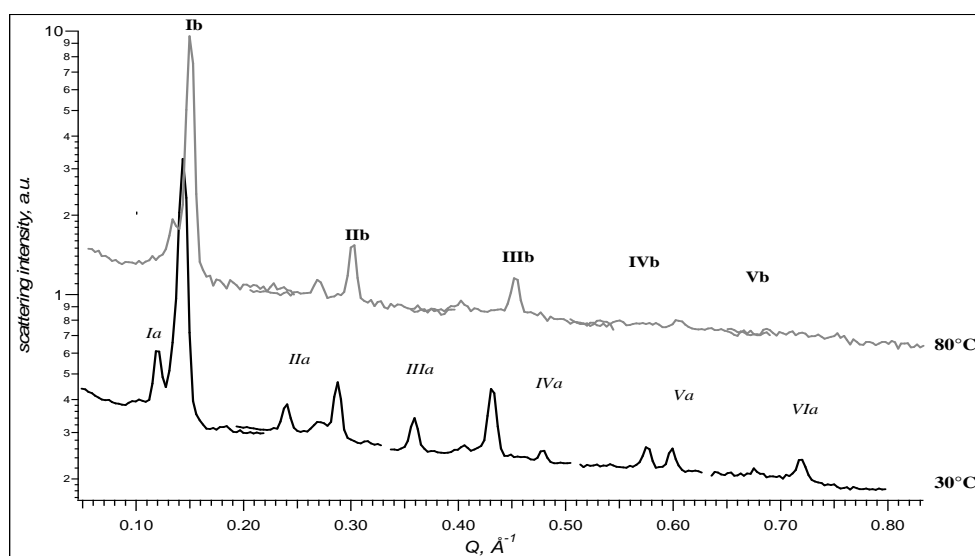
Fig. 8-11 Comparison of the neutron diffraction pattern for the quaternary membrane composed of CER[AP]/CHOL/TA/ ChS (55/25/15/5, w/w) measured as rocking curve either at 30°C or 80°C at 57% RH, 8% D_2O respectively. For better understanding the two phases of the system have been indicated: $Ia - VIa$ indicate the 6 diffraction orders of the FFA-rich phase, while $Ib–Vb$ indicate the 5 diffraction orders of the main phase, respectively.

In case of the membrane with TA the intensity of the peaks corresponding to the TA-rich phase decreases slightly when the temperature reaches 80°C (see Fig. 8-11). For the membrane containing CA the same behaviour was found. This is a result of an increased solubility of the FFA fraction upon temperature increase. This is consistent with results received from FT-IR investigation performed by Chen and co-workers [150]. They studied the phase behaviour of a sphingosine-type ceramide, CER[NS] in mixtures with stearic acid. They also found a separated fatty acid-rich phase, which disappears at around 50°C, while at higher temperatures the two components appear to be quite miscible and a preferential association of the fatty acid occurs with the base chain of CER[NS]. In another study on monolayers [151],

the influence of the ceramide acyl-chain length in mixtures with FFA of different chain length were investigated. Their results illustrate, that the short acyl-chain ceramide showed a higher tendency to mix with the short chain palmitic acid, while the long alkyl-chain ceramide mixed preferentially with the long chain lignoceric acid, but both ceramides only show a partial miscibility with either fatty acid. It was concluded, that a matching in chain length promotes the miscibility of those lipids. This also is in agreement with the separate FFA-rich phase, because the chain length of the short chain CER[AP] molecule and long chain FFA do not match. On the other hand, in Chapter 8.1 the amount of the BA-rich phase increased when temperature was raised above a temperature of 45°C (57% relative humidity). When analysing the amount of FFA-rich phase from the percentage of the first diffraction order of the three different temperatures it becomes evident, that also the amount of the FFA-rich fraction slightly increases at the temperature of 50°C, while at 80°C the amount is reduced again. This is independent of the FFA incorporated in the SC lipid model membrane (see Table 8.4). As in Part1 the measurements were carried out up to a temperature of 65°C, the here presented results are in agreement. Furthermore, after the sample containing TA was cooled back down to 20°C the amount of TA-rich phase is further reduced (5.9 %). Evaluating the fraction of the TA-rich phase after annealing the sample at 100% RH and 75°C resulted even in a further decrease of the TA-rich phase (3.1% of the first order diffraction intensity) indicating that a high temperature as well as a high humidity is necessary for the organisation of the lipids in the lamellar phase, as also described in Chapter 8.1.

Table 8.4 Temperature-dependence of the amount of FFA-rich phase.

Temperature, °C	Amount of TA-rich phase, %	Amount of CA-rich phase, %
30	9.9	4.2
50	11.7	5.2
80	8.8	1.7

In order to monitor changes in the nanostructural alignment of the SC model membrane occurring during the heating process, the neutron scattering length density (SLD) profiles $\rho_s(x)$ across the bilayer were calculated for both phases as described in Chapter 3.3.2. Only the SLD profile of the main phase will be presented further on.

Heating the SC model system containing TA acid first to 30°C, then to 50°C results in only minor differences within the structure of the membrane, as demonstrated in Fig. 8-12. The membrane containing CA shows also no distinct structural changes at the elevated temperature of 50°C (see Fig. 8-13). This is also the case at a slightly higher temperature

(T = 65°C) for the membrane with BA, depicted in Fig. 8-14. These results clearly indicate that the structure of the SC model membrane based on CER[AP] is a very stable one.
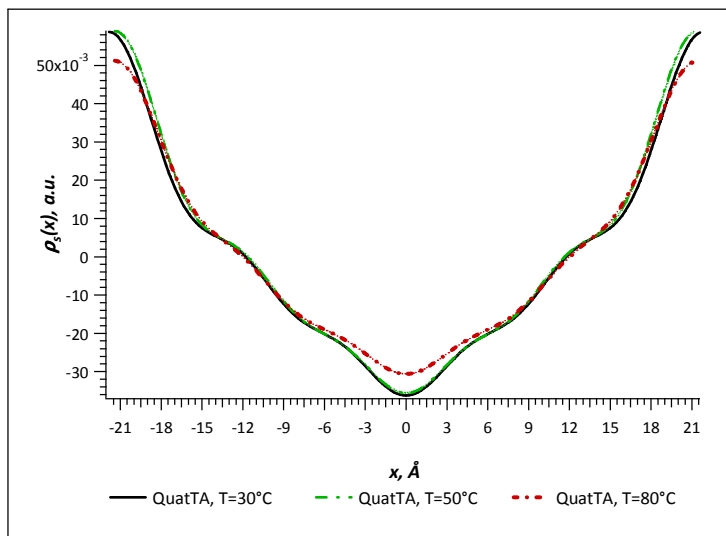
Fig. 8-12 Neutron SLD density profiles of the main phase of the SC lipid model membrane composed of CER[AP]/CHOL/**TA**/ChS (55/25/15/5, w/w) at either 30°C (solid black line), at 50°C (long dash, green line) or T=80°C (red short dashed line). The measurements were carried out at 8% D_2O and 57% RH.
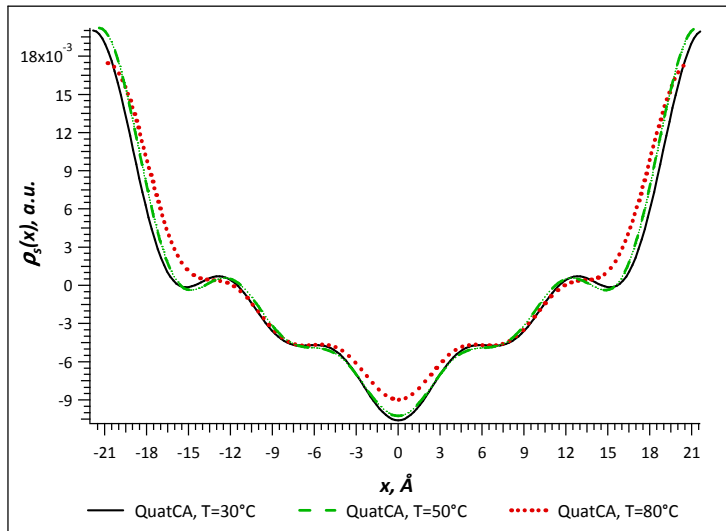
Fig. 8-13 Neutron SLD density profiles of the main phase of the SC lipid model membrane composed of CER[AP]/CHOL/**CA**/ChS (55/25/15/5, w/w) at either 30°C (solid black line), at 50°C (long dash, green line) or T=80°C (red short dashed line). The measurements were carried out at 8% D_2O and 57% RH.
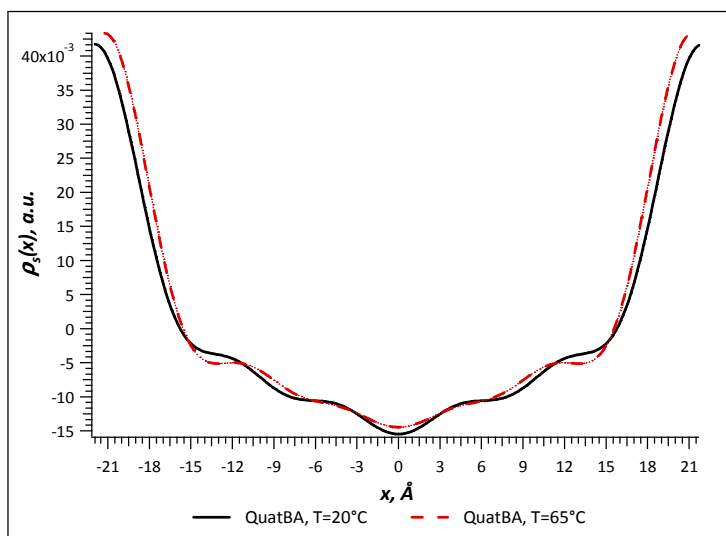
Fig. 8-14 Comparison of the neutron SLD profile of the main phase of the SC lipid model membrane composed of CER[AP]/CHOL/**BA**/ChS (54/9.5/9.5/5) at 20°C with the SLD profile measured at 65°C. Both measurements were performed at 100% D_2O and 57%RH.

To induce structural changes in the membrane higher temperatures than 50 or 65°C are necessary. Increasing the temperature to 80°C results in significant changes in the structure. In Fig. 8-12 the comparison of the SLD profiles of the model membrane containing TA measured at T=30°C and T=80°C, respectively is presented. It reflects, that the main differences in the SLD profiles are localised in the region of polar head groups and in the centre of the membrane, where the CH_3-groups are positioned. This is also the case for the SC model membrane containing CA as depicted in Fig. 8-13. These findings are consistent with investigations on ceramides extracted from bovine brain, which form a crystalline phase and undergo a solid-solid phase transition at 60°C, while the transition towards a more disordered state occurs at 80°C [152].

The changes occurring in the structure due to the increase of the temperature can be explained by the phenomenon of the chain-flip-transition of the ceramide [AP] molecules. The chain-flip-transition was firstly observed by Kiselev and co-workers upon hydrating a SC lipid model membrane similar in composition (CER[AP]/ CHOL/ palmitic acid/ ChS) [28]. At physiological temperatures CER[AP] can be both in fully extended and hairpin conformation in such SC lipid model membranes. In the fully extended conformation (FE) the hydrocarbon chains of CER[AP] are directed oppositely, while the polar head group is positioned within the centre of the membrane. In contrast, the chains in the hairpin conformation point in the same direction (see Fig. 8-15).
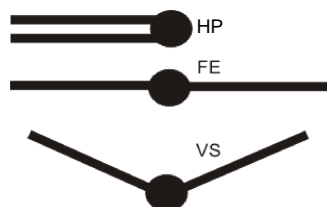
Fig. 8-15. Conformations known for the CER[AP] molecules within a multilayer: *HP* – hairpin (One side) conformation , *FE* – fully extended and *VS* – V shape

In case of a temperature increase it can be supposed that the some amount of the CER[AP] molecules change the conformation from the one-sided to the FE conformation. This is in contrast to the reported chain-flip transition from FE to hairpin conformation under hydration whereby the intermembrane space appears and can be hydrated [28, 82]. In general, such a chain-flip transition is energetically possible as the energy required for this transition amounts only to one-half of the energy necessary for flip-flop transition [84].

From the comparison of the neutron SLD profiles shown in Fig. 8-12 and Fig. 8-13 the transition form hairpin to FE conformation at temperature above 65°C can be underlined:

(i)   the decrease of the neutron SLD in the polar head group region accounts for the fact, that some part the CH_2-groups now reach into the polar head group region when ceramide [AP] has changed from fully extended conformation

(ii) an increase in the SLD in the centre of the membrane, the CH$_3$-group region accounts for the fact that due to the chain-flip-transition some free space results

This is further supported by model calculation of pure CER[AP]. Here, the SLD profile was calculated independently for the FE and the hairpin conformation as demonstrated in Fig. 8-16.
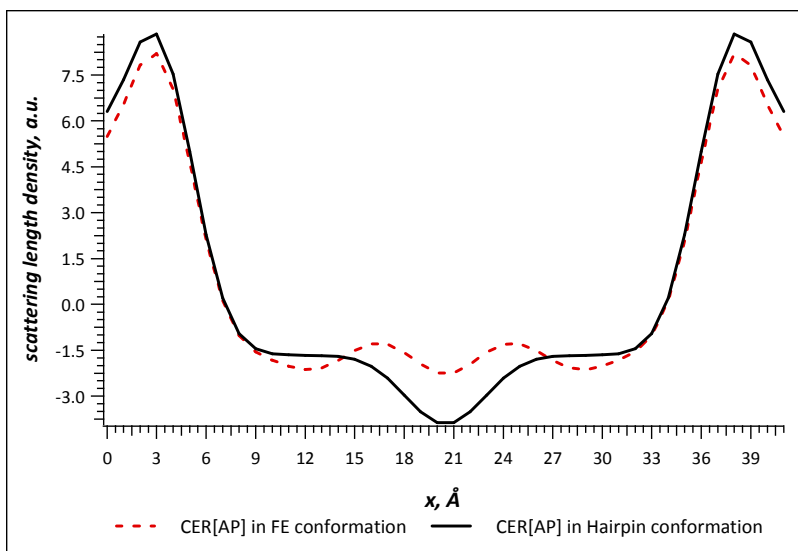
Fig. 8-16 Comparison of the model calculation of the neutron SLD profile of the CER[AP] molecules either in FE or in hairpin conformation.
(Model calculation done by Dr. T Hauß)

Taken together it can be concluded that at temperatures above 65°C some CER[AP] molecules undergo the chain-flip-transition from hairpin to fully extended conformation and that therefore at higher temperatures the fraction of ceramide [AP] molecules in hairpin conformation is decreased. This is of great importance for the maintenance of the barrier properties of the SC, as under elevated temperature the chain-flip transition of the CER[AP] molecules tightens the structure, whereby the CER[AP] molecules in the FE conformation act as an anchor stabilising the membrane structure.

In order to restore the structure to its initial state this process needs to be reversible. This information is of importance as the restoring of the structure to the initial state is necessary to uphold the normal barrier function of the SC. With the intention of verifying the reversibility of the chain-flip-transition of the CER[AP] molecule upon heating, the sample was measured again after cooling back to 20°C and measured afterwards. The neutron SLD profile for the sample containing tetracosanoic acid, displayed in Fig. 8-17 are compared at different states in the heating procedure (before heating at 30°C, after heating and cooling to 20°C and after performing the annealing procedure described for the sample preparation).

As can be seen, the structure is not fully restored to the initial state (T=30°C) after cooling the membrane to 20°C. This can account for the fact that the chain-flip-transition is a slow process similar to the flip-flop transitions. However, at high humidity (100% RH), the

restoration to the initial state is accelerated, the SLD profile measured after heating at 100% RH is more in agreement with the profile measured at the beginning of the experiment.
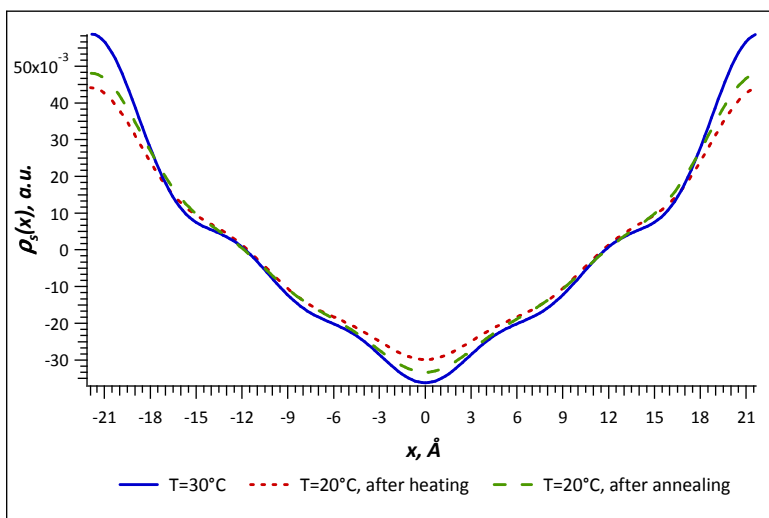
Fig. 8-17 Neutron SLD profiles of the SC model membrane containing TA before (at 30°C, blue solid line) and after heating up to 80°C and cooling back to 20°C (short red dash) as well as after the heating and cooling procedure was finished and the sample was annealed at 75°C and 100% RH (long green dash). All measurements were carried out at 57% RH and 8% D_2O.

8.2.4 Conclusion

The lipid part of the SC is a very effect barrier for substances to leave the skin, as well as for such to penetrate into it. It is necessary to keep the barrier function organised even in dire condition, such as high humidity and increased temperature. Therefore, strategies are needed to upheld structure. One of this is the chain-flip-transition of CER[AP], with which the lipid part of the SC can properly react to changes in the environment.

The investigation of SC lipid model membranes based on CER[AP] with varying FFA showed that in principle such membrane are very stable against heating stress. Raising the temperature up to 50 or 65°C did not induce significant changes in the structure. Only the repeat distance decreased with increasing temperature due to lipid alkyl chain disorder [153, 140, 154] A further increase of the temperature to 80°C resulted in the chain-flip transition of the CER[AP] molecules from the hairpin to the fully extended conformation. This transition is of importance as the fully extended conformation of CER[AP] tightens the adjacent bilayers, whereby the polar head groups are in close proximity to each other. This minimises the intermembrane space, therefore such a structure is not open for a penetration of hydrophilic substances. When the CER[AP] molecules are in the one-sided or hairpin conformation the adjacent bilayers are able to move apart and the intermembrane space can be hydrated whereby the penetration of hydrophilic substances can more easily accomplished.

9 Summary and Perspectives

9.1   English version

The intercellular lipid membranes of the stratum corneum are a biological example for the relationship between the membrane lipid composition, its physical properties and biological function as they have an exceptional composition (mainly ceramides, cholesterol and free fatty acids [43, 45, 46, 155]) as well as physical organisation when compared to most mammalian cell membranes.

To elucidate the special assembly and the properties of the native stratum corneum lipid matrix is a difficult if not impossible task as the natural stratum corneum membranes are very complex. Therefore, in the presented work simplistic, but realistic stratum corneum lipid model membranes were studied. This enabled a systematic investigation of the impact of different lipid species on the structural organisation and properties of such membranes. The model systems chosen for the investigation were usually made up of one or two ceramide species, cholesterol and its derivative cholesterol sulphate and a free fatty acid. To gain specific structural insights the stratum corneum lipid matrices were prepared as oriented multilamellar membranes and studied primarily with neutron diffraction, but also X-ray scattering, differential scanning calorimetry and Raman spectroscopic measurements were used for the characterisation. By analysing the neutron diffraction pattern and further calculating the neutron scattering length density (SLD) profiles the arrangement of the lipids inside the lipid matrix can be concluded.

The first task of in this work was the systematic assessment of the influence of the free fatty acid chain length to a SC lipid model membrane based on ceramide [AP]. This neutron diffraction investigation revealed, that the internal nanostructure of such membranes is not proportionally altered by the increase of the chain length of the free fatty acid from stearic (C18:0) to cerotic (C26:0) acid. It was observed, that an *increase* in the free fatty acid chain length resulted in a *decrease* of the membrane repeat distance. An explanation for this dependency was found to be the partial interdigitation of the longer free fatty acid chain as the free fatty acids tend to "fit" into the membrane size created by ceramide [AP]. This interdigitation creates some free space, wherefore the free fatty acids "pull" the membrane together, a reason for the observed decrease in the membrane thickness. The reason for the interdigitation behaviour of the FFA are the strong intermembrane forces resulting from the very polar short chain phytosphingosine-type ceramide [AP], which creates a superstable nanostructure. Therefore, it was concluded, that ceramide [AP] dictates the main phase of

this SC lipid model membrane. The interactions created by the ceramide [AP] molecules are the major forces which determine the stability of this SC model membrane. Therefore, the ceramide obligates the long chain free fatty acids to either arrange inside this phase or separate to form a free fatty acid-rich phase. Further, the appearance of a "fatty-acid-rich phase" indicates that the longer chained free fatty acids tend towards a formation of a separated phase.

In the next step, the application of the specifically deuterated free fatty acids supplied the *direct* experimental evidence that the long chain free fatty acids due indeed need to protrude into the adjacent layer in order to arrange in the membrane size dictated by ceramide [AP]. Furthermore, the use of the deuterated free fatty acids confirmed the coexistence of free fatty acid-rich phase and main phase, determined by ceramide [AP]. The application of partially deuterated lipids in the neutron diffraction experiment allows the direct localisation of the deuterated part of the lipid within the lipid layer. This is one essential advantage of the applied method.

To gain further insights into the assembling properties of SC lipid matrices and especially of the role of the ceramide species, ceramide [AP] was substituted either by the artificial ceramide [NP]A or [NP]B. Chemically, both differ from the natural ceramide [NP] only by the addition of either one (ceramide [NP]B) or two (ceramide [NP]A) double bonds and further from ceramide [AP] by the absence of the α-hydroxyl group in the fatty acid bound to the phytosphingosine backbone. The ceramide [NP]B-based stratum corneum lipid model membranes exhibited a three phase system in which the ceramide [NP]B molecules adopt different conformations, either fully extended or V-shape conformation. Interestingly, all conformation coexist at defined conditions such as temperature and humidity in contrast to pure native ceramide [NP], where the conformation were found at different experimental conditions [125]. A phase separated membrane is a defective system in the sense of barrier function. As a consequence, it can be assumed that the insertion of ceramide [NP]B in the native stratum corneum could result in an increase in the penetration rate as phase separation can increase the permeability of the stratum corneum lipid barrier. In case of the ability of ceramide [NP]B to reach the intercellular lipid layers of the stratum corneum from an excipient and cause within the lipid matrix a similar phase separation this would cause an decrease of the barrier function and help substance to pass the stratum corneum. Further detailed investigations are necessary to answer the question whether ceramide [NP]B could be used as a penetration enhancer

Stratum corneum lipid model membranes based on ceramide [NP]A on the other hand displayed only a poor lamellar ordering, due to the two double bonds in the ceramide

molecules. The presences of the double bonds disturbs the ordered structure of the stratum corneum lipids, therefore, the membrane fluidity is increased. No highly ordered structure can be formed. An increased fluidity of the stratum corneum lipids causes an increased permeability of the intercellular lipid matrix. Consequently, the disturbance of the natural barrier of the stratum corneum lipids due to the presence of the artificial ceramide [NP]A could also result in an increased permeability. The question whether ceramide [NP]A is suitable to act as an penetration enhancer is yet to be answered.

After evaluating the stratum corneum lipid model membranes based on the artificial ceramides [NP]A and [NP]B the role of the more polar ceramide [AP] in these model matrices was assessed by investigating membranes containing both ceramide [AP] and either ceramide [NP]A or [NP]B in an equal ratio. Independently of the artificial ceramide [NP]-species the addition of ceramide [AP] resulted in well-oriented membranes in which the structural assembly is dictated by ceramide [AP]. The phase separation in the ceramide [NP]B-system disappeared, while model membranes containing mixtures of ceramide [NP]A and ceramide [AP] resulted in well-oriented lamellar membranes. Consequently, the driving forces for the assembling process are again realised by the ceramide [AP] molecules. Again, the role of ceramide [AP] seems to be crucial for the assembling process of such stratum corneum lipid model membranes.

The native stratum corneum contains next to the short chain ceramides also very long chain ω-acylceramides such as ceramide [EOS], which are said to be crucial for proper barrier function of the skin [23, 24]. Further, former studies proclaimed the co-existence of two lamellar phases in the stratum corneum, namely the short-periodicity-phase of approximately 60 Å and long-periodicity-phase of approximately 130 Å [20, 77, 25]. The latter is said to be particularly associated with the presence of ceramide [EOS], which therefore, is regarded to be a prerequisite for proper barrier functions. The existence of the Long-periodicity-phase, its organisation and the inducing or preventing conditions for its formation are currently a matter of debate [69, 68]. Therefore, a stratum corneum lipid system comprising the next to the short chain ceramide [AP] also the very long chain ω-acyl ceramide [EOS], cholesterol and behenic acid as free fatty acid fraction was studied with neutron diffraction. The investigated oriented multilamellar stratum corneum lipid membrane only exhibited the short-periodicity-phase which is consistent with previous studies performed by Kessner and co-workers [81]. The only explanation for such behaviour is that the influence of the head group polarity of ceramide [AP] exceeds the influence of the chain length of ceramide [EOS] in terms of the membrane assembling. The results of this investigation support the phenomena of the *armature reinforcement model*, which was developed for stratum corneum lipid model

membranes based on ceramide [AP] [110]. The results further show the important role of this polar short chain ceramide for the nanostructure of such model membranes and additionally, give new material for the debate on the importance of the short-periodicity-phase for the barrier function of the stratum corneum lipid bilayer.

The lipid part of the stratum corneum is a very effect barrier for substances to leave the skin, as well as for such to penetrate into it. It is necessary to keep the barrier function organised even in dire condition, such as high humidity and increased temperature. Therefore, strategies are needed to upheld structure. One of this is the chain-flip-transition of ceramide [AP], with which the lipid part of the stratum corneum can properly react to changes in the environment.

The investigation of stratum corneum lipid model membranes based on ceramide [AP] with varying free fatty acid showed that in principle such membranes are very stable against heating stress. In this study it was found that raising the temperature up to 50 or 65°C did not induce significant changes in the structure. Only the repeat distance decreased with increasing temperature due to lipid alkyl chain disorder [153, 140, 154]. A further increase of the temperature to 80°C resulted in the chain-flip transition of the ceramide [AP] molecules from the hairpin to the fully extended conformation. This transition is of importance as in the fully extended conformation the polar head groups of ceramide [AP] are in close proximity to each other, which tightens the adjacent bilayers. By this conformational shift the membrane integrity can be upheld ever under severe stress such as increased temperature. When transferring theses results to the native stratum corneum it can be concluded that a severe burning of the skin can destroy the viable parts of the skin, but the barrier function of the skin remains intact.

The application of neutron diffraction for the investigation of the thermotropic response of such complex lipid systems in combination with more conventional techniques such as differential scanning calorimetry and Raman spectroscopy enlarges the knowledge of thermotropic phase transition properties and reveals new structural insights under temperature alteration.

All presented investigations highlight the importance of ceramide [AP] for the structural organisation of the described stratum corneum lipid model membranes. Independently of the applied ceramide species, the assembling process of stratum corneum lipid model membranes was always driven by the very polar short chain ceramide [AP]. Additionally, such model membranes based on ceramide [AP] are not susceptible to changes when the free fatty acid chain length is altered. This gave rise to the conclusion that the head group polarity

of the ceramide molecules exceeds all influences of the other constituents, even the chain length the ω - acyl ceramide [EOS].

The presented results give new material in the debate of the importance of the polar short chain ceramides, in particular the relevance of the head group polarity should be new evaluated. For now only the importance of the long the ω-acyl ceramide for the proper barrier function of the stratum corneum is established [156]. Furthermore, it seems, that the relevance of the short-periodicity-phase for the barrier function of the stratum corneum should be reconsidered.

Future investigations now have to verify the role and function of the head group polarity of the ceramides, in particular of the short chain ceramides. This can be accomplished by a successive substitution of ceramide [AP] in already described stratum corneum lipid model membranes by also short chain ceramides with a decreased head group polarity such as ceramide [AS]. Furthermore, a model membrane similar to the one described in Chapter 7, but containing instead of the ω-acyl ceramide [EOS] the more polar ω-acyl ceramide [EOP] will elucidate, if the influence of the short chain ceramide [AP] can exceed the slightly less polar, but long chain ceramide [EOP]. In another study, the partial substitution of ceramide [EOS] by ceramide [EOP] resulted in a decrease of the intensity of the long-periodicity-phase, which the authors attributed to the head group effect of the more polar ceramide [EOP] by similar chain length of both ceramides [72].

It is also necessary to clarify, whether the free fatty acids can play an essential role for the formation of the long-periodicity-phase. In another prominent study [70], the addition of free fatty acids to mixtures of isolated human ceramides and cholesterol promoted the formation of the short-periodicity-phase, the addition of a mixture of long chain free fatty acids (primarily C22 – C24) resulted in a transition from a hexagonal to an orthorhombic chain packing, which could not be observed when short chain free fatty acids mixtures (C16 – C18) were used [19]. On the other hand, in a study which used synthetically derived ceramides the free fatty acids were found to be required for the proper lipid organisation, only their presence caused the formation of a dominant long-periodicity-phase [72].

In contrast, in the present study no influence to the structure and no orthorhombic chain packing could be observed, which can account for the fact that only *one* type of free fatty acid was applied. If necessary, mixtures of free fatty acids with varying chain length are required to influence the structural assembling process. Furthermore, the question arises whether the amount of free fatty acid within the model membranes can also be a crucial for the structure formation. The mixtures of ceramides, cholesterol and free fatty acids which exhibited the orthorhombic chain packing described by Bouwstra and co-workers [19] were in

an equimolar ratio. This may be an indication, that a higher free fatty acid fraction in such model systems can influence the chain packing. Successive Raman spectroscopic measurements together with neutron diffractions experiments are needed to clarify these questions.

In conclusion, in this thesis many insights into the nanostructure of defined stratum corneum lipid model membranes could be presented. In particular, the important role of ceramide [AP] for the structural assembly could be illustrated and results also support the newly presented theoretical model of the stratum corneum lipid matrix, the *armature reinforcement model*. Further intensive studies in this field are necessary for a better understanding of the organisation of the stratum corneum lipid matrix. Eventually, this is a prerequisite to understand the barrier of the skin and the mechanisms of drug penetration through the stratum corneum.

9.2   German version

Im Vergleich zu den meisten tierischen Zellmembranen nehmen die Lipidmembranen des Stratum corneums eine Sonderstellung ein, bedingt durch ihre außergewöhnliche Lipidzusammensetzung (hauptsächlich Ceramide, Cholesterol und freie Fettsäuren), ihren strukturellen Aufbau und biologische Funktion.

Die Aufklärung des besonderen Aufbaus und der Eigenschaften der nativen Stratum corneum Lipidmatrix ist ein sehr aufwendiges und schwieriges Unterfangen, da die natürliche Stratum corneum Lipidmembranen sehr komplex sind. Die Verwendung von einfachen, aber dennoch realistischen Lipid-Modellmembranen erlaubt eine systematische Untersuchung des Einflusses der verschiedenen Lipidspezies auf den strukturellen Aufbau, auf die Eigenschaften der Membranen und ihrer Funktion innerhalb der Lipidorganisation. Die in dieser Arbeit untersuchten Stratum corneum Lipid-Modellmembranen waren im Allgemeinen aus ein oder zwei Ceramiden, Cholesterol, seinem Derivat Cholesterolsulfat und einer freien Fettsäure zusammengesetzt. Um Einblicke in die Struktur der Stratum corneum Modelmatrices zu erhalten, wurden orientierte multilamellare Membranen mit Hilfe von vor allem Neutronen-, aber auch Röntgenstreuung in Verbindung mit Raman Spektroskopie und Differential Scanning Kalorimetrie untersucht und charakterisiert. Eine genaue Analyse der aus der Neutronendiffraktion resultierenden Diffraktionsmuster und der dann erhältlichen Neutronenstreudichte Profile erlaubt Aussagen über die Anordnung der Lipide innerhalb der Lipidmatrix.

Ein erster Ansatz innerhalb dieser Arbeit war die Untersuchung des Einflusses der Fettsäurekettenlänge auf die Struktur einer auf Ceramid [AP]-basierten Stratum corneum Lipid-Modellmembran. Die systematische Erforschung mit Neutronendiffraktion ergab, dass die interne Nanostruktur solcher Membranen *nicht* durch die Verlängerung der Fettsäurekette beeinflusst wird. Es wurde lediglich beobachtet, dass mit zunehmender Kettenlänge der Fettsäure der lamellare Wiederholabstand abnahm. Dies kann nur dadurch erklärt werden, dass die längerkettigen Fettsäuren sich partiell in der Membrane verzahnen, um sich an die von Ceramid [AP] vorgegebenen Membrandicke anzupassen. Diese Verzahnung bewirkt ein „Zusammenziehen" der Membran, ein Grund für die beobachtete Verringerung der Membrandicke. Eine Ursache für die Verzahnung der Fettsäuren findet sich in den starken intermembranären Kräften der Ceramid [AP] Moleküle, die für eine hoch stabile Nanostruktur sorgen. Das sehr polare, kurzkettige Ceramid [AP] erzwingt die Anordnung der anderen Komponenten in dieser Modellmembran, wobei die Wechselwirkungen der Ceramid [AP] Moleküle die Hauptkräfte darstellen und auch die Stabilität bedingen. Demzufolge zwingt Ceramid [AP] die langkettigen Fettsäuren sich innerhalb der Membran zu arrangieren, oder aber als eine eigene „Fettsäure-reichen" Phase zu separieren. Das Auftreten einer solchen Fettsäure-reichen lässt darauf schließen, dass die langkettigen Fettsäuren zu der Bildung einer eigenen Phase neigen.

Durch den Einsatz von speziell deuterierten Fettsäuren konnte auf direktem Weg belegt werden, dass die langen Fettsäureketten die Membran durchdringen und sich dadurch in der von Ceramid [AP] erzwungenen Membrangröße einordnen können. Des Weiteren konnte mit Hilfe der deuterierten Fettsäuren die Existenz der Fettsäure-reichen Phase bestätigt werden. Die Anwendung partiell deuterierter Lipide in der Neutronenstreuung erlaubt somit eine gezielte Bestimmung der Lage des deuterierten Molekülteils innerhalb der Lipidschicht. Dies ist ein wesentlicher Vorteil der eingesetzten Methode.

Um nun weitere Einblicke in den Aufbau von Stratum corneum Lipidmatrices und speziell die Rolle der Ceramidspezies zu erhalten, wurden Modellmembranen untersucht, die anstelle von Ceramide [AP] ein künstliches Ceramid enthielten. Die verwendeten künstlichen Ceramide [NP]A und [NP]B unterscheiden sich nur durch die Einführung von einer (Ceramid [NP]B) bzw. zwei Doppelbindungen (Ceramid [NP]A) vom natürlich vorkommenden Ceramid [NP] und zusätzlich noch durch das Fehlen der α-Hydroxylgruppe im Phytosphingosingerüst von Ceramid [AP]. Die Ceramid [NP]B-basierten Stratum corneum Lipid-Modellmembranen weisen ein drei Phasen System auf, wobei Ceramid [NP]B in den einzelnen Phasen entweder die V-förmige oder die gestreckte Konformation einnimmt. Interessanterweise co-existieren beide Konformationen bei definierten Bedingungen, wie Temperatur und Feuchtigkeit in der

Membran. Im Gegensatz dazu, wurden die verschiedenen Konformationen des nativen Ceramids [NP] nur bei unterschiedlichen experimentellen Bedingungen gefunden. Bei einem Mehrphasensystem ist die Barrierefunktion beeinträchtigt. Es kann demzufolge angenommen werden, dass eine Integration von Ceramid [NP]B in das native Stratum corneum eine Penetrationsförderung bewirkt, da Phasenseparation im Allgemeinen die Permeabilität der Stratum corneum Lipidbarriere erhöht. Für den Fall, dass Ceramid [NP]B in der Lage ist aus einem Arzneiträger in die Lipidschicht des Stratum corneum zu gelangen und dort eine derartige Phasenseparation bewirkt, könnte Ceramid [NP]B als Penetrationsenhancer eingesetzt werden. Hierzu sind aber weitere umfangreiche Untersuchungen notwendig.

Die Stratum corneum Lipid-Modellmembranen, die Ceramid [NP]A enthielten, bildeten nur ein ein-phasiges System aus. Der Grund hierfür findet sich in der chemischen Struktur des Ceramidmoleküls: die beiden Doppelbindungen im Phytosphingosingerüst stören die geordnete Struktur der Stratum corneum Lipide, wodurch die Fluidität der Membran erhöht ist. Eine hoch geordnete rigide Struktur kann demnach nicht ausbilden. Eine erhöhte Fluidität, bewirkt eine erhöhte Permeabilität der Lipidmatrix. Eine Beeinträchtigung der natürlichen Barriere der Stratum corneum Lipide durch das künstliche Ceramid [NP]A könnte ebenfalls eine Penetrationsverbesserung bewirken, Die Frage, ob nun Ceramid [NP]A als Penetrationsenhancer geeignet ist, bleibt allerdings noch zu beantworten.

Im Weiteren wurden Neutronendiffraktionsuntersuchungen an Modellmembranen durchgeführt, deren Ceramidfraktion aus gleichen Teilen künstlichem Ceramid und Ceramid [AP] bestand, um auf diesem Weg Auskunft über die Bedeutung von Ceramid [AP] zu erhalten. Es hat sich gezeigt, dass unabhängig vom künstlichen Ceramid die Zugabe von Ceramid [AP] in gut orientierten Membranen resultierte, deren struktureller Aufbau eindeutig von Ceramid [AP] bestimmt wird. Die Phasenseparation bei Ceramid [NP]B-basierten Membranen verschwand bei Anwesenheit von Ceramid [AP]. Die Membranen mit Mischungen aus Ceramid [NP]A und Ceramid [AP] zeigten eine hervorragend geordnete Lamellarstruktur, die wiederum durch Ceramid [AP] bestimmt wird. Die Antriebskräfte für den Aufbauprozess werden erneut durch Ceramid [AP] beisteuert. Aus diesen Untersuchungen geht hervor, dass Ceramid [AP] entscheidend für den strukturellen Aufbauprozess von Stratum corneum Lipid-Modellmembranen ist.

Das native Stratum corneum enthält neben den kurzkettigen Ceramiden auch die sehr langen omega-acyl-Ceramide wie Ceramid [EOS]. Von diesen ω-acyl-Ceramiden wird angenommen, dass sie besonders wichtig für die ordnungsgemäße Barrierefunktion der Haut sind. In vorangegangenen Studien wurde die Koexistenz von zwei lamellaren Phasen, der „Short-periodicity-Phase" von ca. 60 Å und der „Long-periodicity-Phase" von ca. 130 Å

beschrieben. Es wird angenommen, dass die Long-periodicity-phase sich nur ausbildet, wenn Ceramid [EOS] vorhanden ist, demzufolge wird die Präsenz von Ceramid [EOS] als eine Grundvoraussetzung für die Barrierefunktion der Haut angesehen. Allerdings, werden die Existenz der Long-periodicity-phase, ihr Aufbau sowie Bedingungen, die ihre Ausbildung fördern bzw. hindern zurzeit kontrovers diskutiert. Ein Betrag zu dieser Debatte lieferten die in dieser Arbeit durchgeführten Strukturuntersuchungen an einer Lipid-Modellmembran, die aus den Ceramiden [AP] und [EOS], sowie Cholesterol und freier Fettsäure (Behensäure) besteht. Es hat sich in den Untersuchungen gezeigt, dass trotz Präsenz des langkettigen Ceramids [EOS] keine Long-periodicity-phase ausgebildet wird und *nur* die Short-periodicity-phase detektierbar war. Auch ternäre Stratum corneum Lipid-Modellmembranen, denen die Fettsäurekomponente fehlte, zeigten ein vergleichbares Verhalten, auch hier wurde die Long-periodicity-phase nicht gefunden [81]. Ein solches Verhalten lässt sich nur dadurch erklären, dass die polaren Kopfgruppen von Ceramid [AP] einen größeren Einfluss auf den Aufbauprozess der Membran ausüben, als die langen Alkylketten des Ceramids [EOS].

Durch diese Ergebnisse wird das von Kiselev und Mitarbeitern vorgeschlagene Modell zur Beschreibung der Stratum corneum Nanostruktur, das *„Armature-reinforcement"*-Modell unterstützt [82]. Die Untersuchungen an Modellmembranen mit Ceramid [AP] und Ceramid [EOS] haben auch dazu beigetragen, dass die Bedeutung der Short-periodicity-phase für die Barrierefunktion der Stratum corneum Lipidmatrix neu überdacht werden muss.

Auch in Stresssituationen, wie erhöhte Temperatur ist es wichtig, die Barrierefunktionen des Stratum corneum aufrechtzuerhalten. Es sind also Strategien von Nöten, die die Struktur unter solchen Bedingungen bewahren. Eine dieser Strategien ist das so genannte „Chain-flip-transition" der Ceramid [AP] Moleküle, mit der auf entsprechende Veränderungen in der Umwelt reagiert werden kann. Dabei können die Ceramid [AP] Moleküle von der gestreckten in die einseitige Konformation bzw. umgekehrt, wechseln.

Die in dieser Arbeit beschriebenen Untersuchungen an Ceramid [AP]-basierten Stratum corneum Lipid-Modellmembranen haben gezeigt, dass im Prinzip diese Membranen einer Beeinflussung durch Hitze recht gut wieder stehen können. Eine Temperaturerhöhung bis zu 50 bzw. 65°C konnte nur unwesentliche Veränderungen in der Gesamtstruktur der Lipidschichten bewirken. Allein der lamellare Wiederholabstand verringerte sich kontinuierlich mit zunehmender Temperatur, bedingt durch die zunehmende der Unordnung der Alkylketten [153, 140, 154]. Eine weitere Erhöhung der Temperatur auf 80°C bewirkte die oben beschriebene Chain-Flip-transition, bei der Ceramid [AP] Moleküle von der einseitigen in die gestreckten Konformation wechseln. Eine derartige Konformationsänderung festigt die

benachbarten Doppelschichten, der intermembranäre Zwischenraum wird durch die enge Nachbarschaft der Kopfgruppen verringert.

Es konnte im Rahmen der vorliegenden Arbeit gezeigt werden, dass die Anwendung der Neutronendiffraktion in Verbindung mit den eher konventionellen Techniken wie Differential-Scanning-Kalorimetrie und Raman Spektroskopie das Wissen über das thermotrope Phasenverhalten solch komplexer Systeme erweitert. Insbesondere die Neutronendiffraktion lieferte unmittelbar strukturelle Daten über die lamellare Anordnung bei Temperaturveränderung, wobei zusätzlich durch die Auswertung des ersten Strukturfaktors Information über die Veränderungen in den polaren Kopfgruppen erhältlich war.

Alle hier vorgestellten Untersuchungen an Stratum corneum Lipid-Modellmembranen haben die besondere Bedeutung von Ceramid [AP] für die strukturelle Anordnung dieser Membranen hervorgehoben. Unabhängig von der zusätzlich verwendeten Ceramidart wurde der Aufbauprozess der Modellmembran immer durch das kurzkettige, polare Ceramid [AP] bestimmt. Weiterhin hat auch die Verlängerung der Fettsäurekettenlänge keinen Einfluss auf die Struktur der Membran. Demzufolge lässt sich schlussfolgern, dass die Polarität der Kopfgruppe des Ceramids die Einflüsse aller anderen Komponenten überwiegt, ebenso die Kettenlänge des ω-acyl-Ceramids [EOS].

Die hier vorgestellten Ergebnisse lassen die kurzkettigen Ceramide in einem neuen Licht erscheinen, insbesondere die Polarität ihrer Kopfgruppe scheint entscheidend für die strukturelle Anordnung der Lipide zu sein. Bisher konnte nur die Bedeutung des ω-acyl-Ceramids [EOS] für die Barrierefunktion des Stratum corneums belegt werden [156]. Weiterhin sollte auch die Bedeutung der Short-periodicity-Phase für die Barrierefunktion innerhalb des Stratum corneums neu überdacht werden.

Die zukünftigen Untersuchungen müssen nun die Bedeutung der einzelnen Ceramidklassen, insbesondere der kurzkettigen Ceramide und deren Kopfgruppenpolarität weiter prüfen. Dies kann durch einen sukzessiven Austausch des sehr polaren kurzkettigen Ceramids [AP] in den bereits beschriebenen Stratum corneum Lipid-Modellmembranen durch ebenfalls kurzkettige Ceramide mit verringerter Kopfgruppenpolarität wie Ceramid [AS] erfolgen. Weiterhin sollten Untersuchungen an Modelmembranen ähnlich denen in Kapitel 7 beschriebenen zeigen, ob ein Austausch des ω-acyl Ceramids [EOS] durch das etwas polarere ω-acyl Ceramid [EOP] den Einfluss von Ceramid [AP] übertreffen kann. In einer vorangegangenen Untersuchung hat ein partieller Austausch von Ceramid [EOS] durch [EOP] eine Verminderung der Long-periodicity-phase geführt hat, welche die Autoren auf den Kopfgruppeneffekt des polareren Ceramids [EOP] zurückführten, wobei die Kettenlänge beider Ceramide annähernd gleich war [72].

Es sollte auch geklärt werden, ob die Fettsäure eine wesentliche Rolle für die Ausbildung der Long-periodicity-phase einnehmen kann. In anderen Studie wurde festgestellt, dass die Zugabe von freien Fettsäuren zu Mischungen aus isolierten humanen Ceramiden und Cholesterol die Bildung der Short-periodicity-phase fördert [70]. Weiterhin hat sich in einer weiteren Studie gezeigt, dass die Zugabe einer Fettsäuremischungen aus langkettigen Fettsäuren (überwiegend C22 – C24) zu Mischungen aus Ceramiden und Cholesterol einen Übergang von einer hexagonalen zu einer orthorhombischen Kettenpackung herbeiführt, in Anwesenheit einer Fettsäuremischung aus überwiegend kurzkettigen Fettsäuren (C16 – C18) konnte dies nicht beobachtet werden [19].

Im Gegensatz dazu, konnte in den hier vorgestellten Untersuchungen eine orthorhombische Kettenanordnung nicht beobachtet werden. Ein Grund hierfür könnte die Verwendung von nur *einer* Fettsäureart sein. Wie bereits oben erläutert müssen gegebenenfalls Fettsäurenmischungen mit verschiedenen Kettenlängen zu gegen sein, um einen Einfluss auf die Strukturausbildung nehmen zu können. Weiterhin stellt sich die Frage, ob der Anteil an Fettsäure in den Modellmembranen auch eine Bedeutung besitzt. Die von Bouwstra und Mitarbeiter [24] beschrieben Mischungen aus Ceramiden, Cholesterol und freien Fettsäuren waren alle in einem equimolaren Verhältnis, gegebenenfalls ein Grund dafür, dass dort die orthorhombische Kettenpackung im Gegensatz zu der hier präsentierten Arbeit nicht beobachtet wurde. Dies ist möglicherweise ein Hinweis, dass ein höherer Fettsäureanteil in solchen Modelsystemen die Kettenpackung beeinflussen kann. Weiterführende Raman spektroskopische Untersuchungen in Verbindung mit Neutronendiffraktion sind erforderlich, um diese Frage zu klären.

Zusammenfassend lässt sich feststellen, dass viele neue Einblicke in die Nanostruktur von definierten Stratum corneum Lipid-Modellmembranen präsentiert werden konnten. Insbesondere die bedeutsame Rolle von Ceramid [AP] konnte belegt werden. Alle vorgestellten Ergebnisse fließen in das von Kiselev und Mitarbeitern [82] entwickelte *„Armature-reinforcement"*-Model mit ein und unterstützen dieses. Weitere intensive Untersuchungen sind nötig, um die die strukturelle Anordnung der Lipide in der Stratum corneum Lipidlamellae besser zu verstehen, was letztendlich die Voraussetzung für ein besseres Verständnis der Barrierefunktion des Stratum corneums und der Mechanismen der Arzneistoffpenetration ist.

Literature

[1]   R.F. Rushmer, K.J. Buettner, J.M. Short and G.F. Odland, The skin, *Science* 154 **(1966)** 343-8.

[2]   P.W. Wertz and B. van den Bergh, The physical, chemical and functional properties of lipids in the skin and other biological barriers, *Chem Phys Lipids* 91 **(1998)** 85-96.

[3]   C.M. Chuong, B.J. Nickoloff, P.M. Elias, L.A. Goldsmith, E. Macher, P.A. Maderson, J.P. Sundberg, H. Tagami, P.M. Plonka, K. Thestrup-Pederson, B.A. Bernard, J.M. Schroder, P. Dotto, C.M. Chang, M.L. Williams, K.R. Feingold, L.E. King, A.M. Kligman, J.L. Rees and E. Christophers, What is the 'true' function of skin?, *Exp Dermatol* 11 **(2002)** 159-87.

[4]   G. Thews, E. Mutschler and P. Vaupel, Anatomie, Physiologie Pathophysiologie des Menschen, 5 ed., Wissenschaftliche Vertragsgesellschaft mbH, Stuttgart, 1999.

[5]   W.F. Loomis, Skin-pigment regulation of vitamin-D biosynthesis in man, *Science* 157 **(1967)** 501-6.

[6]   M.F. Holick, J.A. MacLaughlin, M.B. Clark, S.A. Holick, J.T. Potts, Jr., R.R. Anderson, I.H. Blank, J.A. Parrish and P. Elias, Photosynthesis of previtamin D3 in human skin and the physiologic consequences, *Science* 210 **(1980)** 203-5.

[7]   M. Schiller, M. Raghunath, U. Kubitscheck, T.E. Scholzen, T. Fisbeck, D. Metze, T.A. Luger and M. Bohm, Human Dermal Fibroblasts Express Prohormone Convertases 1 and 2 and Produce Proopiomelanocortin-Derived Peptides, 117 **(2001)** 235.

[8]   T. Winsor and G.E. Burch, Differential roles of layers of human epigastric skin on diffusion rate of water, *Arch Intern Med* 74 **(1944)** 428-436.

[9]   P.M. Elias, Epidermal lipids, barrier function, and desquamation, *J Invest Dermatol* 80 Suppl **(1983)** 44s-49s.

[10]   M.A. Lampe, A.L. Burlingame, J. Whitney, M.L. Williams, B.E. Brown, E. Roitman and P.M. Elias, Human stratum corneum lipids: characterization and regional variations, *J Lipid Res* 24 **(1983)** 120-30.

[11]   M.A. Lampe, M.L. Williams and P.M. Elias, Human epidermal lipids: characterization and modulations during differentiation, *J Lipid Res* 24 **(1983)** 131-40.

[12]   P.M. Elias and D.S. Friend, The permeability barrier in mammalian epidermis, *J Cell Biol* 65 **(1975)** 180-91.

[13]   H.E. Bodde, I. Vandenbrink, H.K. Koerten and F.H.N. Dehaan, Visualization of Invitro Percutaneous Penetration of Mercuric-Chloride - Transport through Intercellular Space Versus Cellular Uptake through Desmosomes, *J Control Release* 15 **(1991)** 227-236.

[14] P. Talreja, N.K. Kleene, W.L. Pickens, T.F. Wang and G.B. Kasting, Visualization of the lipid barrier and measurement of lipid pathlength in human stratum corneum, *AAPS PharmSci* 3 **(2001)** E13.

[15] J.A. Bouwstra, G.S. Gooris, J.A. van der Spek and W. Bras, Structural investigations of human stratum corneum by small-angle X-ray scattering, *J Invest Dermatol* 97 **(1991)** 1005-12.

[16] J.A. Bouwstra, G.S. Gooris, J.A. van der Spek, S. Lavrijsen and W. Bras, The lipid and protein structure of mouse stratum corneum: a wide and small angle diffraction study, *Biochim Biophys Acta* 1212 **(1994)** 183-92.

[17] J.A. Bouwstra, G.S. Gooris, W. Bras and D.T. Downing, Lipid organization in pig stratum corneum, *J Lipid Res* 36 **(1995)** 685-95.

[18] S.E. Friberg and D.W. Osborne, Interaction of a Model Epidermal Lipid with a Vegetable Oil Adduct, *J Disper Sci Technol* 8 **(1987)** 249-258.

[19] J.A. Bouwstra, G.S. Gooris, K. Cheng, A. Weerheim, W. Bras and M. Ponec, Phase behavior of isolated skin lipids, *J Lipid Res* 37 **(1996)** 999-1011.

[20] T.J. McIntosh, M.E. Stewart and D.T. Downing, X-ray diffraction analysis of isolated skin lipids: reconstitution of intercellular lipid domains, *Biochemistry* 35 **(1996)** 3649-53.

[21] J.A. Bouwstra, G.S. Gooris, F.E. Dubbelaar, A.M. Weerheim, A.P. Ijzerman and M. Ponec, Role of ceramide 1 in the molecular organization of the stratum corneum lipids, *J Lipid Res* 39 **(1998)** 186-96.

[22] D. Kuempel, D.C. Swartzendruber, C.A. Squier and P.W. Wertz, In vitro reconstitution of stratum corneum lipid lamellae, *Biochim Biophys Acta* 1372 **(1998)** 135-40.

[23] J.A. Bouwstra, F.E. Dubbelaar, G.S. Gooris, A.M. Weerheim and M. Ponec, The role of ceramide composition in the lipid organisation of the skin barrier, *Biochim Biophys Acta* 1419 **(1999)** 127-36.

[24] J.A. Bouwstra, G.S. Gooris, F.E. Dubbelaar and M. Ponec, Phase behavior of lipid mixtures based on human ceramides: coexistence of crystalline and liquid phases, *J Lipid Res* 42 **(2001)** 1759-70.

[25] T.J. McIntosh, Organization of skin stratum corneum extracellular lamellae: diffraction evidence for asymmetric distribution of cholesterol, *Biophys J* 85 **(2003)** 1675-81.

[26] W.M. Holleran, Y. Takagi and Y. Uchida, Epidermal sphingolipids: Metabolism, function, and roles in skin disorders, *FEBS Lett* 580 **(2006)** 5466.

[27] Y. Masukawa, H. Narita, E. Shimizu, N. Kondo, Y. Sugai, T. Oba, R. Homma, J. Ishikawa, Y. Takagi, T. Kitahara, Y. Takema and K. Kita, Characterization of overall ceramide species in human stratum corneum, *J Lipid Res* 49 **(2008)** 1466-76.

[28]   M.A. Kiselev, N.Y. Ryabova, A.M. Balagurov, S. Dante, T. Hauss, J. Zbytovska, S. Wartewig and R.H. Neubert, New insights into the structure and hydration of a stratum corneum lipid model membrane by neutron diffraction, *Eur Biophys J* 34 **(2005)** 1030-40.

[29]   W.C. Fritsch and R.B. Stoughton, The Effect of Temperature and Humidity on the Penetration of C14 Acetylsalicylic Acid in Excised Human Skin, *J Invest Dermatol* 41 **(1963)** 307-11.

[30]   B. Idson, Percutaneous absorption, *J Pharm Sci* 64 **(1975)** 901-24.

[31]   R.J. Scheuplein, Permeability of the Skin: A review of major concepts and some new developments, *J Investig Dermatol* 67 **(1976)** 676.

[32]   R.E. Zimmerer, K.D. Lawson and C.J. Calvert, The effects of wearing diapers on skin, *Pediatr. Dermatol.* 3 **(1986)** 95-101.

[33]   Encarta. Vol. 2009, Microsoft Inc. **2009**.

[34]   G.L. Wilkes, Superstructure in Stratum Corneum of Neonatal Rat, *Biochim Biophys Acta* 304 **(1973)** 290-293.

[35]   P. Fritsch, Dermatologie und Venerologie: Lehrbuch und Atlas, Springer, Berlin, 1998.

[36]   G.F. Odland, A submicroscopic granular component in human epidermis, *J Invest Dermatol* 34 **(1960)** 11-5.

[37]   P.M. Elias, Epidermal lipids, membranes, and keratinization, *Int J Dermatol* 20 **(1981)** 1-19.

[38]   L. Landmann, [The permeability barrier of the skin], *Pharm. Unserer Zeit* 20 **(1991)** 155-63.

[39]   A.S. Michaels, S.K. Chandrasekaran and J.E. Shaw, Drug permeation through human skin: Theory and invitro experimental measurement, *AIChE J.* 21 **(1975)** 985-996.

[40]   B.W. Barry, Mode of action of penetration enhancers in human skin, *J Control Release* 6 **(1987)** 97.

[41]   R.H.H. Neubert, W.A. Wohlrab and W.C. Marsch, Dermatopharmazie. Vehikel, Wirkstoffe, Pharmakologie, Wissenschaftliche Verlagsgesellschaft mbH, Stuttgart, 2001.

[42]   A. Weerheim and M. Ponec, Determination of stratum corneum lipid profile by tape stripping in combination with high-performance thin-layer chromatography, *Arch Dermatol Res* 293 **(2001)** 199.

[43]   G. Gray and H. Yardley, Different populations of pig epidermal cells: isolation and lipid composition, *J Lipid Res* 16 **(1975)** 441-447.

[44]   G. Gray and H. Yardley, Lipid compositions of cells isolated from pig, human, and rat epidermis, *J Lipid Res* 16 **(1975)** 434-440.

[45]   G.M. Gray and R.J. White, Glycosphingolipids and Ceramides in Human and Pig Epidermis, *J Investig Dermatol* 70 **(1978)** 341.

[46]   H.J. Yardley and R. Summerly, Lipid composition and metabolism in normal and diseased epidermis, *Pharmacol Ther* 13 **(1981)** 383.

[47]   W.M. Holleran, M.Q. Man, W.N. Gao, G.K. Menon, P.M. Elias and K.R. Feingold, Sphingolipids are required for mammalian epidermal barrier function. Inhibition of sphingolipid synthesis delays barrier recovery after acute perturbation, *J Clin Invest* 88 **(1991)** 1338-45.

[48]   L. Coderch, O. Lopez, A. de la Maza and J.L. Parra, Ceramides and skin function, *Am J Clin Dermatol* 4 **(2003)** 107-29.

[49]   P.W. Wertz and D.T. Downing, Ceramides of pig epidermis: structure determination, *J Lipid Res* 24 **(1983)** 759-65.

[50]   S. Motta, M. Monti, S. Sesana, R. Caputo, S. Carelli and R. Ghidoni, Ceramide composition of the psoriatic scale, *Biochim Biophys Acta* 1182 **(1993)** 147-51.

[51]   K. Raith, H. Farwanah, S. Wartewig and R.H.H. Neubert, Progress in the analysis of Stratum corneum ceramides, *Eur J Lipid Sci Tech* 106 **(2004)** 561-571.

[52]   M. de Jager, G. Gooris, M. Ponec and J. Bouwstra, Acylceramide head group architecture affects lipid organization in synthetic ceramide mixtures, *J Invest Dermatol* 123 **(2004)** 911-6.

[53]   M. Mao-Qiang, P.M. Elias and K.R. Feingold, Fatty acids are required for epidermal permeability barrier function, *J Clin Invest* 92 **(1993)** 791-8.

[54]   F. Bonte, A. Saunois, P. Pinguet and A. Meybeck, Existence of a lipid gradient in the upper stratum corneum and its possible biological significance, *Arch Dermatol Res* 289 **(1997)** 78-82.

[55]   L. Norlen, I. Nicander, A. Lundsjo, T. Cronholm and B. Forslind, A new HPLC-based method for the quantitative analysis of inner stratum corneum lipids with special reference to the free fatty acid fraction, *Arch Dermatol Res* 290 **(1998)** 516.

[56]   P.W. Wertz. in (Jolles, P., Zahn, H. and Hocker, H., eds.) *Hair: Biology and structure*, Birkhauser Verlag, Basel **1996**, pp. 227- 238.

[57]   D. Kessner, M.A. Kiselev, T. Hauss, S. Dante, S. Wartewig and R.H.H. Neubert, Localisation of partially deuterated cholesterol in quaternary SC lipid model membranes: a neutron diffraction study, *Eur Biophys J Biophy* 37 **(2008)** 1051-1057.

[58]   T.J. McIntosh, The effect of cholesterol on the structure of phosphatidylcholine bilayers, *Biochim Biophys Acta* 513 **(1978)** 43-58.

[59]   S. Bhattacharya and S. Haldar, Interactions between cholesterol and lipids in bilayer membranes. Role of lipid headgroup and hydrocarbon chain-backbone linkage, *Biochim Biophys Acta* 1467 **(2000)** 39-53.

[60]   J. Czub and M. Baginski, Comparative molecular dynamics study of lipid membranes containing cholesterol and ergosterol, *Biophys J* 90 **(2006)** 2368-82.

[61]   P.W. Wertz, Lipids and barrier function of the skin, *Acta Derm Venereol Suppl (Stockh)* 208 **(2000)** 7-11.

[62]   M.L. Williams and P.M. Elias, Stratum corneum lipids in disorders of cornification: increased cholesterol sulfate content of stratum corneum in recessive x-linked ichthyosis, *J Clin Invest* 68 **(1981)** 1404-10.

[63]   J. Sato, M. Denda, J. Nakanishi, J. Nomura and J. Koyama, Cholesterol sulfate inhibits proteases that are involved in desquamation of stratum corneum, *J Invest Dermatol* 111 **(1998)** 189-93.

[64]   P.M. Elias, D. Crumrine, U. Rassner, J.-P. Hachem, G.K. Menon, W. Man, M.H.W. Choy, L. Leypoldt, K.R. Feingold and M.L. Williams, Basis For Abnormal Desquamation And Permeability Barrier Dysfunction in RXLI, *J Investig Dermatol* 122 **(2004)** 319.

[65]   K.C. Madison, D.C. Swartzendruber, P.W. Wertz and D.T. Downing, Presence of intact intercellular lipid lamellae in the upper layers of the stratum corneum, *J Invest Dermatol* 88 **(1987)** 714-8.

[66]   D.C. Swartzendruber, P.W. Wertz, D.J. Kitko, K.C. Madison and D.T. Downing, Molecular-Models of the Intercellular Lipid Lamellae in Mammalian Stratum-Corneum, *J Investig Dermatol* 92 **(1989)** 251-257.

[67]   N. Ohta, S. Ban, H. Tanaka, S. Nakata and I. Hatta, Swelling of intercellular lipid lamellar structure with short repeat distance in hairless mouse stratum corneum as studied by X-ray diffraction, *Chem Phys Lipids* 123 **(2003)** 8.

[68]   A. Al-Amoudi, J. Dubochet and L. Norlen, Nanostructure of the epidermal extracellular space as observed by cryo-electron microscopy of vitreous sections of human skin, *J Investig Dermatol* 124 **(2005)** 764-777.

[69]   S. Pfeiffer, G. Vielhaber, J.P. Vietzke, K.P. Wittern, U. Hintze and R. Wepf, High-pressure freezing provides new information on human epidermis: Simultaneous protein antigen and lamellar lipid structure preservation. Study on human epidermis by cryoimmobilization, *J Investig Dermatol* 114 **(2000)** 1030-1038.

[70]   J.A. Bouwstra, G.S. Gooris, F.E. Dubbelaar, A.M. Weerheim and M. Ponec, pH, cholesterol sulfate, and fatty acids affect the stratum corneum lipid organization, *J Investig Dermatol Symp Proc* 3 **(1998)** 69-74.

[71]   M.W. de Jager, G.S. Gooris, I.P. Dolbnya, W. Bras, M. Ponec and J.A. Bouwstra, The phase behaviour of skin lipid mixtures based on synthetic ceramides, *Chem Phys Lipids* 124 **(2003)** 123-34.

[72]   M.W. de Jager, G.S. Gooris, M. Ponec and J.A. Bouwstra, Lipid mixtures prepared with well-defined synthetic ceramides closely mimic the unique stratum corneum lipid phase behavior, *J Lipid Res* 46 **(2005)** 2649-56.

[73]   S.H. White, D. Mirejovsky and G.I. King, Structure of lamellar lipid domains and corneocyte envelopes of murine stratum corneum. An X-ray diffraction study, *Biochemistry* 27 **(1988)** 3725-32.

[74]   J.C. Garson, J. Doucet, J.L. Leveque and G. Tsoucaris, Oriented structure in human stratum corneum revealed by X-ray diffraction, *J Invest Dermatol* 96 **(1991)** 43-9.

[75]   G.C. Charalambopoulou, T.A. Steriotis, T. Hauss, A.K. Stubos and N.K. Kanellopoulos, Structural alterations of fully hydrated human stratum corneum, *Physica B: Condensed Matter* 350 **(2004)** E606.

[76]   B. Forslind, A domain mosaic model of the skin barrier, *Acta Derm Venereol* 74 **(1994)** 1-6.

[77]   J.A. Bouwstra, F.E. Dubbelaar, G.S. Gooris and M. Ponec, The lipid organisation in the skin barrier, *Acta Derm Venereol Suppl (Stockh)* 208 **(2000)** 23-30.

[78]   L. Norlen, Skin barrier structure and function: The single gel phase model, *J Investig Dermatol* 117 **(2001)** 830-836.

[79]   M.W. de Jager, G.S. Gooris, I.P. Dolbnya, W. Bras, M. Ponec and J.A. Bouwstra, Novel lipid mixtures based on synthetic ceramides reproduce the unique stratum corneum lipid organization, *J Lipid Res* 45 **(2004)** 923-32.

[80]   M.W. de Jager, G.S. Gooris, I.P. Dolbnya, M. Ponec and J.A. Bouwstra, Modelling the stratum corneum lipid organisation with synthetic lipid mixtures: the importance of synthetic ceramide composition, *Biochim Biophys Acta* 1664 **(2004)** 132-40.

[81]   D. Kessner, M. Kiselev, S. Dante, T. Hauss, P. Lersch, S. Wartewig and R.H.H. Neubert, Arrangement of ceramide [EOS] in a stratum corneum lipid model matrix: new aspects revealed by neutron diffraction studies, *Eur Biophys J Biophy* 37 **(2008)** 989-999.

[82]   M. Kiselev, Conformation of ceramide 6 molecules and chain-flip transitions in the lipid matrix of the outermost layer of mammalian skin, the stratum corneum, *Crystallogr Rep+* 52 **(2007)** 528.

[83]   G.C. Charalambopoulou, T.A. Steriotis, T. Hauss, K.L. Stefanopoulos and A.K. Stubos, A neutron-diffraction study of the effect of hydration on stratum corneum structure, *Appl Phys a-Mater* 74 **(2002)** S1245-S1247.

[84] F.X. Contreras, G. Basanez, A. Alonso, A. Herrmann and F.M. Goni, Asymmetric addition of ceramides but not dihydroceramides promotes transbilayer (flip-flop) lipid motion in membranes, *Biophys J* 88 **(2005)** 348-59.

[85] R.N. McElhaney, Differential scanning calorimetric studies of lipid-protein interactions in model membrane systems, *Biochimica et Biophysica Acta (BBA) - Reviews on Biomembranes* 864 **(1986)** 421.

[86] M. Epple, Applications of Temperature-Resolved Diffraction Methods in Thermal-Analysis, *J. Therm. Anal.* 42 **(1994)** 559-593.

[87] R. Singh, C. V. Raman and the Discovery of the Raman Effect, *Physics in Perspective (PIP)* 4 **(2002)** 420.

[88] N. Colthup, L. Daly and S. Wiberley, Introduction to Infrared and Raman spectroscopy, 3 ed., Academic Press 1990.

[89] H.H. Mantsch, Vibrational spectroscopy of lipids: a historical perspective, *Chem Phys Lipids* 96 **(1998)** 3-7.

[90] R. Mendelsohn and D.J. Moore, Vibrational spectroscopic studies of lipid domains in biomembranes and model systems, *Chem Phys Lipids* 96 **(1998)** 141-57.

[91] R. Mendelsohn, M.A. Davies, J.W. Brauner, H.F. Schuster and R.A. Dluhy, Quantitative-Determination of Conformational Disorder in the Acyl Chains of Phospholipid-Bilayers by Infrared-Spectroscopy, *Biochemistry* 28 **(1989)** 8934-8939.

[92] S. Abbate, G. Zerbi and S.L. Wunder, Fermi Resonances and Vibrational-Spectra of Crystalline and Amorphous Polymethylene Chains, *J. Phys. Chem.* 86 **(1982)** 3140-3149.

[93] S. Abbate, S.L. Wunder and G. Zerbi, Conformational Dependence of Fermi Resonances in Normal-Alkanes - Raman-Spectra of 1,1,1,4,4,4-Hexadeuteriobutane, *J. Phys. Chem.* 88 **(1984)** 593-600.

[94] R.G. Snyder and J.H. Schachtschneider, Vibrational analysis of the n-paraffins I : Assignments of infrared bands in the spectra of C3H8 through n-C19H40, *Spectrochimica Acta* 19 **(1963)** 116.

[95] K.G. Brown, E. Bicknell-Brown and M. Ladjadj, Raman-active bands sensitive to motion and conformation at the chain termini and backbones of alkanes and lipids, *J. Phys. Chem.* 91 **(1987)** 3436-3442.

[96] I. Pascher, M. Lundmark, P.G. Nyholm and S. Sundell, Crystal-Structures of Membrane-Lipids, *Biochim Biophys Acta* 1113 **(1992)** 339-373.

[97] M. Kobayashi, F. Kaneko, K. Sato and M. Suzuki, Vibrational spectroscopic study on polymorphism and order-disorder phase transition in oleic acid, *The Journal of Physical Chemistry* 90 **(1986)** 6378.

[98]   C.R. Cantor and P.R. Schimmel, Biophysical Chemistry: Part II: Techniques for the Study of Biological Structure and Function, W.H. Freeman and Co., San Franscisco, 1980.

[99]   M. Tomita, T. Hasegawa, T. Tsukihara, S. Miyajima, M. Nagao and M. Sato, Two concentric protein shell structure with spikes of silkworm Bombyx mori cytoplasmic polyhedrosis virus revealed by small-angle neutron scattering using the contrast variation method, *J. Biochem. (Tokyo).* 125 **(1999)** 916-922.

[100]   T. Gutberlet, U. Heinemann and M. Steiner, Protein crystallography with neutrons - status and perspectives, *Acta Crystallogr D* 57 **(2001)** 349-354.

[101]   T. Hauss, S. Dante, N.A. Dencher and T.H. Haines, Squalane is in the midplane of the lipid bilayer: implications for its function as a proton permeability barrier, *Biochim Biophys Acta* 1556 **(2002)** 149-54.

[102]   N.P. Franks and W.R. Lieb, The structure of lipid bilayers and the effects of general anaesthetics. An X-ray and neutron diffraction study, *J Mol Biol* 133 **(1979)** 469-500.

[103]   M.C. Wiener and S.H. White, Fluid Bilayer Structure Determination by the Combined Use of X-Ray and Neutron-Diffraction .1. Fluid Bilayer Models and the Limits of Resolution, *Biophys J* 59 **(1991)** 162-173.

[104]   D.L. Worcester, Neutron diffraction studies of biological membranes and membrane components, *Brookhaven Symp Biol* **(1976)** III37-III57.

[105]   J.F. Nagle and S. Tristram-Nagle, Structure of lipid bilayers, *Biochim Biophys Acta* 1469 **(2000)** 159-95.

[106]   B. Dahlen and I. Pascher, Molecular Arrangements in Sphingolipids - Thermotropic Phase-Behavior of Tetracosanoylphytosphingosine, *Chem Phys Lipids* 24 **(1979)** 119-133.

[107]   G. Buldt, H.U. Gally, A. Seelig, J. Seelig and G. Zaccai, Neutron diffraction studies on selectively deuterated phospholipid bilayers, *Nature* 271 **(1978)** 184.

[108]   T. Hauss, G. Buldt, M.P. Heyn and N.A. Dencher, Light-induced isomerization causes an increase in the chromophore tilt in the M intermediate of bacteriorhodopsin: a neutron diffraction study, *Proc Natl Acad Sci U S A* 91 **(1994)** 11854-8.

[109]   S. Dante, T. Hauss and N.A. Dencher, Insertion of externally administered amyloid beta peptide 25-35 and perturbation of lipid bilayers, *Biochemistry* 42 **(2003)** 13667-72.

[110]   M.A. Kiselev, N.Y. Ryabova, A.M. Balagurov, D. Otto, S. Dante, T. Hauss, S. Wartewig and R.H.H. Neubert, Ceramide 6 Influence on the Structure and Hydration of Multilamellar Dipalmitoylphosphatidylcholine Membrane, *Poverchnost. X-ray, synchrotron and neutron investigations* 6 **(2006)** 30-37.

[111] M. Seul and M.J. Sammon, Preparation of Surfactant Multilayer Films on Solid Substrates by Deposition from Organic Solution, *Thin Solid Films* 185 **(1990)** 287-305.

[112] G.K. Menon, New insights into skin structure: scratching the surface, *Adv Drug Deliv Rev* 54 Suppl 1 **(2002)** S3-17.

[113] P.W. Wertz, W. Abraham, L. Landmann and D.T. Downing, Preparation of liposomes from stratum corneum lipids, *J Invest Dermatol* 87 **(1986)** 582-4.

[114] R.M. Hatfield and L.W. Fung, Molecular properties of a stratum corneum model lipid system: large unilamellar vesicles, *Biophys J* 68 **(1995)** 196-207.

[115] V.I. Gordeliy and M.A. Kiselev, Definition of lipid membrane structural parameters from neutronographic experiments with the help of the strip function model, *Biophys J* 69 **(1995)** 1424-8.

[116] K.M. Keough and P.J. Davis, Gel to liquid-crystalline phase transitions in water dispersions of saturated mixed-acid phosphatidylcholines, *Biochemistry* 18 **(1979)** 1453-9.

[117] C. Huang and J.T. Mason, Structure and properties of mixed-chain phospholipid assemblies, *Biochim Biophys Acta* 864 **(1986)** 423-70.

[118] H.S. Shieh, L.G. Hoard and C.E. Nordman, Crystal structure of anhydrous cholesterol, *Nature* 267 **(1977)** 287-9.

[119] J. Huang, J.T. Buboltz and G.W. Feigenson, Maximum solubility of cholesterol in phosphatidylcholine and phosphatidylethanolamine bilayers, *Biochim Biophys Acta* 1417 **(1999)** 89-100.

[120] M.R. Brzustowicz, V. Cherezov, M. Zerouga, M. Caffrey, W. Stillwell and S.R. Wassall, Controlling membrane cholesterol content. A role for polyunsaturated (docosahexaenoate) phospholipids, *Biochemistry* 41 **(2002)** 12509-19.

[121] M.R. Ali, K.H. Cheng and J. Huang, Ceramide drives cholesterol out of the ordered lipid bilayer phase into the crystal phase in 1-palmitoyl-2-oleoyl-sn-glycero-3-phosphocholine/cholesterol/ceramide ternary mixtures, *Biochemistry* 45 **(2006)** 12629-38.

[122] M.A. Fox and J.K. Whitesell, Organische Chemie – Grundlagen, Mechanismen, bioorganische Anwendungen., Spektrum Akademischer Verlag, Heidelberg, 1995.

[123] S. Raudenkolb, W. Hubner, W. Rettig, S. Wartewig and R.H. Neubert, Polymorphism of ceramide 3. Part 1: An investigation focused on the head group of N-octadecanoylphytosphingosine, *Chem Phys Lipids* 123 **(2003)** 9-17.

[124] S. Raudenkolb, S. Wartewig and R.H. Neubert, Polymorphism of ceramide 3. Part 2: A vibrational spectroscopic and X-ray powder diffraction investigation of N-octadecanoyl phytosphingosine and the analogous specifically deuterated d(35) derivative, *Chem Phys Lipids* 124 **(2003)** 89-101.

[125] S. Raudenkolb, S. Wartewig and R.H. Neubert, Polymorphism of ceramide 6: A vibrational spectroscopic and X-ray powder diffraction investigation of the diastereomers of N-(alpha-hydroxyoctadecanoyl)-phytosphingosine, *Chem Phys Lipids* 133 **(2005)** 89-102.

[126] P. Garidel, Structural organisation and phase behaviour of a stratum corneum lipid analogue: ceramide 3A, *Phys Chem Chem Phys* 8 **(2006)** 2265-2275.

[127] A.C. Williams and B.W. Barry, Penetration enhancers, *Adv Drug Deliver Rev* 56 **(2004)** 618.

[128] M.R. Brzustowicz, V. Cherezov, M. Caffrey, W. Stillwell and S.R. Wassall, Molecular organization of cholesterol in polyunsaturated membranes: microdomain formation, *Biophys J* 82 **(2002)** 285-98.

[129] H. Farwanah, R. Neubert, S. Zellmer and K. Raith, Improved procedure for the separation of major stratum corneum lipids by means of automated multiple development thin-layer chromatography, *J Chromatogr B Analyt Technol Biomed Life Sci* 780 **(2002)** 443-50.

[130] D.C. Carrer, S. Schreier, M. Patrito and B. Maggio, Effects of a short-chain ceramide on bilayer domain formation, thickness, and chain mobililty: DMPC and asymmetric ceramide mixtures, *Biophys J* 90 **(2006)** 2394-403.

[131] S. Raudenkolb, S. Wartewig, G. Brezesinski, S.S. Funari and R.H. Neubert, Hydration properties of N-(alpha-hydroxyacyl)-sphingosine: X-ray powder diffraction and FT-Raman spectroscopic studies, *Chem Phys Lipids* 136 **(2005)** 13-22.

[132] D. Kessner, G. Brezesinski, S.S. Funari, B. Dobner and R.H.H. Neubert, Impact of the long chain omega-acyl ceramides on the Stratum corneum lipid nanostructure. Part 1: Thermotropic phase behaviour of CER[EOS] and CER[EOP] studied using X-ray powder diffraction and FT-Raman spectroscopy., *Chem Phys Lipids* accepted **(2009)**.

[133] J. Zbytovská. in *Mathematisch-Naturwissenschaftlich-Technischen Fakultät*, Martin-Luther-Universität Halle-Wittenberg, Halle/Saale **2006**.

[134] S.G. Black and G.S. Dixon, Alternating current calorimetry of dimyristoylphosphatidylcholine multilayers: hysteresis and annealing near the gel to liquid-crystal transition, *Biochemistry* 20 **(1981)** 6744.

[135] P. Garidel and A. Blume, Interaction of alkaline earth cations with the negatively charged phospholipid 1,2-dimyristoyl-sn-glycero-3-phosphoglycerol: A differential scanning and isothermal titration calorimetric study, *Langmuir* 15 **(1999)** 5526-5534.

[136] J.M. Holopainen, J. Lemmich, F. Richter, O.G. Mouritsen, G. Rapp and P.K. Kinnunen, Dimyristoylphosphatidylcholine/C16:0-ceramide binary liposomes studied by differential scanning calorimetry and wide- and small-angle x-ray scattering, *Biophys J* 78 **(2000)** 2459-69.
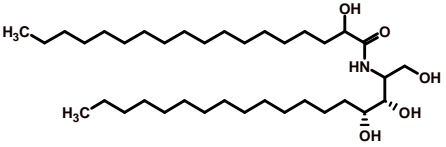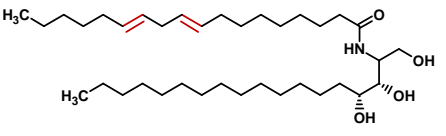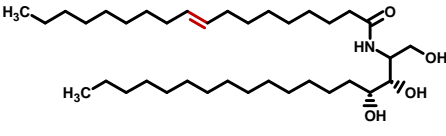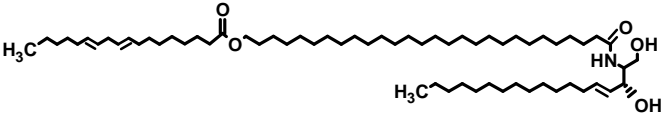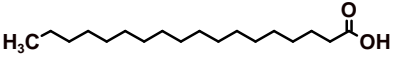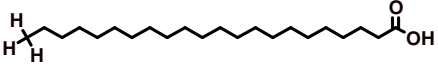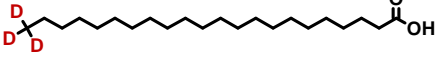
[137]   H.H. Mantsch and R.N. McElhaney, Phospholipid phase transitions in model and biological membranes as studied by infrared spectroscopy, *Chem Phys Lipids* 57 **(1991)** 213-26.

[138]   R.A. MacPhail, H.L. Strauss, R.G. Snyder and C.A. Elliger, Carbon-hydrogen stretching modes and the structure of n-alkyl chains. 2. Long, all-trans chains, *The Journal of Physical Chemistry* 88 **(1984)** 341.

[139]   R. Wang, J. Guo, G. Baran and S.L. Wunder, Characterization of the State of Order of Octadecylsilane Chains on Fumed Silica, *Langmuir* 16 **(1999)** 576.

[140]   G.M. Golden, D.B. Guzek, A.H. Kennedy, J.E. McKie and R.O. Potts, Stratum corneum lipid phase transitions and water barrier properties, *Biochemistry* 26 **(1987)** 2382-8.

[141]   B. Ongpipattanakul, M.L. Francoeur and R.O. Potts, Polymorphism in stratum corneum lipids, *Biochimica et Biophysica Acta (BBA) - Biomembranes* 1190 **(1994)** 122.

[142]   M. de Jager, W. Groenink, I.G.R. Bielsa, E. Andersson, N. Angelova, M. Ponec and J. Bouwstra, A novel in vitro percutaneous penetration model: evaluation of barrier properties with p-aminobenzoic Acid and two of its derivatives, *Pharm Res* 23 **(2006)** 951-60.

[143]   R. Ionov and A. Angelova, Swelling of bilayer lipid membranes, *Thin Solid Films* 284-285 **(1996)** 812.

[144]   B.D. Ladbrooke and D. Chapman, Thermal analysis of lipids, proteins and biological membranes a review and summary of some recent studies, *Chem Phys Lipids* 3 **(1969)** 356.

[145]   Z. Veksli, N.J. Salsbury and D. Chapman, Physical studies of phospholipids. XII. Nuclear magnetic resonance studies of molecular motion in some pure lecithin-water systems, *Biochim Biophys Acta* 183 **(1969)** 434-46.

[146]   H. Pfeiffer, H. Binder, G. Klose and K. Heremans, Hydration pressure and phase transitions of phospholipids: II. Thermotropic approach, *Biochimica et Biophysica Acta (BBA) - Biomembranes* 1609 **(2003)** 152.

[147]   V. Velkova and M. Lafleur, Influence of the lipid composition on the organization of skin lipid model mixtures: An infrared spectroscopy investigation, *Chem Phys Lipids* 117 **(2002)** 63-74.

[148]   M.A. Kiselev, P. Lesieur, A.M. Kisselev, C. Grabielle-Madelmond and M. Ollivon, DMSO-induced dehydration of DPPC membranes studied by X-ray diffraction, small-angle neutron scattering, and calorimetry, *J. Alloys Compd.* 286 **(1999)** 195-202.

[149]   S.N. Shashkov, M.A. Kiselev, S.N. Tioutiounnikov, A.M. Kiselev and P. Lesieur, The study of DMSO/water and DPPC/DMSO/water system by means of the X-ray, neutron small-angle scattering, calorimetry and IR spectroscopy, *Physica B* 271 **(1999)** 184-191.

[150]   H. Chen, R. Mendelsohn, M.E. Rerek and D.J. Moore, Effect of cholesterol on miscibility and phase behavior in binary mixtures with synthetic ceramide 2 and octadecanoic acid. Infrared studies, *Biochim Biophys Acta* 1512 **(2001)** 345-56.

[151]   E. Sparr, L. Eriksson, J.A. Bouwstra and K. Ekelund, AFM study of lipid monolayers: III. Phase behavior of ceramides, cholesterol and fatty acids, *Langmuir* 17 **(2001)** 164-172.

[152]   D.J. Moore, M.E. Rerek and R. Mendelsohn, FTIR spectroscopy studies of the conformational order and phase behavior of ceramides, *J Phys Chem B* 101 **(1997)** 8933-8940.

[153]   B.F. Van Duzee, Thermal analysis of human stratum corneum, *J Investig Dermatol* 65 **(1975)** 408.

[154]   R.O. Potts and M.L. Francoeur, Lipid biophysics of water loss through the skin, *Proc Natl Acad Sci U S A* 87 **(1990)** 3871-3.

[155]   N.Y. Schurer, G. Plewig and P.M. Elias, Stratum-Corneum Lipid Function, *Dermatologica* 183 **(1991)** 77-94.

[156]   J.A. Bouwstra and M. Ponec, The skin barrier in healthy and diseased state, *Biochim Biophys Acta* 1758 **(2006)** 2080-95.

Appendix

Appendix A

Table A Chemical structures of the lipids used for the preparation of the SC lipid model membranes.

Substance (Abbreviation)	Chemical structure
Ceramide [AP] (CER[AP]) *N- (α -Hydroxyoctadecanoyl)- phytosphingosine*	
Ceramide [NP] type A (CER[NP]A) *N-Linoeoyl-phytosphingosine*	
Ceramide [NP] type B (CER[NP]B) *N-Oleoyl-phytosphingosine*	
Ceramide [EOS] (CER[EOS]) *30-Linoyloxy-triacontanoyl- sphingosine*	
Cholesterol (CHOL)	
Cholesterol sulphate (ChS)	
Palmitic acid (PA)	
Stearic acid (SA)	
Behenic acid (BA) Behenic-d$_{22,22,22}$ acid (d$_{22}$BA) Behenic-d$_{7,7,8,8}$ acid (d$_{7}$BA)	
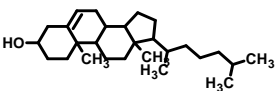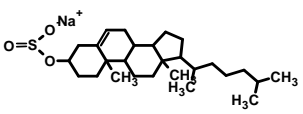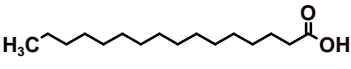
119
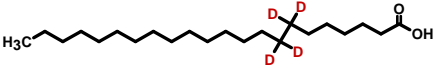
| Tetracosanoic acid (TA) | |
| Cerotic acid (CA) Cerotic-d$_{12,12,13,13}$ acid (d$_{12}$CA) | |

All ceramides were generously donated by Evonik Goldschmidt GmbH (Essen, Germany). Aside from ceramide [EOS], the ceramides were used as received (chemical purity above 96%). In order to increase the chemical purity of CER[EOS] above 96%, the substance was treated using the Middle Pressure Liquid Chromatographic (MPLC) technique on a silica gel column with a chloroform/methanol gradient.

Cholesterol, cholesterol sulphate and the protonated free fatty acids palmitic, docosanoic (behenic), tetracosanoic acid and hexacosanoic (cerotic) acid were purchased from Sigma-Aldrich (Taufkirchen, Germany), while the deuterated fatty acid species, docosanoic-7,7,8,8-d$_4$-acid (99,2 atom% D) and docosanoic-22,22,22-d$_3$-acid (99,2 atom% D) were obtained from Dr. Ehrenstorfer GmbH (Augsburg, Germany). These other lipids were all used as received.

Appendix B

Method:

Neutron diffraction with membrane diffractometer diffractometer V1 (Berlin Neutron Scattering Centre, Berlin Germany) in the reflection setup

- cold source and a neutron wavelength λ of 5.23 Å.
- 2D-position sensitive ^{3}He detector, sensitive area :19 cm x 19 cm, pixel size: 1.5 mm x 1.5 mm
- distance sample to detector: 102.4 cm.

### 1.) Model calculations of the SLD profile
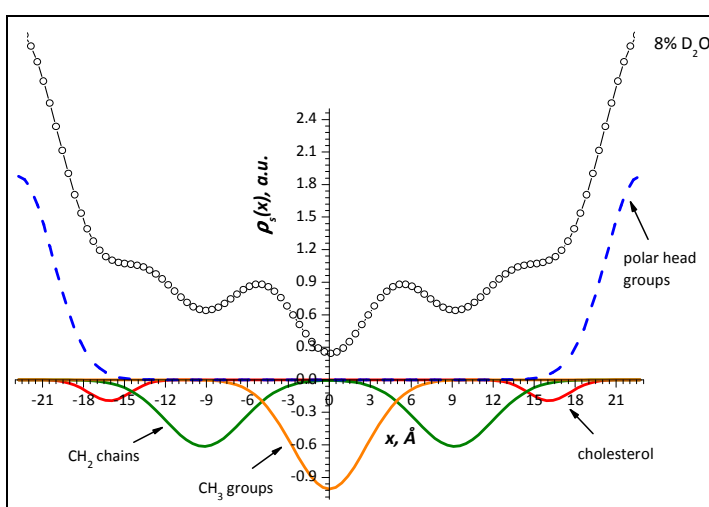
Fig. B 1 Model calculations of the neutron SLD profile of the BA-rich phase of the SC lipid system containing behenic acid. The fitted curves for each group: polar head groups $(-\,-$dash$)$; CH$_2$-groups (dark green), CH$_3$-group (orange), cholesterol (red).

### 2.) Water distribution function
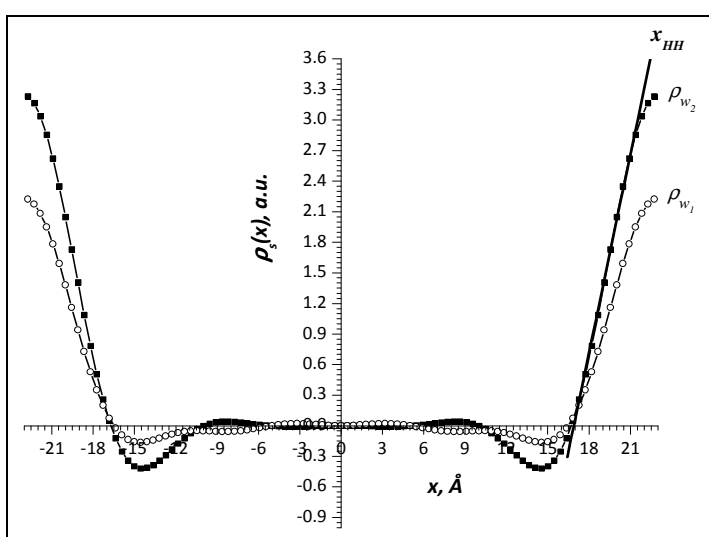
Fig. B 2 Water distribution function $\rho_w(x)$ of the BA-rich phase across the CER[AP]/CHOL/ BA/ChS membrane. The *HH* boundary is determined via linear fit as demonstrated here.

3.) SLD profile of QuatSA
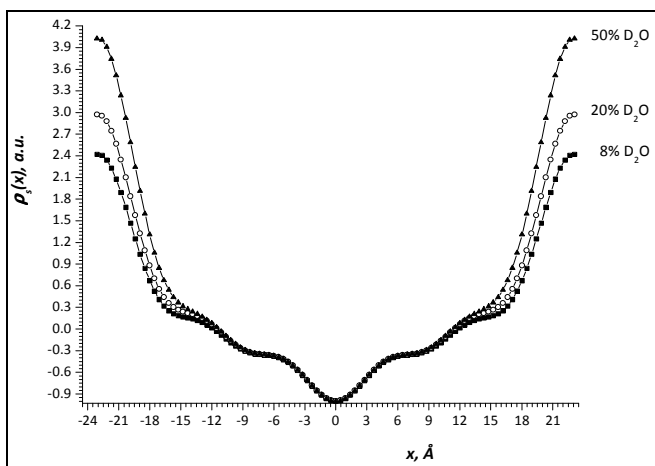
Fig. B 3 The neutron SLD profiles of the main phase of the quaternary SC model membrane composed of CER[AP]/CHOL/SA/ChS (55/25/15/5, w/w) at different D_2O contents (8, 20 and 50%), measured at 57% RH and 20°C.

4.) SLD profile of QuatTA
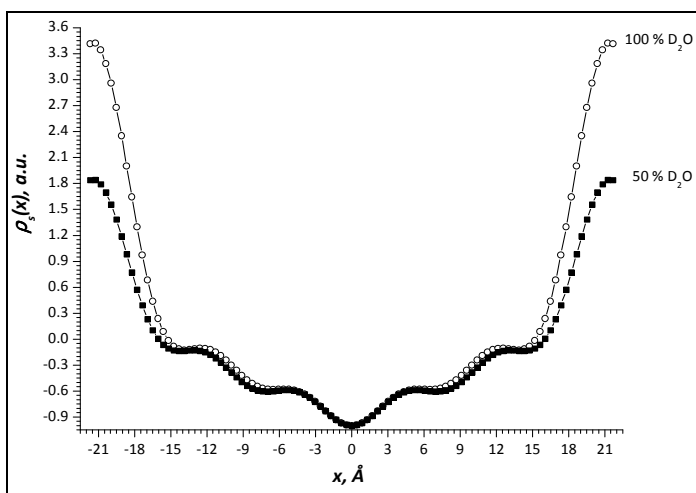
Fig. B 4 The neutron SLD profiles of the main phase of the quaternary SC model membrane composed of CER[AP]/CHOL/TA/ChS (55/25/15/5, w/w) at different D_2O contents (50 and 100%), measured at 57% RH and 20°C.

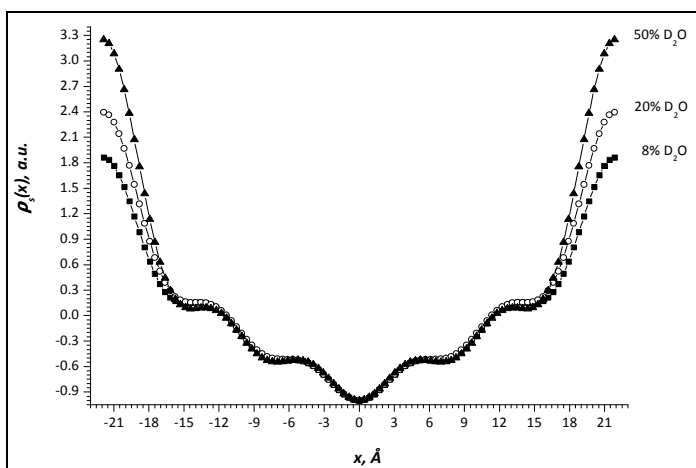### 5.) SLD profile of QuatCA

Fig. B 5 The neutron SLD profiles of the main phase of the quaternary SC model membrane composed of CER[AP]/CHOL/CA/ChS (55/25/15/5, w/w) at different D_2O contents (8, 20 and 50%), measured at 57% RH and 20°C.
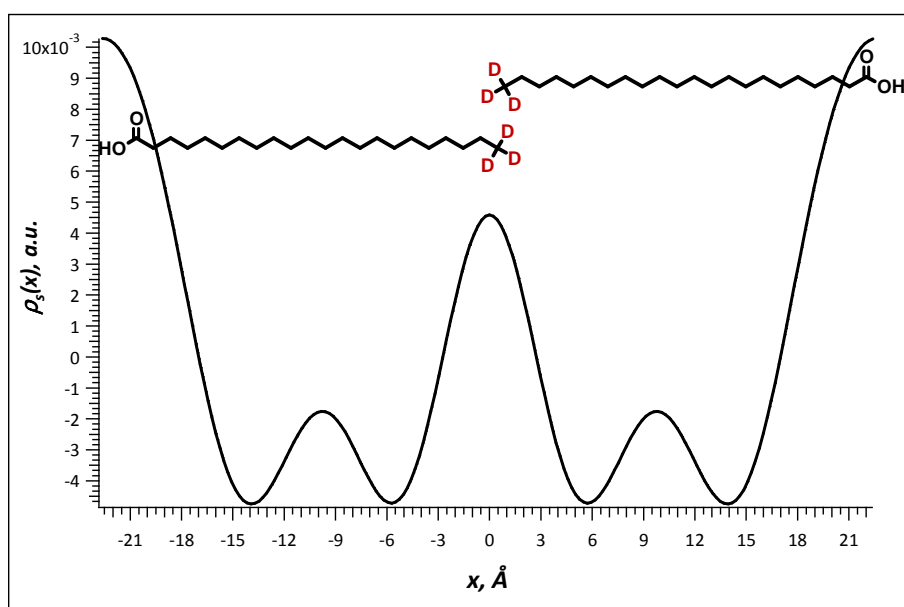
Appendix C

Method:

Neutron diffraction with membrane diffractometer diffractometer V1 (Berlin Neutron Scattering Centre, Berlin Germany) in the reflection setup

- cold source and a neutron wavelength λ of 5.23 Å.
- 2D-position sensitive [3]He detector, sensitive area :19 cm x 19 cm, pixel size: 1.5 mm x 1.5 mm
- distance sample to detector: 102.4 cm.

1) Identification of the FFA-rich phase by applying a specifically deuterated FFA.


Fig. C 1 Neutron SLD profiles at 8% D_2O of the SC lipid model membrane composed of CER[AP]/CER[NP]B/CHOL/ d_{22}BA/ChS (27.5/27.5/25/15/5, w/w). For illustration two terminally deuterated behenic acid molecules have been added.

Appendix D

Method:

Neutron diffraction with membrane diffractometer diffractometer V1 (Berlin Neutron Scattering Centre, Berlin Germany) in the reflection setup

- cold source and a neutron wavelength λ of 5.23 Å.
- 2D-position sensitive [3]He detector, sensitive area :19 cm x 19 cm, pixel size: 1.5 mm x 1.5 mm
- distance sample to detector: 102.4 cm.
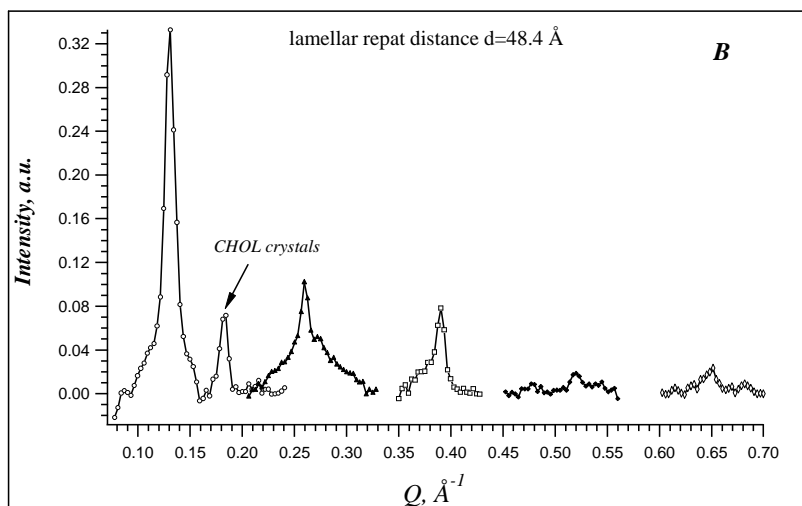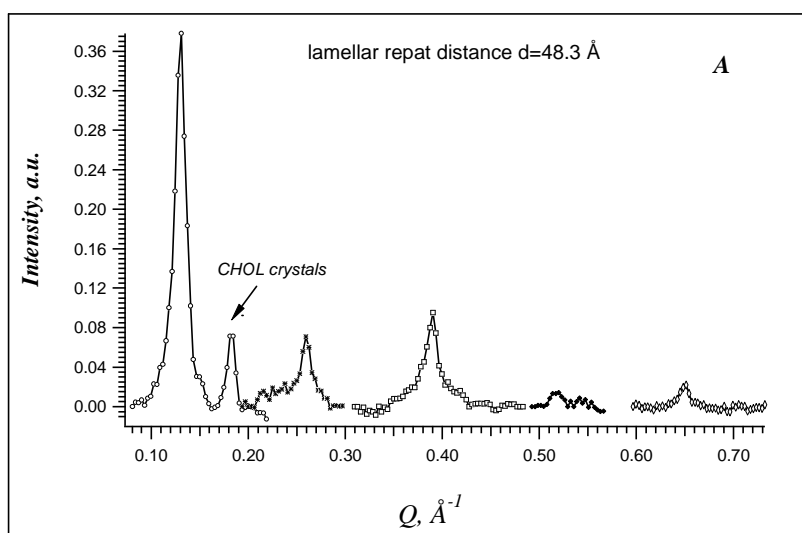
Fig. D 1 Neutron diffraction patterns of the CER[EOS]/ CER[AP]/ CH/ BA membrane at 57% RH (**A**) and at 98% RH (**B**). Measurements were done at a D_2O/ H_2O contrast of 8/ 92 and T=32°C.

List of Publications

Research articles (to October 2009)

○ **A. Ruettinger**, M.A. Kiselev, T. Hauss, S. Dante, A.M. Balagurov and R.H.H. Neubert, Fatty Acid Interdigitation in Stratum Corneum Model Membranes: A Neutron Diffraction Study, *Eur Biophys J Volume 37* (2008) 759-771.

○ D. Kessner, A. **Ruettinger,** M.A. Kiselev, S. Wartewig, R.H.H. Neubert Properties of ceramides and their impact on the stratum corneum structure, Part 2: Stratum corneum lipid model systems - A review, *Skin Pharmacol Physiol 21*:58-74

○ **A. Schroeter**, M.A. Kiselev, T. Hauß, S. Dante and R.H.H. Neubert, Evidence of Free Fatty Acid Interdigitation in Stratum Corneum Model Membranes Based on Ceramide [P] by Deuterium Labelling, *Biochimica et Biophysica Acta (BBA) - Biomembranes 1788* (2009) 2203.

○ **A. Schröter**, D. Kessner, M.A. Kiselev, T. Hauß, S. Dante and R.H.H. Neubert, Basic Nanostructure of Stratum Corneum Lipid Matrices Based on Ceramides [EOS] and [AP]: A Neutron Diffraction Study, *Biophysical Journal 97* (2009) 1114.

○ **A. Schröter, M.A. Kiselev,** T. Hauß, R.H.H. Neubert Phase state and structure of stratum corneum model membranes based on ceramide [AP] - 1. Thermotropic phase behaviour of SC lipid model systems and phase separation of behenic acid in multilamellar SC lipid layers, *submitted to Chemistry and Physic of Lipids* (2009)

○ **A. Schröter, M.A. Kiselev,** T. Hauß, R.H.H. Neubert Phase state and structure of stratum corneum model membranes based on ceramide [AP] - 2. Nanostructural phase transitions in lamellar SC model membrane, *submitted to Chemistry and Physic of Lipids* (2009)

○ **A. Schröter,** T. Hauß, R.H.H. Neubert Structural organisation of stratum corneum model membranes based on the artificial ceramides [NP]A and [NP]B, *submitted to Biophysical Journal* (2009)

Reports

○ **A. Ruettinger**, M. Kiselev M, D. Otto, B. Dobner, R. Neubert, S. Dante S, T. Hauß, Influence of the fatty acid chain length to the structure of a stratum corneum model membrane, *HMI Experimental report,* Berlin, Germany 2006

○ D. Kessner, M. Kiselev, A. **Ruettinger,** R. Neubert, S. Dante, T. Hauß Investigation of deuterium labeled stratum corneum lipid model membranes. *HMI Experimental report,* Berlin, Germany 2006

○ D. Kessner, M. Kiselev, A. **Ruettinger,** R. Neubert, S. Dante, T. Hauß Investigation of Ceramid 1 based stratum corneum lipid model membranes. *HMI Experimental report,* Berlin, Germany 2007

○ **A. Ruettinger**, MA. Kiselev, D. Kessner, S. Dante, T. Hauß, R. Neubert.
Investigation of Stratum corneum lipid model membranes using deuterated fatty acids.
HMI Experimental report, Berlin, Germany 2007

○ **A. Ruettinger**, MA. Kiselev, R. Neubert, S. Dante, T. Hauß,
Structural assembly of Stratum corneum model membranes based on ceramide [NP].
HMI Experimental report, Berlin, Germany 2007

○ D. Kessner, M. Kiselev, A. **Ruettinger,** S. Dante, T. Hauß, R. Neubert
Confirmation of proposed SC lipid model, the armature reinforcement model*. HMI Experimental report,* Berlin, Germany 2007

○ **A. Ruettinger,** R. Neubert, R. Koehler, R. Steitz.
Investigations of the influence of the pH and enhancers on lipid bilayers modelling the stratum corneum*. HMI Experimental report,* Berlin, Germany 2007

○ **A. Schroeter,** T. Engelbrecht, R. Neubert, T. Hauß
Role of ceramide [AP] and ceramide [EOS] in the structural assembly of stratum corneum model membrane. *HMI Experimental report,* Berlin, Germany 2008

Oral presentations

○ **A. Schröter,** D. Kessner, T. Engelbrecht, MA. Kiselev, R. Neubert,
Role of ceramide [AP] for the structural assembly of stratum corneum lipids, *Gordon Research Conference on Barrier Function of Mammalian Skin*, Waterville Valley Resort, NH, USA 2009

○ **A. Rüttinger**, D. Kessner, M.A. Kiselev, R.H.H. Neubert
Insights into the nanostructure of stratum corneum lipid model membranes, *6th World Meeting on Pharmaceutics, Biopharmaceutics and Pharmaceutical Technology,* Barcelona, Spain 2008

○ **A. Rüttinger**
Einfluss der Fettsäurekettenlänge auf die Struktur einer Stratum corneum Lipidmodellmembran. *Kolloqium „SC Lipid Modellmembranen",* Evonik Goldschmidt GmbH, Essen, Germany 2007

○ A. Ruettinger, M. Kiselev, J. Zbytovska, S. Wartewig, R. Neubert.
Investigation of Stratum Corneum Lipid Model Membranes, *Perspectives in Percutaneous Penetration,* La Grand Motte, France 2006

○ A.Rüttinger, M. Kiselev, R. Neubert, S. Wartewig
Einblicke in die Struktur von Stratum corneum Lipid-Modellmembranen, *Doktorandentagung,* Jena, Germany 2005

○ **A. Ruettinger**, R. Neubert
X-ray- and Neutronscattering of Stratum Corneum Lipid Model Membranes *Workshop Earthscience and nanoscience with neutrons at IBR-2/IBR-2M* (JINR Dubna)" GFZ Potsdam, Germany 2005

Poster presentations

○ **A. Schroeter,** D. Kessner, T. Engelbrecht, MA. Kiselev, R. Neubert,
Role of ceramide [AP] for the structural assembly of stratum corneum lipids, *Gordon Research Conference on Barrier Function of Mammalian Skin*, Waterville Valley Resort, NH, USA, 2009

○ **A. Rüttinger**, D. Kessner, M.A. Kiselev, R.H.H. Neubert
Insights into the nanostructure of stratum corneum lipid model membranes, *6th World Meeting on Pharmaceutics, Biopharmaceutics and Pharmaceutical Technology,* Barcelona, Spain, 2008

○ **A. Ruettinger**, A., MA. Kiselev, S. Dante, T. Hauß, RHH. Neubert,
Structural Influence of the chain length of the fatty acids in a Stratum corneum model membrane based on Ceramide [AP], *Jahrestagung der Deutschen Pharmazeutische Gesellschaft*, Erlangen 2007

○ **A. Ruettinger**, A., MA. Kiselev, S. Dante, T. Hauss, RHH. Neubert,
Influence of the fatty acid chain length on a stratum corneum model membrane based on ceramide [AP], *Gordon Research Conference on Barrier Function of Mammalian Skin,* Newport, Rhode Island, USA 2007

○ **A. Ruettinger**, M. Kiselev, S. Dante, T. Hauss, R.H.H. Neubert
Neutron diffraction studies on the structural organisation of a stratum corneum lipid model system based on a synthetic ceramide, *4th Polish-German Symposium,* Halle 2007

○ **A. Ruettinger**, M. Kiselev, S Dante, T Hauss, R. Neubert
Neutron diffraction studies on the structural organisation of a stratum corneum lipid model system based on CER[AP], Hahn-Meitner Users Meeting, Berlin, Germany, 2007

○ **A. Ruettinger**, M. Kiselev, J. Zbytovská, D. Kessner, S. Dante, T. Hauss, R. Neubert,
Investigation of Stratum Corneum Lipid Model Membranes, *International society of skin pharmacology and physiology,* Rome 2006

○ R. Neubert, M. Kiselev, J. Zbytovska, **A. Ruettinger**, D. Otto, S. Wartewig,
New insights into the structure of a stratum corneum lipid model matrix, *5th World Meeting on Pharmaceutics, Biopharmaceutics and Pharmaceutical Technology*, Geneva 2006

○ **A. Ruettinger**, M. Kiselev, J. Zbytovska, S. Wartewig, R. Neubert,
Investigation of Stratum Corneum Lipid Model Membranes, *Perspectives in Percutaneous Penetration*, La Grand Motte 2006

○ MA. Kiselev, J. Zbytovska, D. Otto, **A. Ruettinger**, S. Wartewig, R. Neubert,
New insights into the structure of a stratum corneum lipid model matrix, Gordon Research Conference on Barrier Function of Mammalian Skin*,* South Hadley, MA, USA 2005

Acknowledgements

In the first place I would like to thank my advisor Prof. Dr. rer. nat. habil. Dr. h.c. Reinhard Neubert for the very interesting subject of my PhD work. His willingness to discuss a problem, his inspiration, trust in my person and the provided freedom in research established good working conditions.

I would like to express my appreciation and gratitude to Dr. Thomas Hauß, (Helmholtz Zentrum Berlin für Materialien und Energie Berlin, Germany) for the help in the neutron diffraction experiments, fruitful discussions and careful reading of my various manuscripts. I also like to thank him for the model scattering length density calculations of the ceramide [AP] molecules in the different conformations.

Thank-you to Dr. Mikhail Kiselev (Frank Laboratory of Neutron Physics, Joint Institute for Nuclear Research, Dubna, Moscow Region, Russia) for his help in the analysis of the neutron diffraction data and his readiness for discussions.

I would like to thank Dr. Thomas Müller and Dr. Christoph Wagner (Institute of Chemistry, Martin Luther University Halle-Wittenberg, Germany) for the assistance with the X-ray measurements.

I'm also grateful to Mrs. Heike Rudolf and Mrs. Kerstin Schwarz for the technical assistance with the Raman spectroscopy and differential scanning calorimetry measurements, respectively.

Many thanks to Sandra Heuschkel, Christian Schmelzer, Alexandra Göbel, Anke Hinder, Doreen Kessner and all the other colleagues for the friendly atmosphere in our group, their insights, inputs and support.

I would like to pay my special thank to my husband, my daughter Luise, my parents and my brother for their support and appreciation of my work. They all gave me strength and motivation to get things finished.

Without all of you I could not have made this work possible.

Curriculum vitae

Personal details

Name:	Annett Schröter,
Maiden name:	Rüttinger
Born:	10.10.1979 in Halle/ Saale, Germany
Nationality	German
Marital status	Married, 1 Daughter

Education

1991 - 1999	Thomas-Müntzer-Gymnasium, Halle (Abitur)
09/1996 – 06/1997	Ithaca High School in Ithaca, New York, USA
03/1999	Participation at "jugend forscht" in the field of biology, 1st place in the regional competition and special prize of the Bayer Bitterfeld GmbH, Greppin, Germany
07/1999	Participation at the „8. Landeswettbewerb Unsere Umwelt – ihr Schutz" in Halle, Germany
10/1999 – 09/2003	Pharmacy studies at Martin Luther University Halle-Wittenberg in Halle, Germany
11/2003 – 04/2004	Diploma thesis in pharmaceutical biology in the group of Prof. Dr. W. Roos, Martin Luther University, Halle-Wittenberg: "Fluorescence microscopic measurement and manipulation of the cellular Glutathion pool in Eschscholzia cell cultures ", Halle, Germany
05/2004 – 10/2004	Practical training at the "Neue Apotheke", Halle, Germany
12/2004	Approbation as a pharmacist, Martin Luther University Halle-Wittenberg, Halle, Germany
06/2005	Diploma degree in pharmacy, Martin Luther University Halle-Wittenberg, Halle, Germany

Professional Experience

05/2005 – 09/2008	Ph.D. student in the group of Prof. Dr. Dr. h. c. R. Neubert, Institute of Pharmacy, Department of Pharmaceutical Technology and Biopharmacy, Martin Luther University Halle-Wittenberg, Halle,

Germany

10/2005	Participation at the "Photons and Neutrons Research on Advanced Material" Autumn School on Application of Neutrons and Synchrotron Radiation in Engineering Materials Science, Hamburg, Germany
Since 10/2009	Research and teaching assistant in the group of Prof. Dr. Dr. h. c. R. Neubert at the department of Pharmaceutical Technology and Biopharmacy, at the Institute of Pharmacy, Martin Luther University Halle- Wittenberg in Halle, Germany

Eidesstattliche Erklärung

Hiermit erkläre ich gemäß § 5 Absatz 2b der Promotionsordnung der Naturwissenschaftliche Fakultät I (Biowissenschaften) der Martin-Luther-Universität Halle-Wittenberg, dass ich die Ergebnisse der vorliegenden Dissertationsarbeit

The role of ceramide [AP] for the structural assembly of stratum corneum lipid model membranes

am Institut für Pharmazeutische Technologie und Biopharmazie der Martin-Luther-Universität Halle-Wittenberg selbständig und ohne fremde Hilfe erarbeitet und verfasst habe. Ferner habe ich nur die in der Dissertation angegebenen Literaturstellen und Hilfsmittel verwendet und die entnommenen und benutzten Literaturstellen auch als solche kenntlich gemacht. Weiterhin habe ich die vorliegende Arbeit bisher keiner anderen Prüfungsbehörde vorgelegt.

Halle (Saale), im Oktober 2009   Annett Schröter